Gait Event Detection Algorithms for Free-Living Stair Ambulation

Bachelor's Thesis in Medical Engineering

submitted
by

Liv Herzer

born 03.09.1999 in Nürnberg

Written at

Machine Learning and Data Analytics Lab
Department Artificial Intelligence in Biomedical Engineering
Friedrich-Alexander-Universität Erlangen-Nürnberg (FAU)

Advisors:
Nils Roth M. Sc., Arne Küderle M. Sc., Dr.-Ing. Felix Kluge, Prof. Dr. Bjöern Eskofier
(Machine Learning and Data Analytics Lab, FAU Erlangen-Nürnberg)
Dr. phil. Heiko Gaßner
(Department of Molecular Neurology, University Hospital Erlangen)

Started: 11.01.2021

Finished: 25.06.2021

Ich versichere, dass ich die Arbeit ohne fremde Hilfe und ohne Benutzung anderer als der angegebenen Quellen angefertigt habe und dass die Arbeit in gleicher oder ähnlicher Form noch keiner anderen Prüfungsbehörde vorgelegen hat und von dieser als Teil einer Prüfungsleistung angenommen wurde. Alle Ausführungen, die wörtlich oder sinngemäß übernommen wurden, sind als solche gekennzeichnet.

Die Richtlinien des Lehrstuhls für Bachelor- und Masterarbeiten habe ich gelesen und anerkannt, insbesondere die Regelung des Nutzungsrechts.

Erlangen, den 25. Juni 2021

Übersicht

Eine quantitative Ganganalyse des Treppensteigens kann sowohl helfen das Risiko eines Sturzes realistisch einzuschätzen als auch einen tieferen Einblick in allgemeine gesundheitliche Verfassung und den Verlaufstand neurodegenerativer Krankheiten bieten. Treppensteigen stellt eine größere Belastung für das Gleichgewichts- und Bewegungssystem dar als das Gehen in der Ebene und ist ein elementarer Bestandteil des Alltags. Dennoch wird es in den meisten Gangstudien nicht berücksichtigt, da es an robusten Methoden zur Analyse mangelt. Ein Home-Monitoring über einen längeren Zeitraum liefert ein realistischeres Bild des Gangzustandes als Ganglaboranalysen. Für ersteres können Inertialsensoren eingesetzt werden, da diese leicht sind und sich unauffällig in den Alltag eingliedern lassen. Viele relevante Gangparameter basieren auf dem Erst- und Letztkontakt des Fußes mit dem Boden innerhalb eines Schrittzyklus, daher ist eine präzise Erkennung dieser Ereignisse notwendig. Algorithmen, die diese Ereignisse detektieren, wurden oft lediglich für Gehen in der Ebene oder auf einzelnen Treppen in Laborumgebungen validiert.

In dieser Arbeit wurde deshalb zunächst ein Datensatz mit Treppenlaufszenarien aus dem Außenbereich zusammengestellt. Hierbei wurden von den 20 gesunden Studienteilnehmer:innen gezielt sowohl die präferierte Ganggeschwindigkeit von langsam bis schnell auf drei verschiedenen Treppen variiert, als auch verschiedene Treppenlaufstrategien angewandt, sodass insgesamt über 31 000 Schritte annotiert werden konnten.

Der zweite Teil dieser Arbeit bestand aus der Entwicklung eines Algorithmus zur Gangereignisdetektion anhand der Daten der an beiden Füßen getragenen Inertialsensoren, der insbesondere für Treppensteigen zuverlässig funktioniert. Hierfür wurde zunächst die Funktionsweise zweier Algorithmen aus der Literatur auf dem Treppendatensatz evaluiert und gegen die Referenzdaten von Drucksensorsohlen validiert. Der darauffolgend entwickelte Algorithmus detektiert den Letztkontakt im Minimum der Winkelgeschwindigkeit um die mediolaterale Achse und den Erstkontakt an der Stelle des steilsten Abstiegs der Tiefpass-gefilterten anterior-posterioren Beschleunigung. Die Detektion beider Gangereignisse beim Treppensteigen war hierbei wesentlich zuverlässiger als bei den ebenfalls evaluierten Algorithmen aus der Literatur, die einerseits niedrige Erkennungsraten aufgrund von für wechselnde Schrittmuster unpassenden Schwellwertimplementierungen hatten und andererseits insgesamt nicht auf die unterschiedlichen Signalcharakteristika beim Treppensteigen vorbereitet waren. Der hier vorgestellte Algorithmus erkannte bei präferierter Ganggeschwindigkeit den Erstkontakt mit einem mittleren Fehler von 4.6 ± 16.9 ms und 5.9 ± 16.0 ms und den Letztkontakt mit einem mittleren Fehler von -2.1 ± 35.8 ms und -6 ± 20 ms für Treppenauf- bzw. -abstieg, sodass die Schwung- und Standphasen mit mittleren absoluten Fehlern unter 42.9 ms für den Treppenaufstieg und unter 26.2 ms für den Treppenabstieg berechnet werden konnten. Der entwickelte Algorithmus ist somit für eine Anwendung in der lebensnahen Ganganalyse geeignet, muss jedoch zukünftig in Bezug auf seine Anwendbarkeit bei pathologisch veränderten Gangmustern geprüft werden, um in Home-Monitoring Studien zum Einsatz kommen zu können.

Abstract

Quantitative gait analysis of stair ambulation can help to assess fall risk as well as provide a deeper insight into overall functional decline and the progression of neurodegenerative diseases. Stair negotiation, whilst posing a greater challenge for the balance and motor system than level walking, is a fundamental part of an independent every-day life. Nevertheless, it is often not included in real-world studies due to lack of robust methods. However, long-term home monitoring provides a more realistic image of every-day gait than gait laboratory analysis. For the former, inertial sensors can be used as they are unobtrusive, light-weight, and low-cost. Many gait parameters of interest are based on the initial and terminal contact gait events, therefore a precise detection of these events is necessary. Algorithms that detect these events have often only been validated for level walking or on single stairs in laboratory environments.

Thus, in this thesis, a dataset with stair ambulation data in a real-world outdoor scenario was compiled. For this purpose, 20 healthy participants were asked to vary their gait speed from preferred to slow and fast on three different stairs, as well as perform different stair negotiation strategies as part of a conducted study. As a result, over 31 000 strides were annotated.

The second part of this thesis consisted of the development of an algorithm for gait event detection based on the data of the inertial sensors worn on both feet, which works reliably for walking on level ground and especially for stair ambulation. For this purpose, the performance of two algorithms from literature was first evaluated on the obtained dataset and validated against the reference data from pressure sensor insoles. The algorithm subsequently developed detects the terminal contact of the foot with the ground at the minimum angular velocity around the medio-lateral axis and the initial contact at the point of steepest descent of the low-pass filtered anterior-posterior acceleration. The detection of both gait events during stair ambulation was substantially more reliable compared to the likewise evaluated algorithms from the literature, which struggled on one hand with low detection rates due to threshold implementations unfitting for changing stride patterns and on the other hand were overall not prepared for the different signal characteristics during stair ambulation. The proposed algorithm at preferred gait speed detected initial contact with a mean error of 4.6 ± 16.9 ms and 5.9 ± 16.0 ms and terminal contact with a mean error of -2.1 ± 35.8 ms and -6 ± 20 ms for stair ascent and descent, respectively, allowing the swing and stance times for all paces to be computed with mean absolute errors below 42.9 ms for stair ascent and below 26.2 ms for stair descent.

The developed algorithm is thus suitable for application in real-world gait analysis, but needs to be evaluated in the future with respect to its applicability in pathologically altered gait patterns in order to be used in long-term home monitoring studies.

Contents

Chapter 1

Introduction

Human gait is a fascinating and complex motion that has yet to be fully understood and characterized. As it demands a combination of body strength, coordination, and balance, overall psychological, neurological or musculoskeletal changes can also affect gait characteristics [Bro17, Mir19, Liz16, Mui10]. The aim of gait analysis is to identify these characteristics and to derive statements about the person's mental and physical health. Gait characteristics can e.g., involve certain spatio-temporal gait parameters such as *stride time* and *stride length* as well as less straight-forward parameters such as upper trunk sway or dominant frequencies in acceleration patterns [Ram15, Car18, Tun17, Din17].

Gait analysis is often used to monitor disease progression and severity [Sch17, Hau98, Kel19, Liz16]. While gait tests and indices such as the Timed Up and Go Test and Dynamic Gait Index have been the clinical standard to assess a patients health status, they recently were under criticism due to their lack of objectivity, lack of clarity [SC13] and limited responsiveness and sensitivity in certain populations [Par12]. Although attempts have been made to update the current standards (e.g., the modified Dynamic Gait Index [SC13]), the demand for a truly objective gait analysis system that can accurately quantify a persons mobility capabilities persists. To meet these demands, additional technical measurement systems such as instrumented walkways [McD01] and motion capture systems [Car13] have been used as the gold standard of gait analysis. However, these systems are not only expensive, they are also confined to limited laboratory spaces and thus lack relation to real-world gait [Gal19, Bro17]. To solve these problems and furthermore enable easy to use and unobtrusive long-term home monitoring, sensors and especially inertial measurement units (IMUs) attached to the body have been used in many studies in recent years to extract an objectively assessed variety of gait parameters [Won07, Jar18, Sch17, Ram15, Kan15].

IMUs enable a precise calculation of spatio-temporal gait parameters with an accuracy comparable to gold standard systems [Kan15, Ram15, Ber18]. Various forms of the application of IMUs for gait assessment have been patented (Appendix A.1, A.3 and A.2).

Sensor-based gait analysis of patients with neurodegenerative diseases such as Parkinson's disease (PD) and Huntington's disease (HD) revealed an increased variability of certain spatio-temporal gait parameters [Kel19, Hau98]. The degree of variability was a measure of disease severity and, in contrast to HD patients, PD patients exhibited significantly reduced gait speed [Hau98].

In the context of gait analysis, the analysis of stair ambulation is a particular topic of interest, e.g., in the field of fall risk assessment since over 10% of fatal falls happen on stairs [Sta00]. Stair ambulation is a more demanding task than walking on level ground, as it puts additional charge on the balance control system and requires larger moments and range of motion at lower limb joints [Nad03, Con17, McF88]. Nevertheless, it is a crucial part of daily living, an independent lifestyle, and community participation and should therefore be considered in the validation of any gait analysis system developed for home monitoring.

Analysis of stair ambulation also benefits from the use of IMUs, as otherwise complicated sensorized stair setups have to be integrated into the motion laboratory [Ber09]. These setups often only include less than six steps [Col05, OP11, Rie02, McF88] and thus the relation to real-world gait is questionable.

Nonetheless, investigations into the relevance of stair ambulation parameters have yielded promising results even within these laboratory settings. For instance, Oh-Park et al. measured the stair ascent and descent times of community-dwelling older adults on a three step laboratory stair and were able to accurately assess their risk of overall functional decline [OP11].

However, more detailed and realistic insights can be gained from sensor-based gait analysis in real-world stair ambulation scenarios. In this context Wang et al. [Wan17] investigated the differences between semi-unsupervised gait on stairs and flat surfaces with regard to fall risk. Their results suggests that a faster step rate during stair descent is correlated to multiple prospective falls over 12 months. In contrast, no meaningful correlations from gait parameters obtained during level walking or stair ascent were found [Wan17]. This finding falls in line with the fact, that most of the fall accidents on stairs happen during stair descent [Sta00].

On the other hand, Brodie et al. showed that during stair ascent gait strategies related to slower velocity, greater variability in step duration and lower anteroposterior stability were an appropriate behavioural response to fear of falling [Bro15]. These findings suggest that further sensor-based analysis of stair descent as well as stair ascent would be valuable.

The consideration of gait parameters from stair ambulation can also be useful in the context of disease monitoring and classification. For instance, Carpinella et al. were able to detect significant differences in stair ascent gait patterns from patients with multiple sclerosis, stroke, Parkinson's disease, and the healthy control group [Car18]. Their subjects climbed a 10-step stair as described by Shumway-Cook et al. [SC13] while wearing a magneto-inertial sensor at the sternum. Relevant parameters were step frequency, symmetry and regularity, as well as harmonic ratios and trunk sway in all three body directions (anterio-posterior, medio-lateral and vertical).

While many gait analysis systems have only been validated for walking on level ground [Ram15, Hau98, Jar18, Rue10, Bob18], the few that have been validated for stair ambulation still have a questionable applicability for real-world stair ambulation analysis due to laboratory study environments with few steps on a single flight of stairs [OP11, Car18] or a limited number of subjects and strides [For14, Fig18]. However, even validations of gait analysis systems on semi-unsupervised gait sequences on real-world stairs did not consider multiple differently inclined stairs nor did they include varying paces [Col05, Wan17, Wan14, Fig18]. In order to accurately evaluate the applicability of gait analysis systems for real-world gait analysis, these factors need to be considered and integrated accordingly into the study protocol.

Basic gait parameters such as step symmetry, stride time, cadence, and gait speed can be sufficiently calculated without a perfectly accurate detection of initial contact (IC) and terminal contact (TC) of the foot with the ground. However, a precise detection of these gait events is crucial for the calculation of relative gait parameters such as *swing* to *stance time* ratios, as a systematic increase or reduction of relative phase durations would be the consequence of repeated systematic misdetections [Rud21]. Therefore, the development of algorithms for sensor-based gait event detection is currently a highly frequented research topic [Vu20, Bob18, Jar18, Nis21]. Some exemplary gait event detection algorithms are described in the following section.

1.1 State of the Art Sensor-Based Gait Event Detection

The gait event detection algorithms introduced in this section have been chosen due to their similar sensor placement and potential application for stair ambulation. All algorithms extract features either from the medio-lateral angular velocity or the anterio-posterior acceleration or both.

One common peak-based gait event detection algorithm is the one by Formento et al., who used a single-axis rate gyroscope mounted to the preferred shank to determine IC and TC during stair ambulation with a sampling rate of 125 Hz [For14]. Their real-time system adapted from Catalfamo et al. detected IC at the first negative peak in the angular velocity around the medio-

lateral axis after the *swing phase* and TC was located at the second negative peak after a waiting phase of 50% of the last stance time. An additional threshold was used to determine the *swing phase* [Cat10]. The system was tested in a study with seven healthy subjects (8 – 16 years of age, 137 – 187 cm in height and 33.3 – 65.3 kg in mass). Each participant walked approximately 20 m in total on level ground and additionally once ascended and descended a six step staircase. The first five steps had a run of 25.0 cm and a rise of 15.0 cm and the last step had the same run but only a 1 cm rise. The FScan Mobile System was used as a reference and data was sampled at 125 Hz. The measured absolute mean temporal errors were ≤ 40 ms for stair ascent and ≤ 132ms for stair descent (Stair ascent: IC: 21 ± 17 ms, TC: 40 ± 13 ms; Stair descent: IC: 38 ± 36 ms, TC: 132 ± 44 ms) with a detection rate of 93.1% during stair descent and 95.5% during stair ascent. During level walking, this rate was even higher at 99.5% [Cat10]. Similar approaches with shank-mounted or thigh-mounted IMUs have been patented as a real-time exoskeleton control system (Appendix A.1) and as movement detection and classification system e.g., for pedestrian navigation (Appendix A.2).

Rampp et al. also applied a peak-based algorithm to detect the IC. However, they mounted IMUs on both shoes of their subjects laterally below the ankle instead of the shank and detected the TCs at the zero crossing of the gyroscope signal instead of the negative peak [Ram15]. The IMU data was sampled at 102.4 Hz. Their algorithm was specifically developed for partially pathological gait from elderly people, thus the algorithm was validated on gait recordings from 101 geriatric patients (82.1 ± 6.5 years of age, 164.0 ± 10.0 cm in height) with the GAITRite [McD01] system as a reference. The study protocol consisted of a 10 m walk at preferred speed on level ground (sometimes performed with the help of a wheeled walker) and did not involve any stair ambulation. Rampp et al. did not report mean absolute errors for the individual events they detected, but reported mean absolute errors of 25 ± 38 ms for swing time (mean error: -8 ± 45 ms) and 33 ± 61 ms for stance time (mean error: 9 ± 69 ms). The algorithm is described in more detail in Section 4.3. In the course of this thesis, the algorithm was applied to the obtained stair ambulation dataset and results are reported and discussed in Chapter 5 and Section 6.2.

A slightly different approach was described by Figueiredo et al., who aimed to detect gait events in real-time by applying a finite state machine with heuristic decision rules and adaptive thresholds [Fig18]. Like Formento et al., they only used the medio-lateral gyroscope signal recorded with a sampling rate of 100 Hz, but attached the sensor to the instep of the shoe. The system was validated, among other things, by measures of nine healthy subjects (27 ± 7.35 years of age, 170 ± 12 cm in height, 62.63 ± 9.39 kg) in uncontrolled real-life outdoor environments with two force sensitive resistors integrated in the heel and toe area of the shoe as a reference

system. The study protocol included 50 m level-ground walking on a flat and a rough surface, ascending and descending a 10° slope, as well as climbing a eight step staircase, each at preferred, fast and slow speed. However, from their descriptions it is not quite clear, whether they included stair descent into their evaluations. For free-living level walking an accuracy of 100% for IC and 98.64% for TC was reported with temporal errors greater than 100 ms considered a misdetection. For stair climbing these values were significantly worse ($p > 0.052$ for level walking, $p < 0.05$ for stair climbing) at 96.98% and 95.89% for IC and TC, respectively. They did however report extraordinarily small mean errors and standard deviations for both *stride types* with values below 4.8 ± 10.56 ms (TC delay) for level walking and below 6.43 ± 5.7 ms (TC advance) for stair climbing. For the purpose of this thesis, the proposed algorithm was slightly adapted, which is described in more detail in Section 4.4. The resulting algorithm was evaluated and discussed in Chapter 5 and Section 6.3, respectively.

Another option for gait event detection are template-based methods. Bobić et al. adapted two template-based stride segmentation algorithms for gait event detection with foot-mounted IMUs, which recorded data at 100 Hz [Bob18]. The posterior-anterior acceleration and an algorithm adapted from Micó-Amigo et al. [MA16] was used for IC detection. TCs were detected within the medio-lateral gyroscope signal with an adapted subsequence Dynamic Time Warping algorithm from Barth et al. [Bar13]. Measurements were evaluated on four 15 m walks on level ground per subject from 15 patients with PD and 15 age and gender matched healthy controls (52 ± 7 years of age) with the GAITRite platform as reference system. No absolute errors were specified in numbers, however, they did report sensitivity and precision, where every event with an absolute temporal error below 100 ms was considered a true positive. For the control group a sensitivity of $87.7\% \pm 0.08\%$ and $98.6\% \pm 0.02\%$ was achieved for TC and IC, respectively. The algorithms scored higher in precision with $99.4\% \pm 0.02\%$ for TC and $99.8\% \pm 0.01\%$ for IC.

Furthermore, machine learning approaches based on Hidden Markov Models [Mar17, Man19], Linear Discriminant Analysis [Jia18] , Gaussian Mixture Models [Chu13], as well as artificial neural networks [Kon14] are frequently investigated with respect to applicability for gait event detection and gait characterization. However, this thesis will focus on feature-based event detection.

1.2 Purpose of the Thesis

Real-world gait analysis can not yet provide an accurate analysis of stair ambulation, although multiple studies suggest its clinical relevance [Cos02, Kas05, Wan17, Car18]. More robust gait

event detection algorithms for stair ascent and descent are needed to make further studies of the relationship between stair gait parameters and clinically relevant parameters possible. Ideally, the event detection algorithm should be applicable for home-monitoring in order to gain more realistic insights into daily-life gait characteristics.

Although the presented algorithms partially already showed good results even for stair ambulation, so far no proper study has been performed to test these algorithms in sufficient real-life stair ambulation scenarios. These scenarios should involve multiple real-world stairs with different inclinations, which should additionally be negotiated multiple times at different speed. Furthermore, no algorithm has been developed to detect gait events specifically during stair ascent and descent with foot-worn IMUs.

The purpose of this thesis is therefore to develop an accurate gait event detection algorithm for stair ambulation and compare its performance with existing gait event detection algorithms from literature.

For this matter, threshold- and peak-based algorithms were chosen in this thesis, as they are likely more suitable for pathological gait with higher stride-to-stride variability [Bob18]. This will possibly be useful to enhance the probability of a successful application of the algorithm to the *FallRiskPD* dataset (an ongoing long-term home monitoring study with PD patients of the Machine Learning and Data Analytics Lab (Friedrich-Alexander-Universität Erlangen-Nürnberg) and the University Hospital Erlangen) or other real-world studies.

The question to be addressed is: Is it possible to reliably detect initial and terminal contact during stair ascent and descent under realistic conditions with foot-worn IMUs?

In order to answer this question, first a fitting dataset from various real-life stair ambulation scenarios had to be acquired. This process is described in Chapter 3. Subsequently, three different gait event detection algorithms were applied to the obtained dataset and their performance was evaluated with respect to the different *stride types* and paces.

Chapter 2

Fundamentals

In the following chapter, the basics of human gait will be discussed with a particular focus on stair ambulation (Section 2.1), followed by an overview of the function and application of IMUs and the used coordinate frames (Section 2.2). At the end of the chapter, a brief introduction to the Force Sensing Resistors used as a reference system is given (Section 2.3).

2.1 Human Gait

2.1.1 Human Gait Cycle and Gait Metrics

A stride consists of a distinct sequence of gait events and gait phases, which together form the gait cycle depicted in Figure 2.1. One gait cycle or stride is defined as the events and phases between one gait event and its consecutive repetition with the same limb. It is common to choose the initial contact (IC) of one foot with the ground as the start and end point of the gait cycle [Whi07].

This IC or heel strike is followed by a *stance phase* in which the foot is flat on the ground (foot flat) and carries the full body weight. The foot is then gradually extended, first lifting the heel off the ground (HO) and finally pushing off with the toes. This event is called foot off, toe off, or terminal contact (TC) and is the initiation of the *swing phase*, which in turn ends with another IC, completing the gait cycle. In healthy gait, the *swing phase* constitutes approximately 40% of the gait cycle and the *stance phase* constitutes the remaining 60% [Whi07]. The *double support phases* during which both feet have contact with the ground each last for about 10% to 12% of the gait cycle [Pir16].

To evaluate gait, different gait parameters are calculated and examined. Some of the commonly used gait parameters are defined in Table 2.1. On the basis of these parameters, it is possible

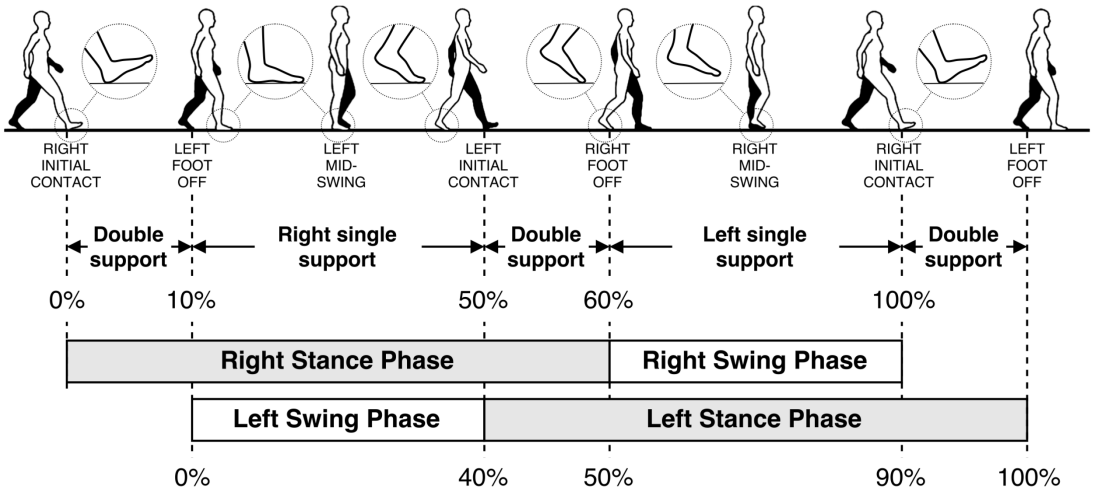

Figure 2.1: **The human gait cycle.** The basic gait events are indicated in the first line. Below that, the different gait phases are shown [Tun17]. The foot off event is also referred to as terminal contact.

to make meaningful statements about a person's health. For instance the increased variance of spatio-temporal gait parameters is distinctive for PD patients [Din17, Kel19]. Additionally, the PD typical *Freezing of Gait* events that often lead to falls are related to an increased *double support time* and typical asymmetries in gait can be read from asymmetrical *swing* to *stance time* ratios [Sta11]. Other parameters such as foot angles at IC and TC might also be interesting to better classify motor impairments in PD [Ngu19]. All these gait parameters depend on correctly detected ICs and TCs.

2.1.2 Stair Ambulation

The movement pattern on stairs is inherently different from walking on level ground. Nevertheless, IC and TC as well as *swing* and *stance phase* can still be identified.

During stair ascent, the *stance phase* is initiated by the weight acceptance with the middle to front portion of the foot [McF88] as seen in the centre picture of Figure 2.2a. Due to the strong knee flexion necessary to lift the body up to the next step, extensive dorsal flexion would be required for a heel strike. Consequentially, the contact happens at the forefoot to allow the ankle to be in a natural angular range [Rie02]. This IC is followed by the pull-up of the body weight and further forward motion until the body weight is fully shifted onto the ipsilateral leg. The TC (Figure 2.2b) then initiates the *swing phase*, which is dominated by the foot clearance motion with

Table 2.1: Common gait parameters that depend on IC and/or TC.[Tun17, Din17, Kan15]

Parameter	Definition
Stride time	Duration of one gait cycle (e.g., from IC to IC).
Stance time	Duration of stance phase, starting with IC and ending with TC of the same foot.
Swing time	Duration of swing phase, starting with TC and ending with IC of the same foot.
Single support time	Duration of the phase during which only one foot touches the ground.
Double support time	Duration of the phases during which both feet touch the ground.
Cadence	Number of steps taken per minute.
Toe-off angle	The angle between the foot and the ground during the TC event.
Heel strike angle	The angle between the foot and the ground during the IC event.

(a) Initial contact. (b) Terminal contact.

Figure 2.2: **Gait events for different stride types.** F. l. t. r.: Level walking, stair ascent, stair descent.

dorsiflexion of the foot and a flexed knee to pull back the leg [McF88]. At the end of the *swing phase* the foot is placed on the next step and a new gait cycle begins.

During stair descent, the *stance phase* also starts with the weight acceptance by the forefoot (Figure 2.2a). This helps to distribute the necessary energy absorption to the ankle as well as to the knee joint, with most of the energy absorbed by the plantar flexors and the knee muscles providing the control [Rie02, McF88]. Other than during stair ascent, the bodyweight is now first moved forward and then vertically. The controlled lowering with the major absorption at the knee ends as soon as the ipsilateral leg is sufficiently placed on the next step. Throughout the lowering phase, the plantar flexors stay active until the TC (Figure 2.2b), to relieve the extremely dorsiflexed position and to help push the swing leg through [McF88]. In the course of the following *swing phase* the leg is first pulled through and at the end the foot is placed on the next step, all while largely maintaining the plantar-flexed position.

2.2 Inertial Measurement Units

Inertial sensors are sensors that measure acceleration or angular velocity. Accelerometers and gyroscopes combined form an Inertial Measurement Unit (IMU). If accelerometers and gyroscopes are provided for three orthogonal directions, this IMU is able to accurately record every motion in the three-dimensional space. Since the realization as micro-electro-mechanical systems (MEMS), inertial sensors have become increasingly low-cost, light-weight, and precise, and are now used in various applications to track orientation and movements [Ben15]. As such, they are commonly used for unobtrusive gait analysis [Cal17, Jar18].

2.2.1 Accelerometer

Most accelerometers follow the same construction basics. A seismic mass is elastically mounted to a fixed point [Woo07]. The force needed to displace this mass by the length Δl is proportional to the stiffness of the mount (e.g., the spring constant k in case of a spring suspension) according to Hook's law:

$$F_s = k \cdot \Delta l \tag{2.1}$$

The acceleration can then be calculated from the mass and the determined force using Newton's law:

$$F = m \cdot a \tag{2.2}$$

In case of an piezoresistive MEMS implementation, the mass is attached to a thin cantilever beam, that is fixed on the other side (Figure 2.3). During acceleration, the inertial force on the mass causes the beam to bend and thus changes the resistance of the piezoresistor in the beam [Bao05]. This resistance is therefore proportional to the acceleration.

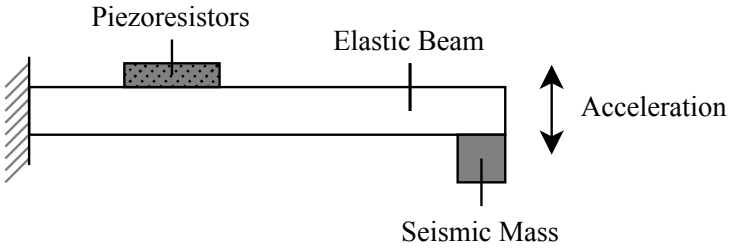

Figure 2.3: **Simplified model of a piezoresistive based MEMS accelerometer.** Adapted from [Alb09]

Additionally to dynamic accelerations, accelerometers also measure the static gravitational acceleration, which can then be used to determine the accelerometers orientation relative to gravity [Bro19]. The measured dynamic acceleration can further be integrated to calculate velocity and displacements.

2.2.2 Gyroscope

Most gyroscopes used today are MEMS rate-gyroscopes, that measure the angular velocity. The angular displacement then has to be obtained via signal integration. All micro-mechanical gyroscopes are vibratory gyroscopes [Bao05]. A simplified model of this type is shown in Figure 2.4. The gyroscope shown has two perpendicular vibration axes x and y. For operation, the mass is driven into vibration along the x-axis with a driving frequency f_d. The gyroscope then makes use of the Coriolis force (Equation 2.3). A mass m moving at a velocity $\boldsymbol{v}$ within a reference frame with angular velocity $\boldsymbol{w}$ experiences the Coriolis force $\boldsymbol{F}_c$.

$$\boldsymbol{F}_c = -2m(\boldsymbol{\omega} \times \boldsymbol{v}) \tag{2.3}$$

If, as in the case of the shown gyroscope, the angular velocity is orthogonal to the drive axis x, the velocity v_d from the driving vibration induces the Coriolis force F_c along the y-axis. The magnitude of this force is also alternating in the driving frequency f_d. The described force generates a measurable vibration in y-direction with an amplitude proportional to the angular velocity [Bao05, Woo07].

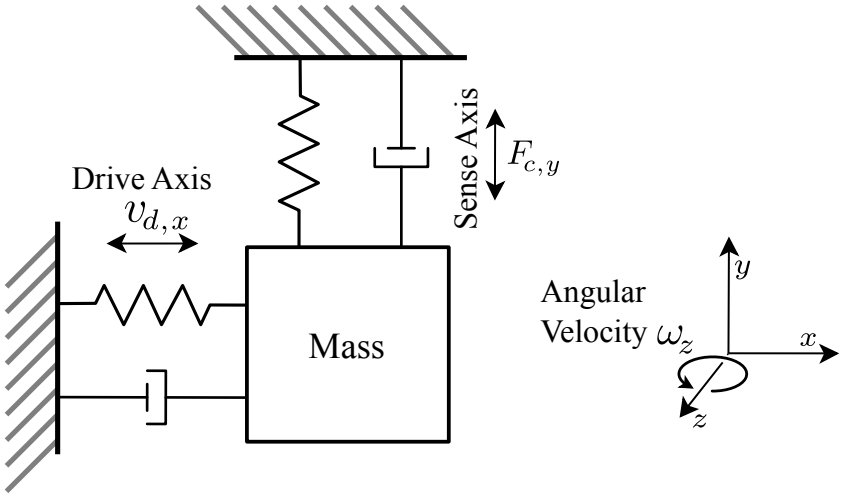

Figure 2.4: **Simplified model of a vibratory gyroscope.** Adapted from [Bao05, Woo07].

Most gyroscopes in use are implemented as 3D systems, that measure angular velocities along three orthogonal axes [Bro19]. Although MEMS devices are far less accurate than optical devices, they are more commonly used due to their light-weight and low-power implementation with shorter start-up times [Woo07].

2.2.3 Coordinate Frames

When working with IMUs it is important to choose a suitable coordinate frame for the specific application.

The sensor's output describes everything from the sensor's perspective. Thus, as the sensor is moved, its coordinate system moves along. Since the sensor is attached to the foot, this coordinate frame is called *Foot Sensor Frame* (FSF). As depicted in Figure 2.5a, this coordinate system is right-handed. It is the same for both feet with the y-axis pointing to the left. The gyroscopes' positive direction is also defined according to the right-hand rule. The signals in the FSF can be used for physical calculations, although it may be useful to first rotate them to fully align the z-axis with the gravity vector to make the calculations more comparable regardless of the exact sensor orientation. For applications that characterize or analyse human motion it can be useful to follow the anatomical direction nomenclature to better understand the interrelations between different sensors attached to the same body regardless of their actual sensor orientation. With sensors centrally attached to the body, e.g., to the lower back or chest, the transformation from x, y, and z coordinates to posterior-anterior, right-left, and superior-inferior, respectively can be achieved by a simple rotation. If, however, the IMUs are attached to opposite-sided extremities, a mirroring along the sagittal plane is necessary to achieve the same signal output regardless of by which extremity it is performed. For the application at the feet the resulting *Foot Body Frame* (FBF) is illustrated in Figure 2.5b. Its axes correspond to the posterior-anterior (pa), medio-lateral (ml), and superior-inferior (si) directions of the body. Due to the mirroring, the coordinate system looses its right-handedness and can therefore no longer be used for any sort of physical calculation, that involves more than one axis. The FBF follows the convention of directions defined by Wu et al. [Wu02].

In order to describe the IMU's movements relative to a global reference frame, a different coordinate frame is needed. This *World Frame* requires continuous orientation estimation and will not be utilized within this thesis.

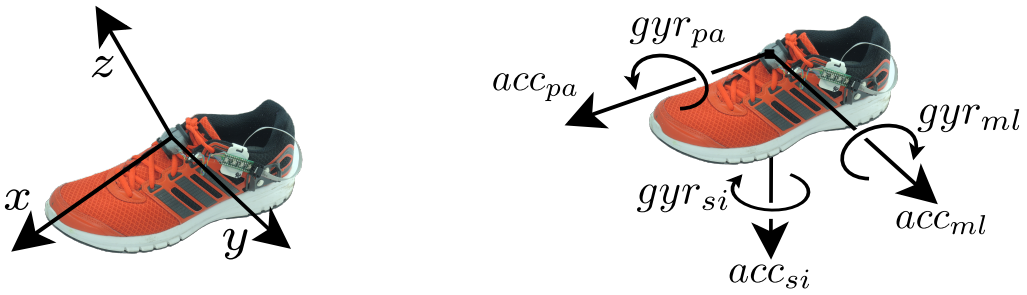

(a) Foot Sensor Frame.

(b) Foot Body Frame.

Figure 2.5: **Foot coordinate systems.** Within the FSF (a) the right foot has exactly the same coordinate system as the left foot with the y-axis to the left. The gyroscope nomenclature follows the right-hand-rule. The FBF (b) for the right foot, however, is mirrored in the sagittal plane.

2.3 Force Sensing Resistors

A Force Sensing Resistor (FSR) is a sensor whose resistance decreases when loaded [Smi02]. This resistance R_{FSR} can be measured through current when applying a voltage. The current through R_{FSR} induces the output voltage along a reference resistance R_{ref}. Because of the usually non-linear behaviour of FSRs regarding the applied voltage, a circuit with an operational amplifier is used to measure R_{FSR} (Figure 2.6). This way, the voltage V_{ref} applied to the FSR is constant. However, due to FSR manufacturing difficulties, a slightly non-linear relationship remains between the output voltage and the applied force or weight. This sensor response is different for every individual sensor. Consequentially the resistance-weight response of every sensor used has to be measured in advance, so that the recorded V_{out} values can be mapped to the corresponding linear weight values.

Most FSRs come in the shape of a thin conductive polymer layer sensor, that can easily be integrated into insoles. In addition, they are low-cost, easy to interface, and have a fast dynamic response [Hau95]. Consequentially, they have been used in gait analysis for many years now, often as reference system to determine the accuracy of accelerometer- and gyroscope-based gait event detection systems [Rue10].

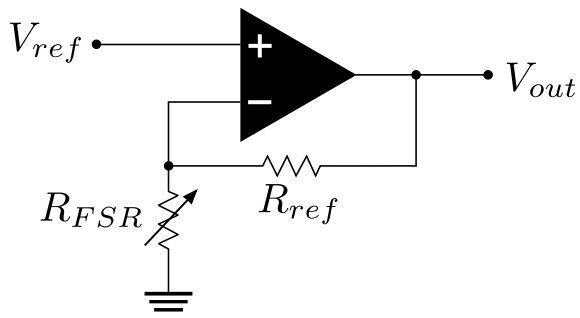

Figure 2.6: Signal conditioning circuit for Force Sensing Resistor.

Chapter 3

Data Acquisition

This chapter describes the various stages of the data acquisition process and its outcome. First, the contents of study protocol are outlined (Section 3.1). Section 3.2 then gives an overview of the sensors and other data generation methods used. Finally, the participants and the obtained dataset are characterized (Section 3.3).

3.1 Study Design

The aim of this thesis was to develop robust gait event detection algorithms for real-world stair ambulation. To do so first of all data is needed of various different realistic stair ambulation scenarios. No such data was available, thus a study had to be conducted to gather the necessary data.

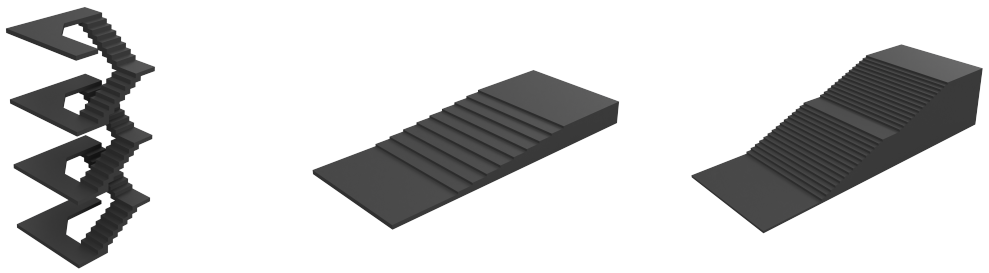

(a) Staircase. (b) Flat stair. (c) Long stair.

Figure 3.1: The stairs selected for the study.

Table 3.1: **Stair characteristics.** Definition of stair features by Startzell et al. [Sta00].

	Number of Steps	Rise [cm]	Run [cm]	Stair Angle	Figure
Staircase	48 (pairs of 8)	17.5	27.0	33.9°	3.1a
Flat Stair	9	13.0	96.5	7.7°	3.1b
Long Stair	29 (15 and 14)	14.5	34.5	22.8°	3.1c

Three stairs outside of the *Universitätsklinikum Erlangen* (Germany) with different inclinations were chosen as a location for the study. These stairs are pictured in Figure 3.1 and their individual characteristics are listed in Table 3.1.

Each stair was ascended and descended four times by every subject: Twice in their preferred walking speed, once at a fast walking pace, and once at a slow pace. The first test at preferred speed was performed with continuous walking on level ground before, after and in between the ascent and descent. During the three other tests per stair the subject started and stopped a few steps before and after each stair ascent or descent, respectively, to always include the transition from level walking to stair ambulation.

In addition, special walking strategies were recorded on the long stair at the end of the study. Each subject once performed the stair ascent and descent placing both feet on each step before a foot is advanced to the next step (*single step* strategy). Afterward they were asked to only take every second step (*double step* strategy). Furthermore, each subject also once walked up and down a 35 m ramp with a 1.9° angle. The full study protocol is listed in Appendix B.2.

3.2 Measurement System

3.2.1 Sensor Setup

Three *NilsPod* (Portabiles GmbH, Erlangen, Germany) inertial sensor units were attached to the instep of the shoe (Figure 3.2) and to the lower back, respectively (Figure 3.3). Each *NilsPod* contains a *BMI160* (Bosch Sensortec GmbH, Reutlingen, Germany) 16-bit IMU with a 3D accelerometer (range $\pm 16\,\mathrm{g}$) and a 3D gyroscope (range $\pm 2000\,^\circ/\mathrm{s}$), and a *BMP280* (Bosch Sensortec GmbH, Reutlingen, Germany) barometer, and is supplied with storage and a battery. All three IMUs were wirelessly synchronized and recorded data with a sampling rate of $204.8\,\mathrm{Hz}$.

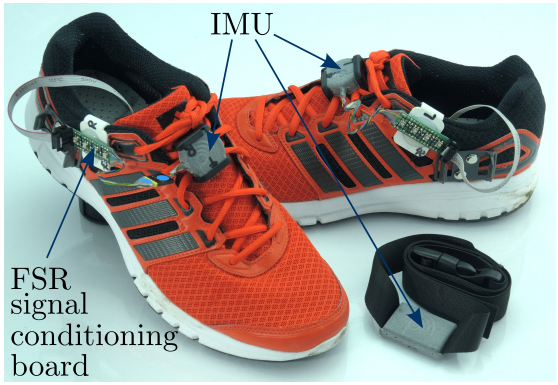

Figure 3.2: IMU sensors attached to the shoes and hip belt.

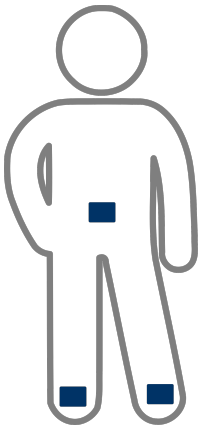

Figure 3.3: IMU placement at instep and lower back.

3.2.2 Ground Truth

The reference values for the evaluation of the gait event detection algorithms were mainly obtained by pressure sensor insoles (Figure 3.4). The data of the insoles was directly recorded by the sensor units and was therefore already synchronized with the respective inertial data streams. Three *RP-S40-ST* (Shenzhen Film Sensor Technology Co., Ltd., Shenzhen, P.R. China) 40 mm × 40 mm thin film FSRs were placed at the anatomical landmarks toes, metatarsal head and heel, respectively (Figure 3.5). These locations were chosen, as they supply sufficient information on IC and TC timing for healthy gait [Kon08, Gon15]. The exact locations are marked as squares on the insole in Figure 3.4. Additionally, the subject's feet were filmed during the study.

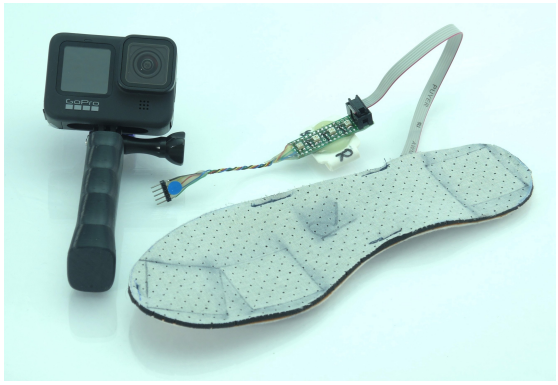

Figure 3.4: Reference system with camera and FSR insole.

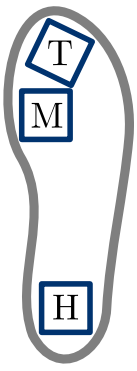

Figure 3.5: FSR placement at heel (H), metatarsal head (M), and toes (T).

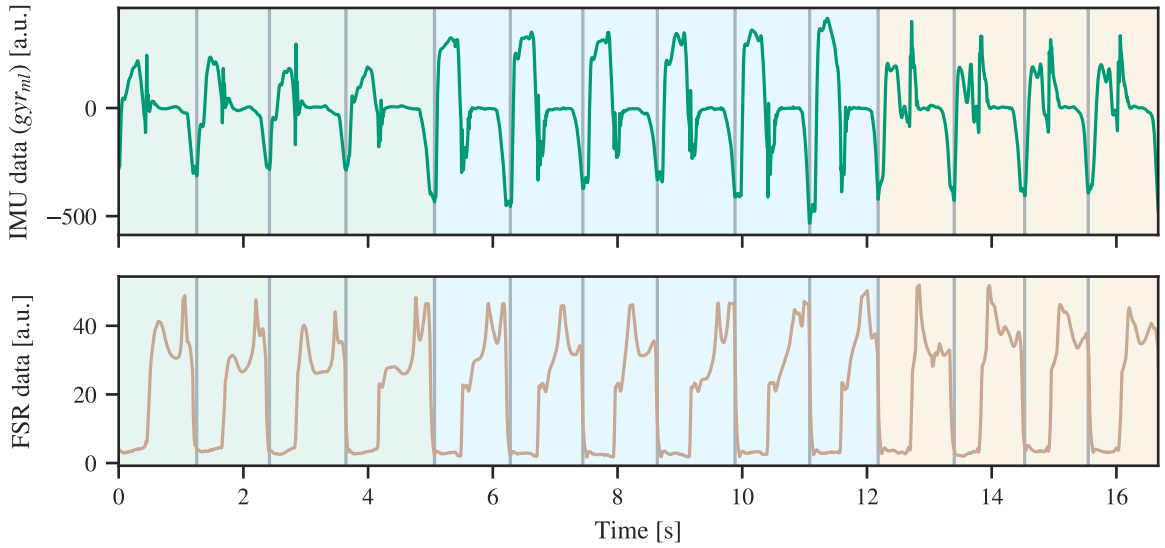

Figure 3.6: **Sensor data with manual labels.** Stair ascent in green, level walking in blue, and stair descent in yellow. The annotated stride borders are shown as grey vertical lines.

Manual Labels

The obtained sensor data was manually annotated after the recording with the help of the video material. Annotations included:

- Stride borders at the minima of the gyr_{ml} signal (pre-annotated with an HMM-algorithm, checks and corrects by hand)
- The current test scenario (which stair, pace, direction, ...)
- The total displacement in vertical direction (e.g., the height of one stair step)
- The stride type (level walking, ascending, ...)

3.3 Dataset

3.3.1 Participants

Twenty healthy subjects participated in the study. The average subject characteristics are listed in Table 3.2. All wore the same pair of running shoes shown in Figure 3.2 either in size 42 or $39\frac{1}{3}$.

Table 3.2: Subject characteristics.

Number of Subjects	20
Age [years] ± SD	27.2 ± 11.3
Height [cm] ± SD	173.4 ± 7.1
Weight [kg] ± SD	68.1 ± 8.6
Sex (m/f)	10 / 10

3.3.2 Recorded Data

In total, the recorded dataset contains 32 365 annotated strides, 31 268 of which are valid. Strides are considered valid in this context, if every ground truth parameter has an anatomically and logically reasonable value. The exact criteria in which cases a stride is considered unrealistic, and thus removed from the ground truth is described in Section 4.6.1. Most strides that have been annotated, but are not considered valid, are strides directly before or after a longer period of standing which are therefore somehow abnormal. Additionally, there are 1097 strides in the dataset, that are actually valid, but do not have an associated *stance time*, because there was no TC available for the next stride. These strides and the invalid strides are not included in Table 3.3.

Most of the strides are at preferred speed. Also, there are substantially more descending strides than ascending strides at preferred speed. This is partially due to the test protocol that requires one additional stair descent on the flat staircase at preferred walking speed to access the long stair.

Table 3.3: **Number of strides in the dataset.** The pace is the given pace for the respective test case. For this reason there are entries for *single* and *double step* during level walking. The strides for ramp ascent and descent are not specifically listed, but they are included in the number of total strides at the bottom.

Pace	Level	Ascending	Descending
Preferred	8655	3856	4239
Fast	851	1753	1860
Slow	1025	1949	1983
Single Step	216	1132	1132
Double Step	127	315	320
Total per Type:	10 874	9005	9534
Total:			31 268

Chapter 4

Methods

The following chapter will present an overview of all the event detection methods that have been applied to the dataset at hand during the course of this thesis. At first, the extraction of the reference values for the ICs and TCs from the FSR data will be described (Section 4.1). Afterwards, the three event detection algorithms to be compared in this thesis will be introduced, starting with two published algorithms: the *RamppEventDetection* algorithm (Section 4.3) as described by Rampp et al. [Ram15] and the *FigueiredoEventDetection* algorithm (Section 4.4) as described by Figueiredo et al. [Fig18]. At last, the advantages and learnings from these two algorithms were combined into the *ComboEventDetection*, which is outlined in Section 4.5. These three algorithms were evaluated as described at the end of this chapter.

4.1 Processing Pressure Sensor Data

4.1.1 Linearization and Scaling

Before conducting the study, the sensor properties of each individual FSR were measured, because they had highly variant sensor responses. A load cell was used to measure the FSR resistance response R_{FSR} to different weights between 0.5 kg and 20 kg, since the signal saturates at over 20 kg. Additionally, the individual reference resistance R_{ref} was calculated from the observed maximum output voltage $V_{out,max}$ and the FSR resistance at 20 kg $R_{FSR@20kg}$ (Equation 4.1). The reference voltage V_{ref} was set to 0.1 V and the maximum possible output voltage was 2.4 V. These measurements were then stored for the linearisation and voltage to weight conversion of the recorded FSR data.

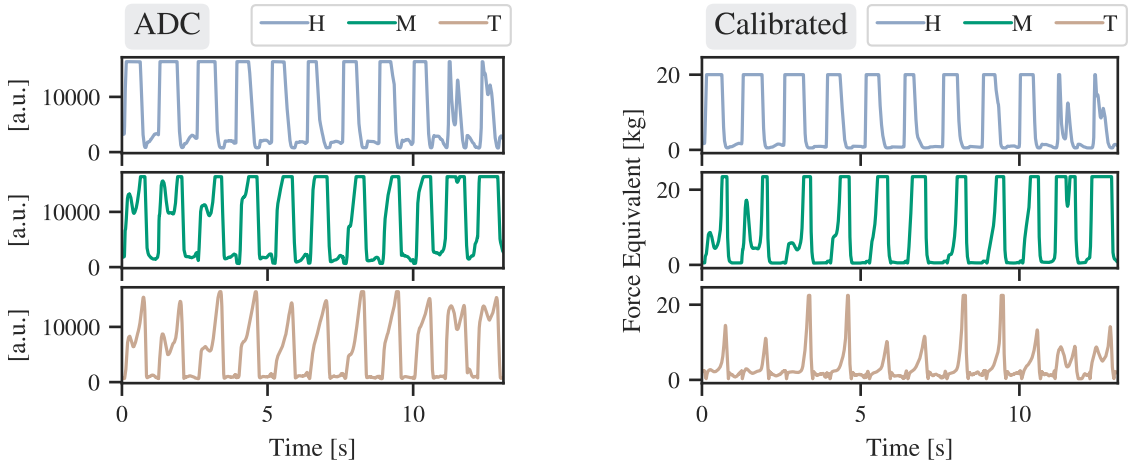

(a) (b)

Figure 4.1: **Calibration of FSR signals.** The data from FSRs at heel (H), metatarsal head (M), and toes (T) in Analog to Digital Converter (ADC) format *(a)* and after linearization and mapping to the corresponding weight values *(b)*.

$$R_{ref} = R_{FSR@20kg} \cdot \left(\left(\frac{V_{out,max}}{V_{ref}} \right) - 1 \right) \tag{4.1}$$

After the study was conducted, the FSR data first had to be converted from the 14-bit Analog to Digital Converter format (Figure 4.1a) to the corresponding voltage value ranging from $0\,\mathrm{V}$ to $2.4\,\mathrm{V}$.

Based on the previously recorded FSR response data an individual conversion function was created for each sensor used. In order to do that, the weight-resistance value pairs stored were first sorted into $0.5\,\mathrm{kg}$ bins ranging from $0.5\,\mathrm{kg}$ to $20\,\mathrm{kg}$ and for each bin the average resistance was calculated. The corresponding output voltages V_{out} were then obtained by simulating a non-inverting operational amplifier (Equation 4.2 and Figure 2.6). This resulted in weight-voltage value pairs for every $0.5\,\mathrm{kg}$ bin. Finally, a 6th order polynomial was fit to these value pairs to achieve a continuous conversion function. The resulting conversion function was applied to the corresponding FSR's data recordings to map the recorded voltages to their weight equivalents (Figure 4.1b).

$$V_{out} = V_{ref} \cdot \left(1 + \left(\frac{R_{ref}}{R_{FSR}} \right) \right) \tag{4.2}$$

The signals obtained this way for each of the three FSRs per foot were then added together to get a total force signal $force_{total}$, since for the purposes of this thesis it did not matter which part of the foot had contact with the ground. Only this sum signal was used for the following detection of the ground truth events.

4.1.2 Edge Detection

After the preprocessing, the pressure signal ideally resembles a square wave signal, that accurately differentiates between only two states: Either the foot does have contact with the floor, or it does not. The IC and TC are defined as the point in time where the foot starts, or stops respectively, to have contact with the ground. Therefore, within an almost ideal signal, the IC is located at the starting point of the rising edge and the TC occurs at the end of the falling edge.

The real pressure signal, however, is not ideal (see Figure 4.2): Its baseline during the swing phase is often not linear due to some pressure applied by foot movements within the shoe. Also, there tends to occur a dip in the middle of the stance phase, because the pressure sensors cover the midfoot area to a lower degree. These irregularities had to be considered during the event detection.

The event detection takes the calibrated data and the segmented stride list as an input. First, the pressure signal is divided into individual strides according to the given stride list. The actual events are then detected on each of these short sequences. The event detection was roughly based on the approach by Hausdorff et al. [Hau95].

Initial Contact Detection

A first rough estimate for the IC was found by applying a threshold at 20% of the subjects body weight. This threshold should not be above the cutoff value of one sensor, but also should be high enough that the noisy baseline stays below.

Starting from this rough estimate the signal is searched backward until the slope of the signal is below 10% of the steepest slope. This derivative is calculated on a smoothed signal to avoid getting stuck in local minima. The smoothed signal was calculated using a centered moving average with a sample window size $n = 11$, which corresponds to roughly 54 ms (Equation 4.3). However, due to the smoothing, rising edges start half the window size earlier than in the original signal. Consequentially, half the window size (here $\lfloor n/2 \rfloor = 5$) was added as a time offset to the

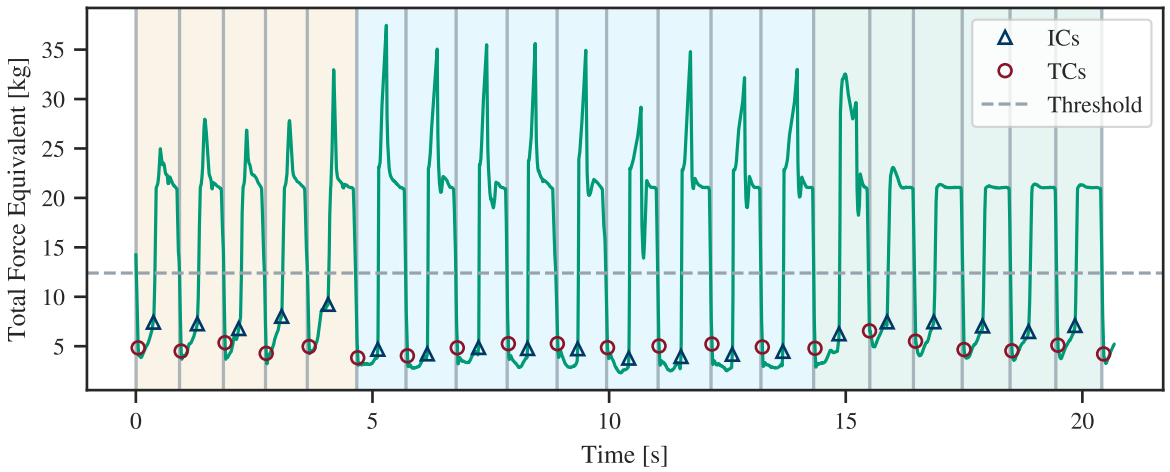

Figure 4.2: **Event detection on the pressure sensor data.** This figure shows a typical pressure signal after the preprocessing with its associated stride borders and detected events. The threshold is set at 20% body weight and the background colors indicate the different *stride types* (f.l.t.r. stair descent in yellow, level walking in blue, stair ascent in green). The baseline during the *swing time* is especially distorted during stair descent and ascent. Also note the cutoff at around $20\,\mathrm{kg}$ during the stair ascent *stance phases*. This cutoff indicates that only one sensor was activated , e.g., because the subject stands on only the ball of the foot during stair ascent.

detected IC to compensate the filter delay.

$$force_{smooth}[t] = \frac{1}{n} \sum_{i=t-\lfloor \frac{n}{2} \rfloor}^{t+\lfloor \frac{n}{2} \rfloor} force_{total}[i] \tag{4.3}$$

Terminal Contact Detection

The TC is located somewhere around the labeled start of the stride, sometimes it even occurs slightly before the *start* label outside of the stride borders. Because of that, the TC detection does not take place on the signal within the stride borders, but rather on the sequence a quarter of the stride time before and after the *start* label. Since this label is already a good estimation, the search starts there. The further search direction is then dependent on whether the value at the *start* label is above or below the threshold.

After that, the more accurate TC is obtained similar to the second part of the IC detection, except the derivative of the smoothed signal is now searched *forward* until the 10% mark is reached. An offset of half the smoothing window size is then *subtracted* from the detected TC,

because due to the smoothing of the signal, rising edges end half the smoothing window size later than in the original signal.

4.2 IMU Data Preprocessing

The accelerometer and gyroscope data was calibrated according to Ferraris et al. [Fer95].

The signals of each sensor in FSF were subsequently transformed so that a z-axis parallel to gravity is obtained. These aligned signals were finally rotated to the symmetrical *Foot Body Frame* (Eq. 4.4 and Eq. 4.5), to make a side-independent gait event detection possible.

$$\text{Left Sensor: } \begin{pmatrix} acc_{pa} \\ acc_{ml} \\ acc_{si} \end{pmatrix} = \begin{pmatrix} acc_{x} \\ acc_{y} \\ -acc_{z} \end{pmatrix}, \begin{pmatrix} gyr_{pa} \\ gyr_{ml} \\ gyr_{si} \end{pmatrix} = \begin{pmatrix} -gyr_{x} \\ -gyr_{y} \\ -gyr_{z} \end{pmatrix} \tag{4.4}$$

$$\text{Right Sensor: } \begin{pmatrix} acc_{pa} \\ acc_{ml} \\ acc_{si} \end{pmatrix} = \begin{pmatrix} acc_{x} \\ -acc_{y} \\ -acc_{z} \end{pmatrix}, \begin{pmatrix} gyr_{pa} \\ gyr_{ml} \\ gyr_{si} \end{pmatrix} = \begin{pmatrix} gyr_{x} \\ -gyr_{y} \\ gyr_{z} \end{pmatrix} \tag{4.5}$$

For the *RamppEventDetection* and the *FigueiredoEventDetection* the acc_{pa} signal was afterwards negated to make the algorithm described by Rampp et al. [Ram15] more easily applicable.

4.3 Rampp Event Detection

The *RamppEventDetection* (RED) algorithm operates on the stride level. This means that the input data in *Foot Body Frame* format was segmented into single stride sequences according to the given *stride borders*. The event detection was then performed on these sequences one at a time. The results and the mechanism of the algorithm are illustrated in Figure 4.3.

4.3.1 Terminal Contact Detection

The TC was detected at the first zero crossing of the gyr_{ml} signal within the labeled stride. The resulting TCs in comparison to their respective reference values are shown in Figure 4.3 in the gyr_{ml} signal for different *stride types*.

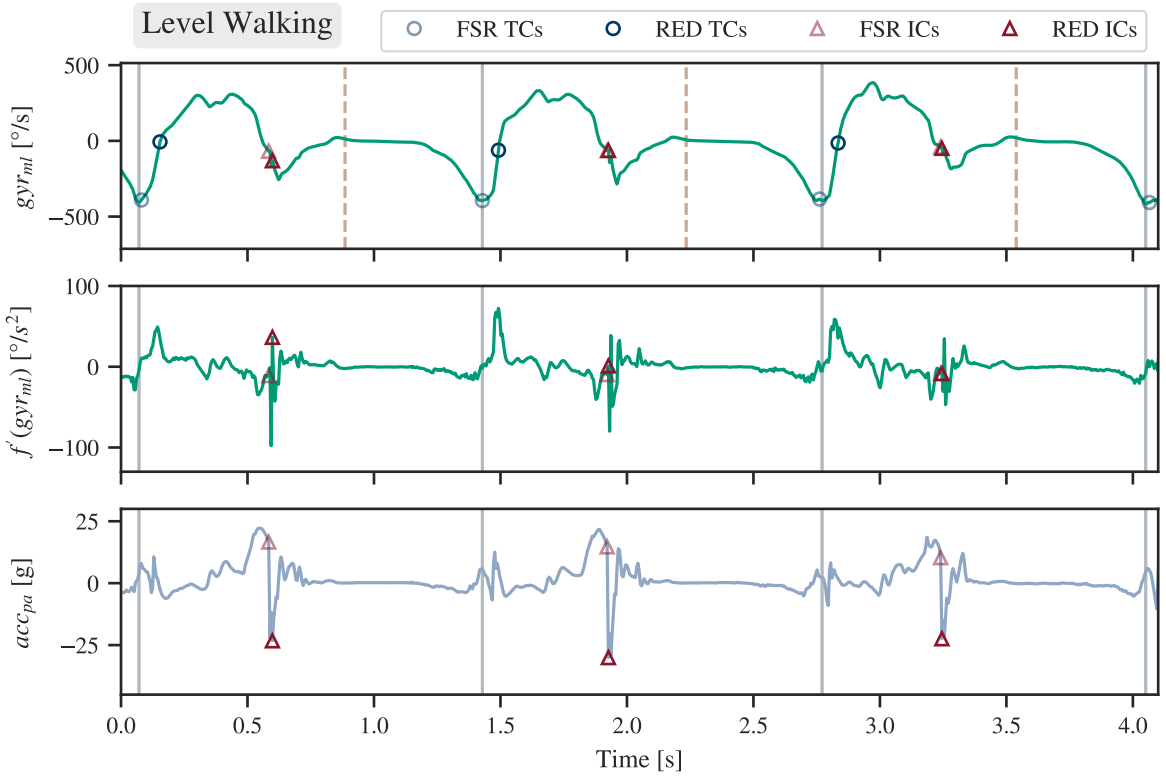
Level Walking
FSR TCs
RED TCs
FSR ICs
RED ICs
gyr_{ml} [°/s]
$f'(gyr_{ml})$ [°/s^2]
acc_{pa} [g]
Time [s]

(a)

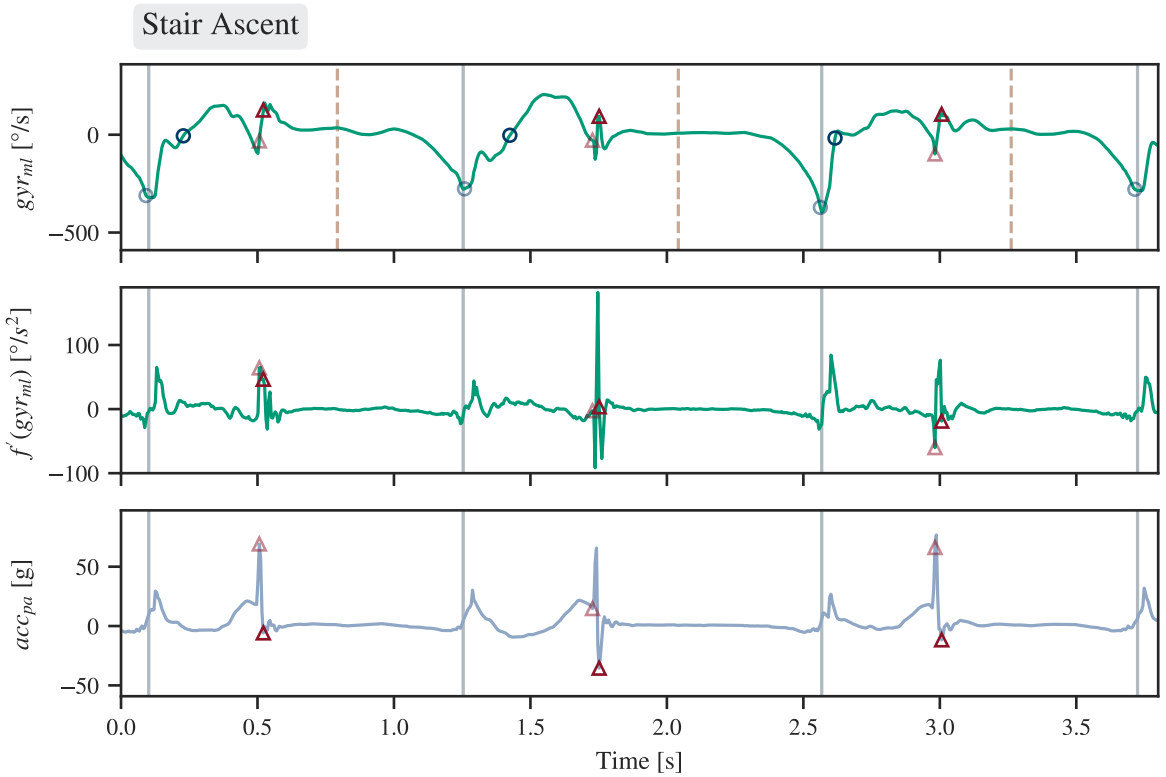
Stair Ascent
gyr_{ml} [°/s]
$f'(gyr_{ml})$ [°/s^2]
acc_{pa} [g]
Time [s]

(b)

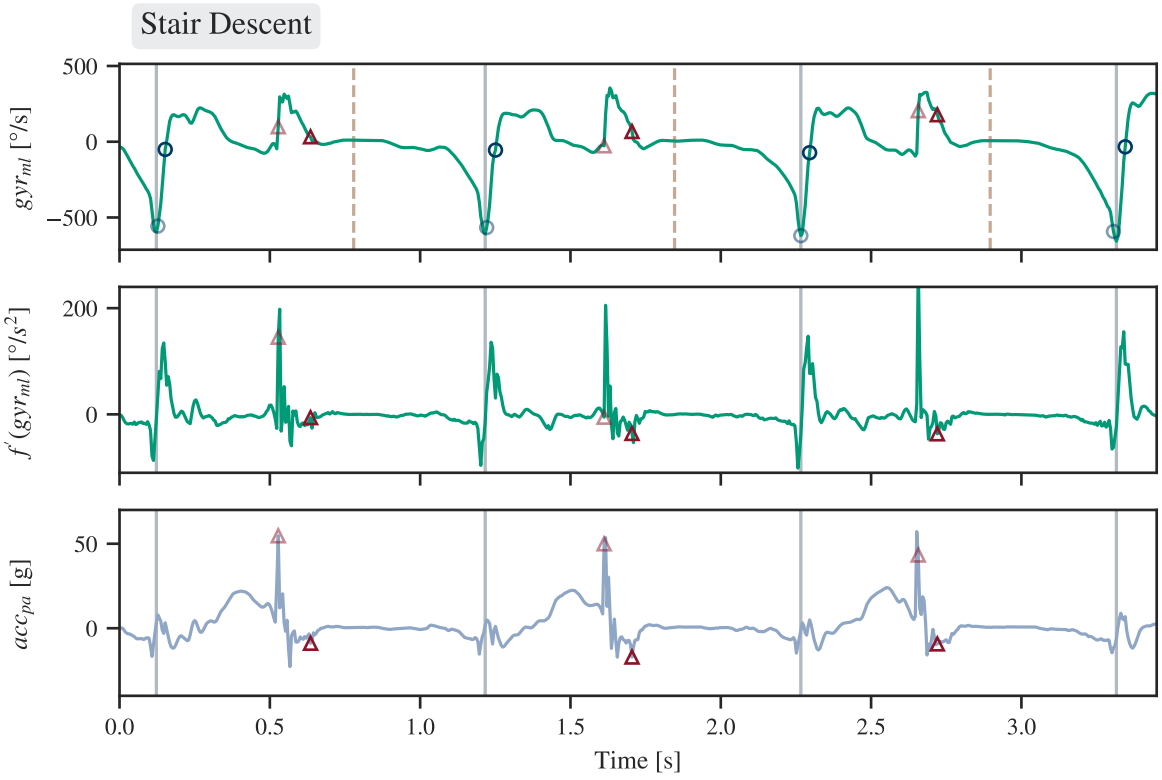

(c)

Figure 4.3: **RamppEventDetection behaviour for different stride types.** This figure shows the three signals that correspond to the three levels of the IC detection for the main *stride types*. The levels are depicted top to bottom starting with the gyr_{ml} signal. The first level search region end at 60% *stride time* is shown as a dashed line. The TCs are depicted at the first zero crossing of the gyr_{ml} signal where they are detected after the respective stride border (light grey lines).

4.3.2 Initial Contact Detection

The IC detection as described by Rampp et al. [Ram15] consists of three levels in which the search region is increasingly narrowed until the event can finally be detected. These levels are depicted from top to bottom for each *stride type* in Figure 4.3.

A first rough search area was defined to start at the gyr_{ml} maximum. This corresponds to the *mid swing* stage during level walking and stair ascent. As a slight deviation from the original paper, the endpoint of this search region was defined as 60% of the stride segments length instead of the original 50% to allow event detection on more variant strides.

This area is narrowed down further to be between the steepest negative slope and the steepest positive slope within the gyr_{ml} signal. These show as a negative and a positive peak respectively in the deviation of the gyr_{ml} signal ($f'(gyr_{ml})$).

The minimum of the gyr_{ml} signal within that area then served as a first IC candidate. This candidate was taken as the basis for the final search: The IC was detected at the minimum of the acc_{pa} signal within the region $80\,\mathrm{ms}$ before and $50\,\mathrm{ms}$ after the detected candidate. Again, the deviation from the originally stated $50\,\mathrm{ms}$ and $30\,\mathrm{ms}$ [Ram15] makes the event detection possible even with higher step variability.

4.4 Figueiredo Event Detection

The algorithm described by Figueiredo et al. [Fig18] was designed to perform gait event detection in real-time. That, however, was not the subject of this thesis. Consequentially, the described algorithm and procedures were adapted to a prerecorded dataset. The algorithm consists of a preprocessing step (section 4.4.1) and a Finite State Machine (FSM) responsible for the actual event detection (section 4.4.2).

4.4.1 Preprocessing

In accordance with Figueiredo et al. [Fig18] the gyr_{ml} signal was exponentially smoothed [Gar85] with a first order digital low-pass filter (Eq. 4.6). The derivative $deriv_{gyr}$ used in the finite state machine (FSM) decision rules (see Table 4.1) was then calculated as the derivative of this smoothed signal to suppress signal noise and avoid minor local extrema (Eq. 4.7).

$$gyr_{ml,smooth}[i] = k \cdot gyr_{ml}[i] + (1-k) \cdot gyr_{ml,smooth}[i-1] \tag{4.6}$$

$$deriv_{gyr} = f'(gyr_{ml,smooth}) \tag{4.7}$$

4.4.2 Finite State Machine

The FSM only takes the gyr_{ml} signal and its preprocessed derivative $deriv_{gyr}$ into account because Figueiredo et al. aimed to use as few sensors and signals as possible [Fig18]. For the purpose of this thesis, the FSM was also provided with the segmented stride list to get the approximate current *stride time*. This is a slight deviation from the original approach by Figueiredo et al. who had to take the *stride time* of the last detected stride instead because of their real-time solution. All signals used by the *FigueiredoEventDetection* (FED) algorithm and the eventually detected events can be seen in Figure 4.5.

The FSM consists of five states corresponding to different gait events (MAX, IC, FF, HO, TC), and additionally a default state (DEF), and a reset state (R) (see Fig. 4.4). This is another deviation from the original paper, which defines six states [Fig18]. Their *mid stance* state was left out, as it was defined to be in the approximate middle between the *foot flat* (FF) and the *heel-off* (HO) event. Consequentially, the *mid stance* state was not relevant for the correct functioning of the FSM. As additionally only IC and TC events were relevant to this thesis, the *mid stance* state could be omitted.

The state transition conditions are specified as decision rules in Table 4.1. A gait event is detected at the index i that first satisfies the corresponding state's decision rule. Each of the decision rules consists of several unique signal characteristics as well as a heuristically determined time range relative to the index of the last relevant maximum of the gyr_{ml} signal (MAX_{idx}, set in the MAX state). The error condition E applies, whenever the regular following decision rule could not be satisfied due to the current index i exceeding this defined time range. Additionally, if the FSM stays longer than five times the current *stride time* in one state (including the DEF state), or if no current stride time is available, the algorithm resets by restarting at the R state.

This R state is also the entry point of the FSM, where all parameters are set to their default values (defined in Table 4.2). In addition, since the segmented stride list was available, the current index i is set to the next labeled stride start to avoid unnecessary computation time for signal sequences without strides. The FSM then immediately transitions into the DEF state, and stays there until the condition R1 is satisfied.

In the following, all decision rules defined in Table 4.1 will be shortly described in the order of their occurrence. The time ranges will not be included in this description, they can, however, be found in the last row of every decision rule in said Table.

The transition into the MAX state takes place at the first local maximum of the gyr_{ml} signal with angular velocities above the MAX_{thr} (R1). The adaptive threshold MAX_{thr} defined as 60% of the mean of the last three maximum values is then updated with the current maximum's value

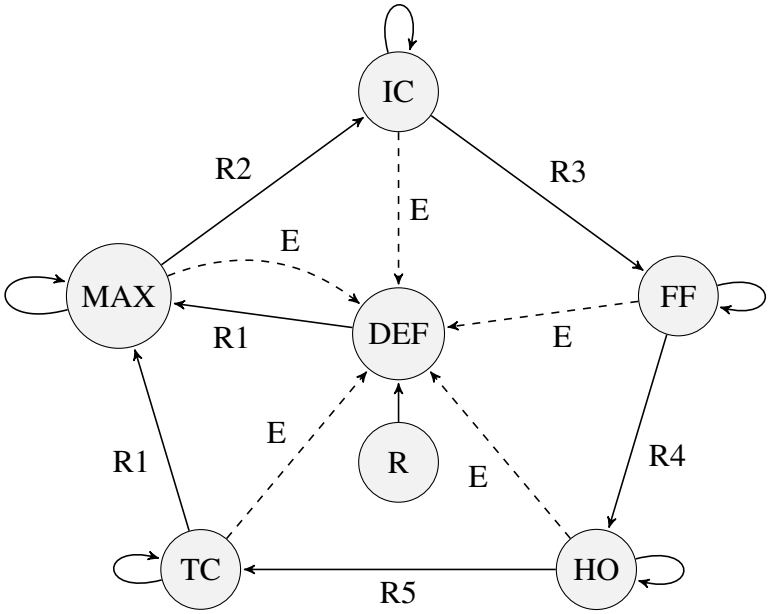

Figure 4.4: **Figueiredo Finite State Machine.** Adapted from Figueiredo et al. [Fig18].

	Decision Rule	State
R1	$(gyr_{ml}[i] > MAX_{thr})$ AND $(deriv_{gyr}[i] < 0)$ AND $(deriv_{gyr}[i-1] > 0)$ AND $(i - MAX_{index} \in [0.7 \cdot stride\_time; 1.3 \cdot stride\_time])$	MAX
R2	$(IC\_thr_{mean} - IC\_thr_{std} < gyr_{ml}[i] < IC\_thr_{mean} + IC\_thr_{std})$ OR $(is\_min$ AND $gyr_{ml}[i] < MAX_{thr})$ AND $(i - MAX_{index} \in [0; 0.4 \cdot stride\_time])$	IC
R3	$(\lvert deriv_{gyr}[i]\rvert \leq 0.2)$ AND $after\_1st\_gyro\_min$ AND $(i - MAX_{index} \in [0.15 \cdot stride\_time; stride\_time])$	FF
R4	$(gyr_{ml}[i] < 0)$ AND $(deriv_{gyr}[i] < 0)$ AND $(deriv_{gyr}[i-1] < 0)$ AND $(deriv_{gyr}[i] > 0.9 \cdot deriv_{gyr}[i-1])$ AND $(i - MAX_{index} \in [0.3 \cdot stride\_time; stride\_time])$	HO
R5	$(gyr_{ml}[i] < MIN_{thr})$ AND $(deriv_{gyr}[i] > 0)$ AND $(deriv_{gyr}[i-1] < 0)$ AND $(i - MAX_{index} \in [0.5 \cdot stride\_time; 1.1 \cdot stride\_time])$	TC

Table 4.1: **Adapted Figueiredo decision rules.** These decision rules adapted from Figueiredo et al. [Fig18] were applied in this thesis. The respective use cases are depicted in the state diagram in Figure 4.4.

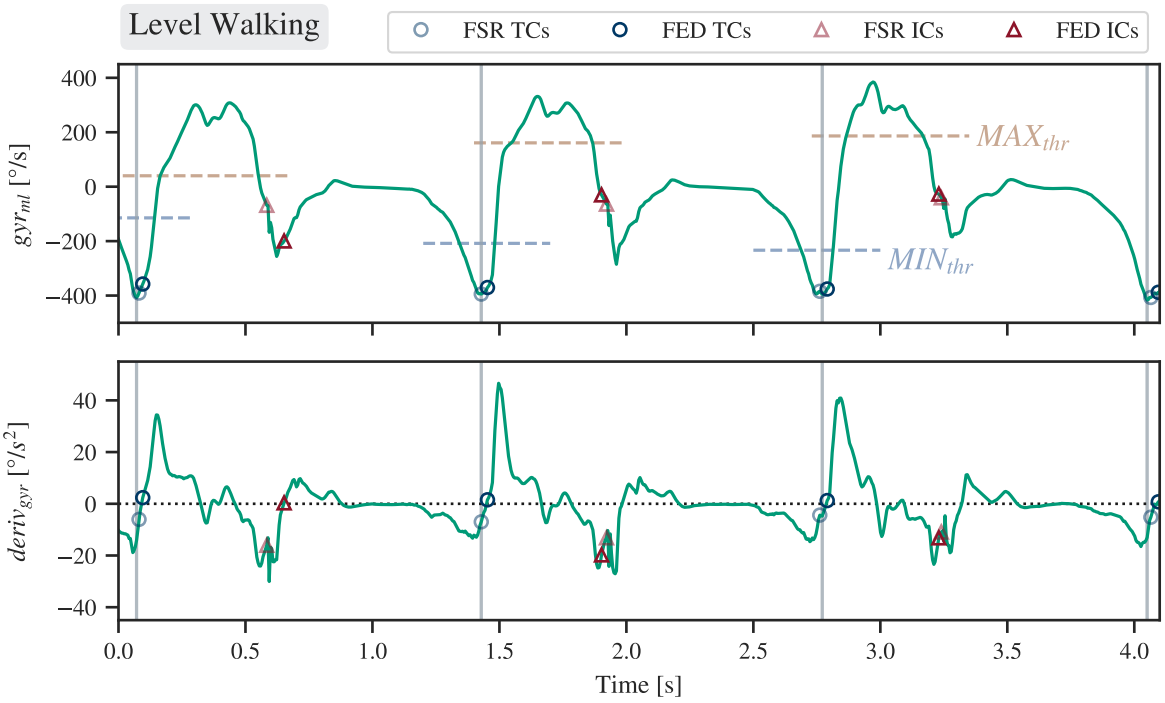
Level Walking
FSR TCs
FED TCs
FSR ICs
FED ICs
MAX_{thr}
MIN_{thr}
gyr_{ml} [°/s]
$deriv_{gyr}$ [°/s^2]
Time [s]

(a)

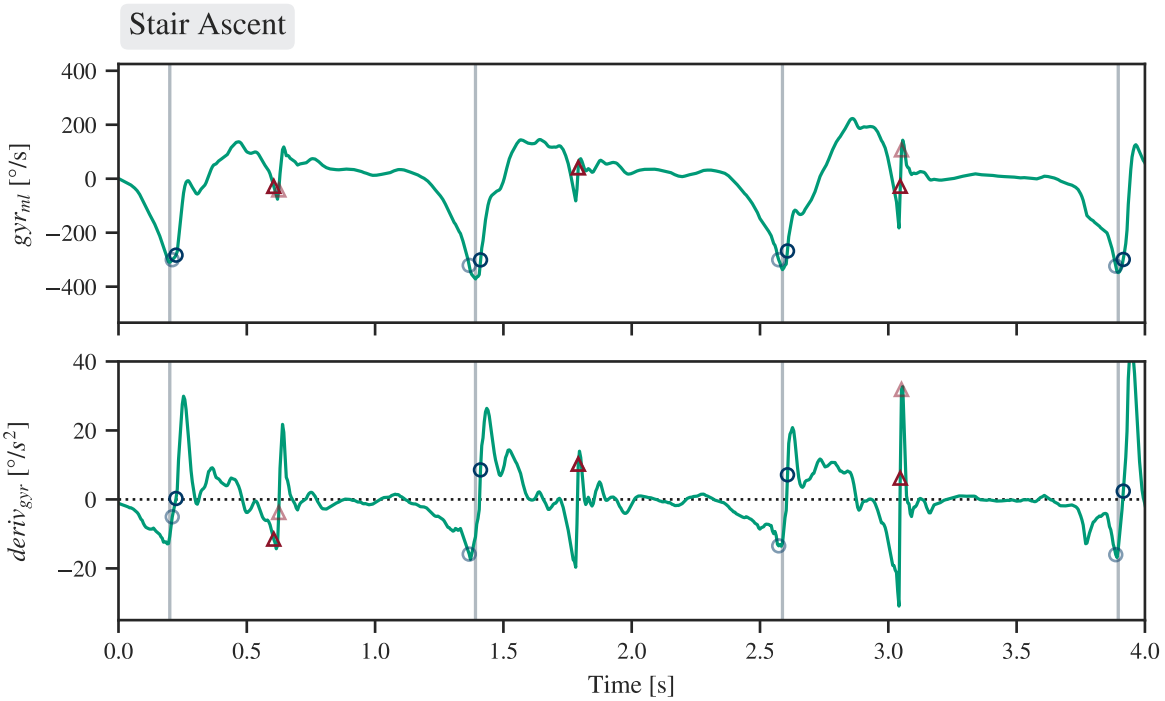
Stair Ascent
gyr_{ml} [°/s]
$deriv_{gyr}$ [°/s^2]
Time [s]

(b)

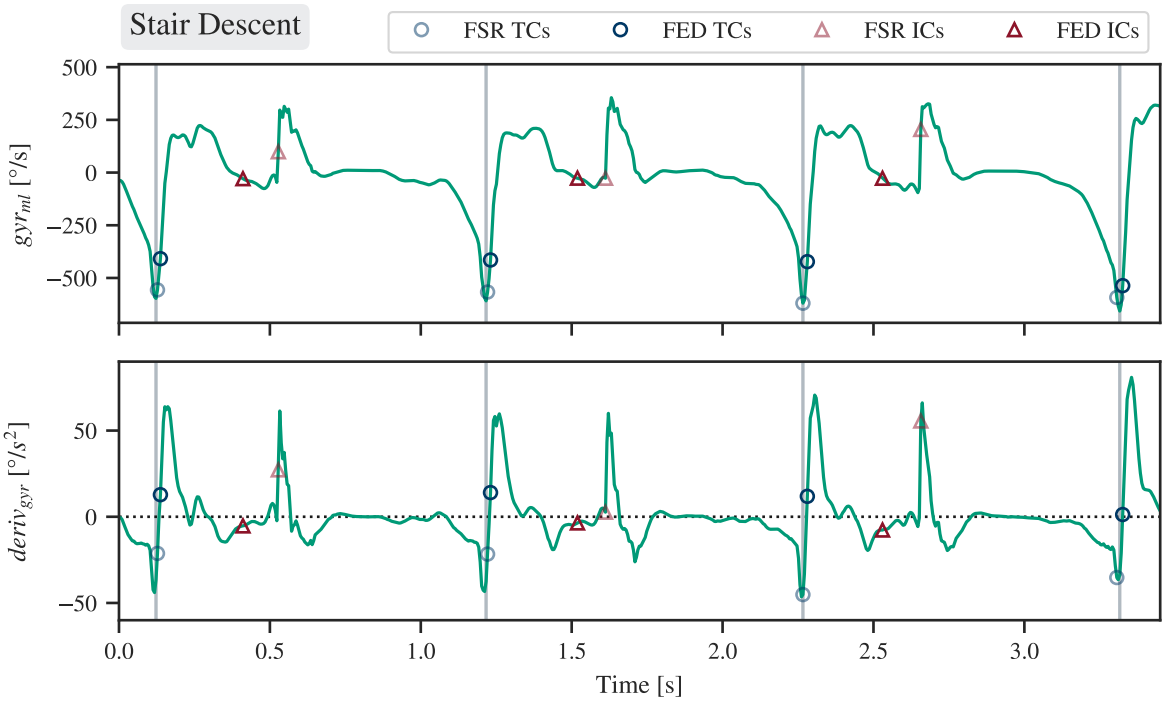

(c)

Figure 4.5: **FigueiredoEventDetection behaviour for different stride types.** The *Figueiredo-EventDetection* algorithm operates exclusively on the two signals shown above for different stride types. The $deriv_{gyr}$ depicted was calculated from a mediolateral gyroscope signal smoothed with $k = 0.2$. The stride borders (light grey lines) provide a current stride time estimate. Note that the adaptive thresholds MAX_{thr} and MIN_{thr} depicted for the level walking signal are still set to their default values in the first stride shown. Two previous strides have been cut out, therefore only from the second stride shown there are enough preceding gyr_{max} values to compute the adaptive threshold properly.

$gyr_{max,n}$ (Table 4.2) as soon as at least three previous values are available. This behaviour can be observed in Figure 4.5. After this maximum was detected and the angular velocity is below the MAX_{thr}, the IC occurs as soon as either a local minimum is reached or the gyr_{ml} value is within the defined range ($IC\_thr_{mean} \pm IC\_thr_{std}$) (R2). The FF state starts after the first minimum once the slope of the gyr_{ml} signal is almost zero (R3). The following HO state was defined as when the angular velocity becomes negative with a sustained downward slope (R4). The TC is then found at the end of that slope at the second minimum of the gyroscope signal. This minimum has to be below the adaptive minimum threshold MIN_{thr} which is calculated equivalently to the adaptive maximum threshold (see Table 4.2 and Fig. 4.5).

4.5 Combined Event Detection for Stair Ambulation

Since the *RamppEventDetection* algorithm (Section 4.3) provided more accurate results for the IC detection and the *FigueiredoEventDetection* (Section 4.4) was better at the TC detection, some elements of these two algorithms were combined and partially improved to form a more robust and accurate gait event detection algorithm for both level walking and stair ambulation. This algorithm works – like the *RamppEventDetection* – on the stride level, meaning the input signals were also segmented into single stride sequences, on which the events were then detected.

The algorithm and its results are illustrated in Figure 4.7.

4.5.1 Terminal Contact Detection

The search region for the TC is firstly narrowed down to a quarter *stride time* before and after the *start* label. The TC was then – according to Figueiredo et al. – defined as the global gyr_{ml} minimum within this segment [Fig18], as especially for slow stair ascent the gyr_{ml} zero crossing used in the *RamppEventDetection* [Ram15] appears well after the actual TC.

Parameter	Default Value	Adaptive Value
MAX_{thr}	$0.7\,\mathrm{rad/s}$ ($40.11\,^\circ/\mathrm{s}$)	$MAX_{thr} = 60\% \cdot \frac{1}{3}\sum_{i=n-2}^{n} gyr_{max,i}$
MIN_{thr}	$-2.0\,\mathrm{rad/s}$ ($-114.59\,^\circ/\mathrm{s}$)	$MIN_{thr} = 60\% \cdot \frac{1}{3}\sum_{i=n-2}^{n} gyr_{min,i}$
IC_thr_{mean}	$-0.5\,\mathrm{rad/s}$ ($-28.65\,^\circ/\mathrm{s}$)	not adaptive
IC_thr_{std}	$0.05\,\mathrm{rad/s}$ ($2.86\,^\circ/\mathrm{s}$)	not adaptive

Table 4.2: Figueiredo default parameter values.

4.5.2 Initial Contact Detection

Low-Pass Filtering of the Acceleration Signal

Rampp et al. detected the IC at the minimum of the acc_{pa} signal [Ram15]. However, a thorough analysis of the signals at hand suggested that the ICs' locations can rather be determined through a low-pass filtered acceleration signal regardless of the *stride type*. The posterior-anterior accelerometer signal was filtered forward and backward with a low-pass *Butterworth filter* h_{butter} with order $n = 1$ and a cutoff frequency f_{cutoff} at four times the stride frequency f_{stride} of the current stride (Equation 4.8 and 4.9) [But30, Gus96]. The filtered signal $acc_{pa,low}$ clearly shows the overall acceleration trend during the course of one stride (Figure 4.6).

$$f_{cutoff} = 4 \cdot f_{stride} = 4 \cdot \frac{1}{t_{stride}} \tag{4.8}$$

$$acc_{pa,low} = reversed\left(h_{butter} * reversed\left(acc_{pa} * h_{butter}\right)\right) \tag{4.9}$$

Search Region and Event Detection

Taking the global gyr_{ml} maximum as the start of the search region as described by Rampp et al. [Ram15] does not work for stair descent, because of the additional peak that occurs after the IC (Figure 4.3c). To address this problem, and ensure the search started after the *midswing*, the first *prominent* peak within the gyr_{ml} signal served as the start of the search region instead. This peak was determined with the `scipy.signal.find_peaks` [Vir20] function and an adaptive prominence value that is lowered until it is very low (0.2 or lower) or at least two peaks have been found. The end of the search region was expanded to 70% of the *stride time* to adapt the event detection to faster paces [Man80].

The search area is then further narrowed down to the area between the maximum in the $acc_{pa,low}$ signal (corresponding to the late *swing phase*, when the foot is decelerated and foot placement is in preparation) and the maximum of the gyr_{ml} derivative.

The rapid deceleration at the end of the *swing phase* (positive peak in the $acc_{pa,low}$ signal) comes to an end as soon as the foot hits the ground, which in turn results in a steep downward slope within the $acc_{pa,low}$ signal. This is visible as a prominent negative peak in the derivative at the approximate IC location (Figure 4.6 and Figure 4.7). This negative peak in the $acc_{pa,low}$ derivative was therefore chosen as the feature for IC detection (Figure 4.7).

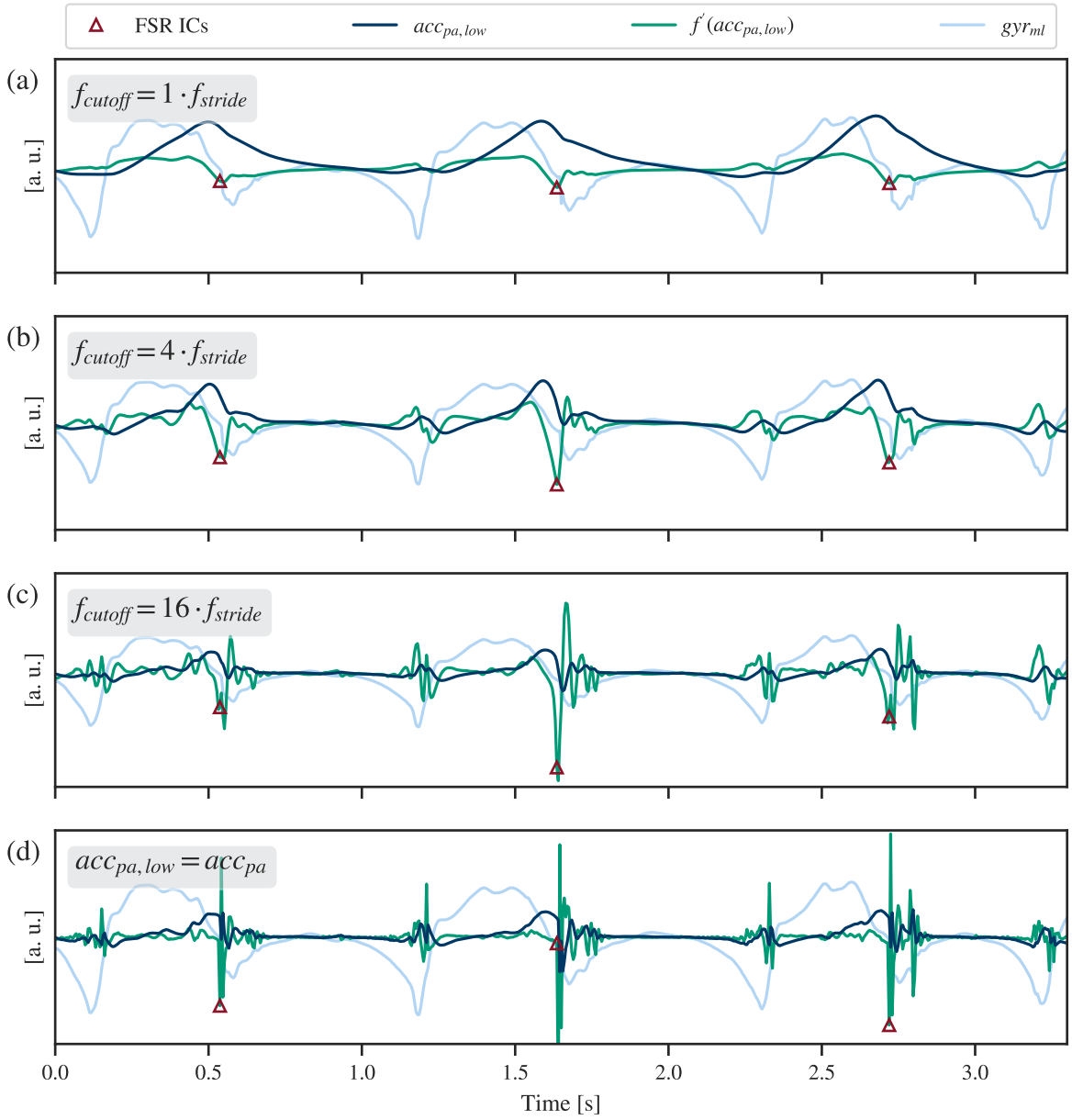

Figure 4.6: **Low-pass filtered posterior-anterior acceleration signal for different cutoff frequencies.** This figure shows the low-pass filtered acc_{pa} signal and its derivative with the ideal ICs. The gyr_{ml} signal was added for orientation. The original acc_{pa} signal and its derivative are depicted in the bottom plot. The IC derivative peak can most clearly be seen with a cutoff frequency $f_{cutoff} = 4 \cdot f_{stride}$ *(b)*. In the original signal *(d)* or for higher cutoff frequencies *(c)* this peak is not as prominent and additionally it is not necessarily the most negative one (e.g., in the third stride there are other peaks almost as negative or even more negative than the IC peak itself).

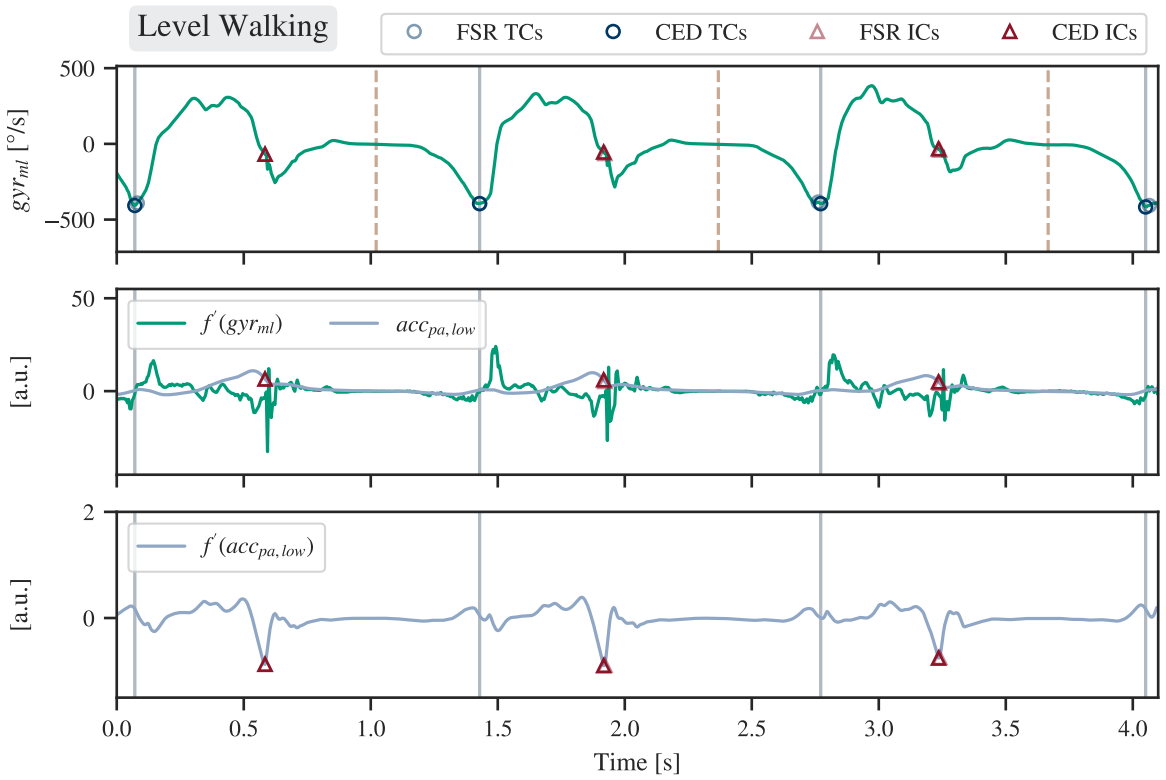
Level Walking
FSR TCs
CED TCs
FSR ICs
CED ICs
gyr_{ml} [°/s]
500
0
−500
[a.u.]
50
0
$f^{'}(gyr_{ml})$
$acc_{pa,low}$
2
0
$f^{'}(acc_{pa,low})$
0.0
0.5
1.0
1.5
2.0
2.5
3.0
3.5
4.0
Time [s]

(a)

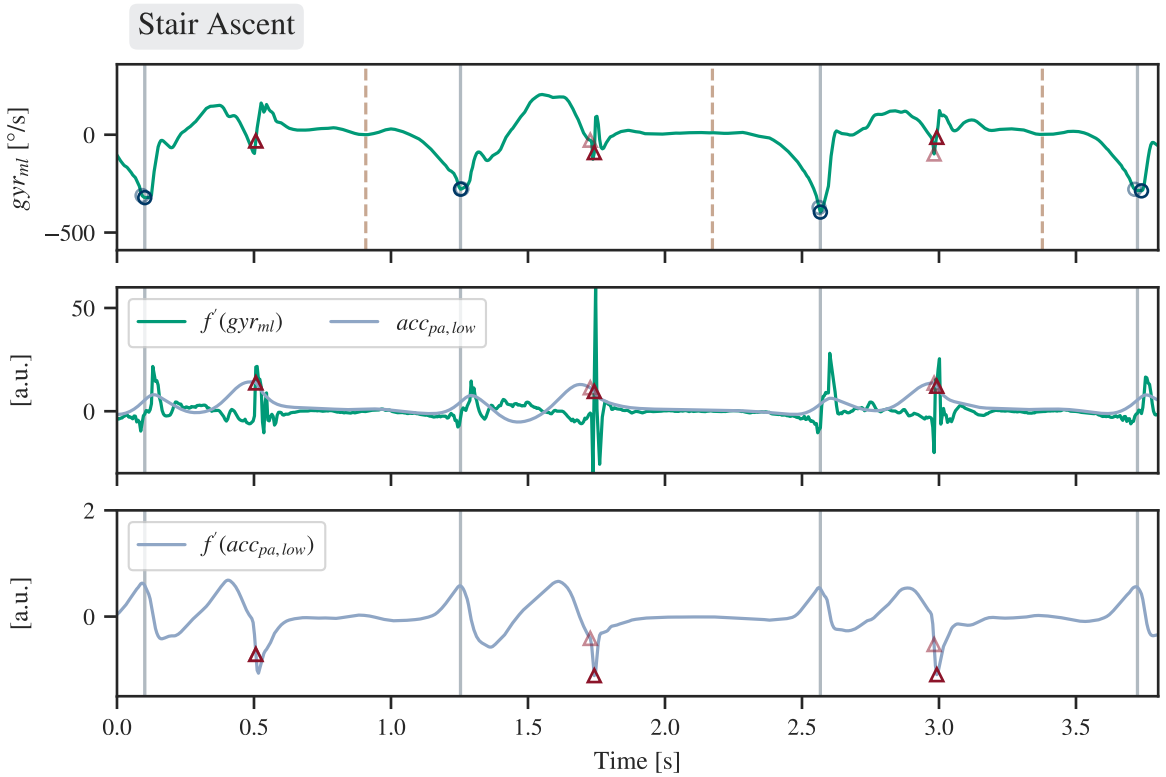
Stair Ascent
gyr_{ml} [°/s]
0
−500
[a.u.]
50
0
$f^{'}(gyr_{ml})$
$acc_{pa,low}$
2
0
$f^{'}(acc_{pa,low})$
0.0
0.5
1.0
1.5
2.0
2.5
3.0
3.5
Time [s]

(b)

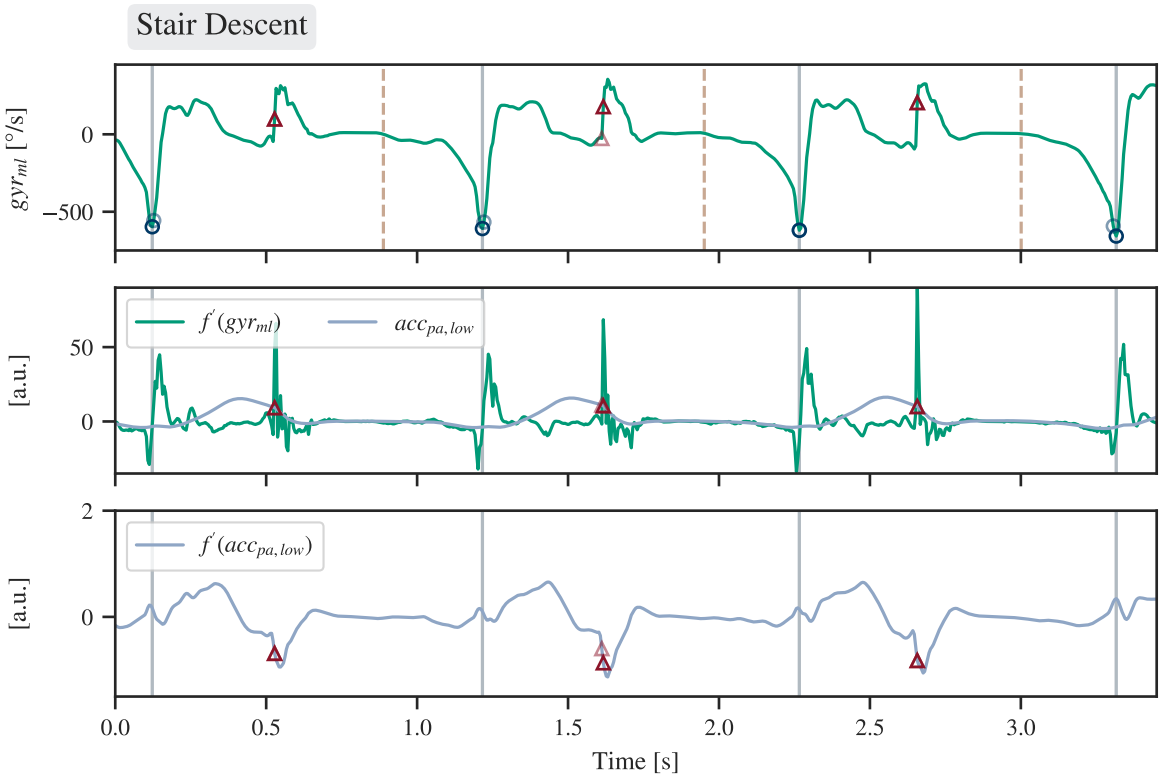

(c)

Figure 4.7: **ComboEventDetection behaviour for different stride types.** The TCs were detected at the minimum of the gyr_{ml} signal. For the IC detection, several levels of search area refinements were needed. These levels are illustrated here from top to bottom for each stride type. Level 1: Search between *midswing* gyr_{ml} peak and 70% of the *stride time* (dashed line). Level 2: Search between late *swing* $acc_{pa,low}$ peak and gyr_{ml} derivative maximum. Level 3: The IC was detected at the minimum of the $acc_{pa,low}$ derivative.

4.6 Evaluation

4.6.1 Postprocessing

Detected events and thus also their corresponding strides were excluded from the final evaluation on the basis of the following criteria:

- wrong order of events within stride
- event in non-plausible area
- *swing time* in non-plausible relation to stride time

For every stride, the TC had to occur before the IC. The ground truth indicates that each TC is located in the close vicinity of the associated stride's start. Adding a generous buffer, the TC was only considered plausible if it was less than $\pm 25\%$ of the stride time away from the *start* label. Based on the assumption that this label is approximately the TC, the distance to the IC is equal to the *swing time*. The *swing time* can take up between 15% and 70% of the stride time, if walking and running [Man80], differently inclined stairs [Rie02] and pathological gait patterns such as in PD [Hau98] are taken into consideration. Consequentially, a stride is regarded as plausible if the distance between the stride's start and the IC as well as the *swing time* are within 15 to 20% of the stride time.

This postprocessing was first applied to the ground truth events based on FSR data, where mostly strides immediately after or before a period of standing where excluded. These strides were removed from the stride list that was then used as an input to the *RamppEventDetection*, *FigueiredoEventDetection* and *ComboEventDetection* algorithms. The detected events where then also cleaned up according to the above described plausibility criteria. Only the events left where included in the evaluation. The percentage of strides in the postprocessed stride list, where the event detection algorithm delivered a plausible result, was given as the detection rate.

4.6.2 Error Measurements

The temporal error d was calculated for every stride (Equation 4.10). The strides were then grouped into logically related groups, e.g., all fast ascending strides or all strides on level ground. For each of these groups (with N strides) several error measurements were calculated, starting with the arithmetic mean (Equation 4.11) and standard deviation of the errors (Equation 4.12).

$$d = event_{IMU} - event_{FSR} \tag{4.10}$$

$$\mu = \frac{1}{N}\sum_{i=0}^{N-1} d_i \tag{4.11}$$

$$\sigma = \sqrt{\frac{1}{N}\sum_{i=0}^{N-1}(d_i - \mu)^2} \tag{4.12}$$

These measures show if the results generally tend to be larger or smaller than the gold standard. However, large negative and positive errors can cancel each other out. Thus, in order to quantify the absolute discrepancy between gold standard and the results of the evaluated method, the mean absolute error MAE was introduced (Equation 4.13). Additionally, the 95th percentile of the absolute difference was given, to get a better understanding of the scattering of the absolute errors. The 95th percentile is defined as the absolute error, that is larger than 95% of the absolute errors.

$$MAE = \frac{1}{N}\sum_{i=0}^{N-1} |d_i| \tag{4.13}$$

Additionally, the *Spearman correlation coefficient* (SCC) is provided for the detected *stride* and *swing times*. It quantifies the statistical dependence between the rankings of the ground truth and the results of the evaluated method.

Chapter 5

Results

In this chapter results of the evaluation are presented, starting with the detection rate of the algorithms. The main focus is on the performance of the algorithms regarding the event detection (Section 5.2 and 5.3), but at the end of the chapter the accuracy of the resulting gait parameters is evaluated as well (Section 5.4).

5.1 Detection Rate

The *Detection rate* is defined as the percent of detected events from the postprocessed stride list, that have been considered plausible. The exact plausibility criteria are explained in Section 4.6.1. *Detection rates* for the different *stride types* are visualized in Figure 5.1. *Single step* and *double step* strategy strides are not included in this figure. A detailed list of the detection rates can be found in the Appendix in Table B.1.

Generally, the FED had the lowest and the CED had the highest detection rates. For fast descent and ascent the FED performance was the worst with a detection rate of 20.0% and 42.3%, respectively. With just over 70%, most events were detected by the FED during level walking and *single step* stair ascent.

The RED performance was similar to the CED performance, except for slightly worse *detection rates* for stair ascent and descent. Again, this was mostly caused by the fast stair descent (82.8%) and ascent (93.2%). However, for slow, normal, and *single step* stair ascent every single event detected by the RED was considered plausible.

The CED showed exceptionally high detection rates, with the worst rate at 98.2% for *double step* stair ascent. The algorithm delivered most plausible results for stair descent with rates between 99.5% (*single step*) and 100.0% (preferred pace).

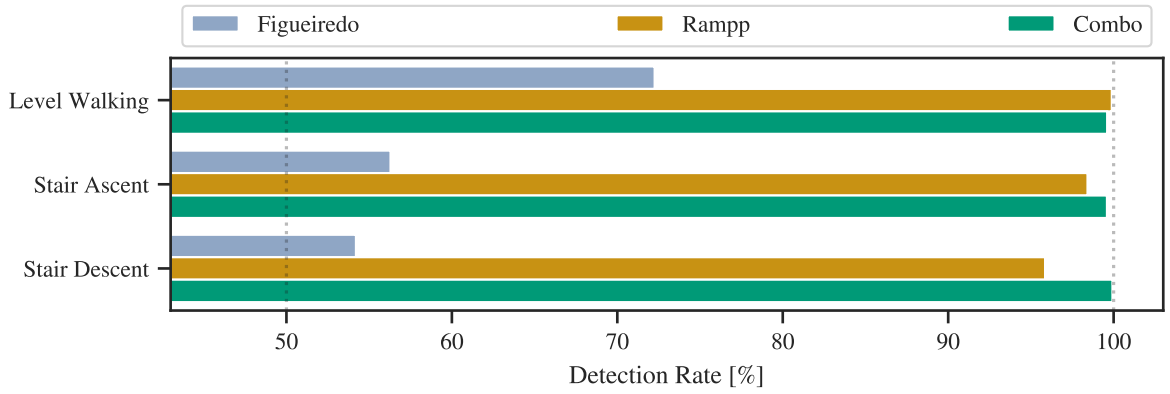

Figure 5.1: **Detection rate.** The percentage of plausible events delivered by the respective algorithm. The *detection rate* is the same for IC and TC because the postprocessing either accepts or rejects the stride as a whole with both events.

5.2 Initial Contact Detection

The IC detection performance of the examined algorithms is visualized in different figures and tables: Mean temporal errors and standard deviation are shown in Figure 5.2 and Table 5.1. Mean absolute errors are depicted in Figure 5.3 and listed together with their 95th percentile in Table 5.2.

The FED algorithm generally performed the worst at IC detection with mean absolute errors between 30.9 ms and 133.7 ms. However, on average it provided slightly better values for stair ascent than RED. RED and CED showed a similar standard deviations throughout, but while RED detected the IC on average always over 14 ms too late, CED's IC detection was on average below 8 ms off.

RED and FED both scored worst for slow descent (44.0 ms and 133.7 ms) but they were also not particularly good at stair descent at a fast or preferred pace.

Overall, the CED algorithm performed best with mean absolute errors below 18.9 ms for all tests. Its IC detection has actually been found to work best for level walking with even smaller scatter and smaller errors than RED.

Table 5.1: Mean errors and standard deviation for different stride types and paces for the IC.

Pace	Type	Rampp Mean Error [ms]	Figueiredo Mean Error [ms]	Combo Mean Error [ms]
Preferred	Asc.	22.4 ± 20.0	14.8 ± 45.9	4.6 ± 16.9
	Desc.	38.6 ± 29.4	-48.6 ± 104.0	5.9 ± 16.0
Slow	Asc.	16.4 ± 33.2	-4.7 ± 57.2	-3.5 ± 30.2
	Desc.	43.4 ± 38.8	-98.1 ± 121.4	3.7 ± 21.0
Fast	Asc.	22.3 ± 26.6	21.8 ± 38.9	7.6 ± 13.3
	Desc.	33.3 ± 23.1	-40.7 ± 71.1	6.9 ± 16.1
Mixed	Level	14.6 ± 23.5	26.2 ± 39.4	-4.5 ± 22.5

Table 5.2: Mean absolute errors and 95th percentile (P_{95th}) for different stride types and paces for the IC.

Pace	Type	Rampp MAE (P_{95th}) [ms]	Figueiredo MAE (P_{95th}) [ms]	Combo MAE (P_{95th}) [ms]
Preferred	Asc.	24.4 (48.8)	30.9 (87.9)	12.9 (29.3)
	Desc.	38.9 (102.5)	95.4 (207.5)	12.0 (34.2)
Slow	Asc.	26.6 (63.5)	36.4 (92.8)	18.9 (53.7)
	Desc.	44.0 (127.0)	133.7 (263.7)	13.1 (34.2)
Fast	Asc.	27.8 (53.7)	31.5 (92.8)	12.0 (29.3)
	Desc.	34.2 (73.2)	65.6 (147.0)	11.7 (34.2)
Mixed	Level	17.2 (53.7)	38.5 (78.1)	9.1 (24.4)

5.3 Terminal Contact Detection

The TC detection performance of the investigated algorithms is visualised as the observed relative and absolute temporal errors in Figure 5.2 and Figure 5.3, respectively. Additionally, the exact numbers for mean errors and standard deviation are provided in Table 5.3, and mean absolute errors and their 95th percentile are listed in Table 5.4.

Every examined algorithm produced the worst TC detection results for slow stair ascent. RED always detected the TCs on average more than 30 ms too late especially for stair ascent with mean errors well above 97 ms. The lowest error rates for RED occurred during (fast) stair descent with mean absolute errors still over 30 ms.

Table 5.3: Mean errors and standard deviation for different stride types and paces for the TC.

Pace	Type	Rampp Mean Error [ms]	Figueiredo Mean Error [ms]	Combo Mean Error [ms]
Preferred	Asc.	111.9 ± 52.0	3.6 ± 28.2	-2.1 ± 35.8
	Desc.	39.2 ± 18.4	9.4 ± 19.5	-6.1 ± 20.0
Slow	Asc.	130.8 ± 70.1	-2.3 ± 33.0	-1.3 ± 44.8
	Desc.	45.7 ± 23.4	6.8 ± 30.1	-7.2 ± 26.9
Fast	Asc.	97.6 ± 45.1	2.4 ± 34.5	-3.7 ± 32.9
	Desc.	30.2 ± 20.2	7.0 ± 13.9	-12.6 ± 18.8
Mixed	Level	54.3 ± 24.9	10.3 ± 21.4	-4.8 ± 34.6

Table 5.4: Mean absolute errors and 95th percentile (P_{95th}) for different stride types and paces for the TC.

Pace	Type	Rampp MAE (P_{95th}) [ms]	Figueiredo MAE (P_{95th}) [ms]	Combo MAE (P_{95th}) [ms]
Preferred	Asc.	112.3 (185.5)	20.0 (53.7)	30.2 (58.6)
	Desc.	40.5 (68.4)	15.6 (36.6)	14.7 (39.1)
Slow	Asc.	131.4 (234.4)	24.5 (63.5)	35.8 (78.1)
	Desc.	46.3 (83.0)	19.4 (48.8)	19.7 (53.7)
Fast	Asc.	97.7 (169.2)	20.7 (53.7)	28.4 (53.7)
	Desc.	32.6 (58.6)	11.8 (29.3)	16.2 (39.1)
Mixed	Level	55.3 (83.0)	17.9 (43.9)	23.9 (58.6)

FED and CED also performed best during stair descent, but with mean absolute errors less than half as high at no more than 19.7 ms. FED peaked for fast stair descent and detected 95% of the TCs with an absolute error below 29.3 ms.

CED tended to detect the TCs a few milliseconds too early. It delivered the best results for stair descent with at best a mean absolute error of 14.7 ms at the preferred pace.

5.4 Calculated Parameters

Mean errors and standard deviation between the detected *swing times* and the ground truth *swing time* values are listed in Table 5.5, mean absolute errors and SCCs are listed in Table 5.7. The respective values for the *stance times* are listed in Table 5.6 and 5.8. Additionally, the relationship

between detected and ground truth values for both temporal gait parameters is visualised in Figure 5.4 and Bland-Altmann-Plots are provided for all *stride types* in Figure 5.5.

RED and CED provided the worst *swing time* calculation results for stair ascent, while especially the stair ascent seems to be a strength of the FED algorithm.

For stair ascent, RED was particularly bad with mean absolute errors ≥ 77.0 ms. For stair descent, however, its mean absolute errors were ≤ 34 ms and the SCC between the ground truth and the values calculated by RED was between 0.82 and 0.87.

The highest SCC between the FED results and the ground truth was 0.81 for fast stair ascent. The mean absolute errors for stair ascent and level walking were similar and ranged from 38.4 ms to 47.0 ms. For slow and preferred stair descent, however, the *swing time* could only be calculated with mean absolute errors of ≥ 100 ms and correspondingly low SCCs.

Similar to RED, the *swing time* calculations by the CED algorithm were also the most accurate for stair descent. The algorithm was able to achieve mean absolute errors between 21.1 ms and 26.2 ms and SCCs between 0.87 and 0.93 The largest deviations were found for slow and fast stair ascent, but the mean absolute errors there were still below 36 ms.

For *stance time* calculations the mean absolute errors and their scatter were very similar with respect to the different algorithms, *stride types*, and paces (compare the MAE(P_{95th}) columns in Table 5.7 and Table 5.8). However, the SCCs were significantly higher for the *stance time* calculations. FED achieved SCCs ranging from 0.52 for stair descent at preferred pace to 0.93 for slow and fast ascent. RED performed better with SCCs between 0.85 (preferred ascent) and 0.97 (fast descent). This was surpassed by the performance of the CED with all SCCs ≥ 0.91 and reaching 0.97 for slow descent.

Table 5.5: Mean errors and standard deviation for different stride types and paces for the *swing time*.

Pace	Type	Rampp Mean Error [ms]	Figueiredo Mean Error [ms]	Combo Mean Error [ms]
Preferred	Asc.	-89.5 $\pm$ 57.0	11.2 $\pm$ 53.4	6.7 $\pm$ 40.3
	Desc.	-0.6 $\pm$ 36.3	-58.0 $\pm$ 105.7	12.1 $\pm$ 26.2
Slow	Asc.	-114.4 $\pm$ 79.8	-2.3 $\pm$ 66.1	-2.2 $\pm$ 56.1
	Desc.	-2.3 $\pm$ 45.3	-104.9 $\pm$ 124.4	11.0 $\pm$ 35.2
Fast	Asc.	-75.3 $\pm$ 51.7	19.4 $\pm$ 51.0	11.3 $\pm$ 36.4
	Desc.	3.1 $\pm$ 33.5	-47.7 $\pm$ 71.3	19.5 $\pm$ 25.2
Mixed	Level	-39.7 $\pm$ 34.6	15.9 $\pm$ 45.3	0.3 $\pm$ 38.6

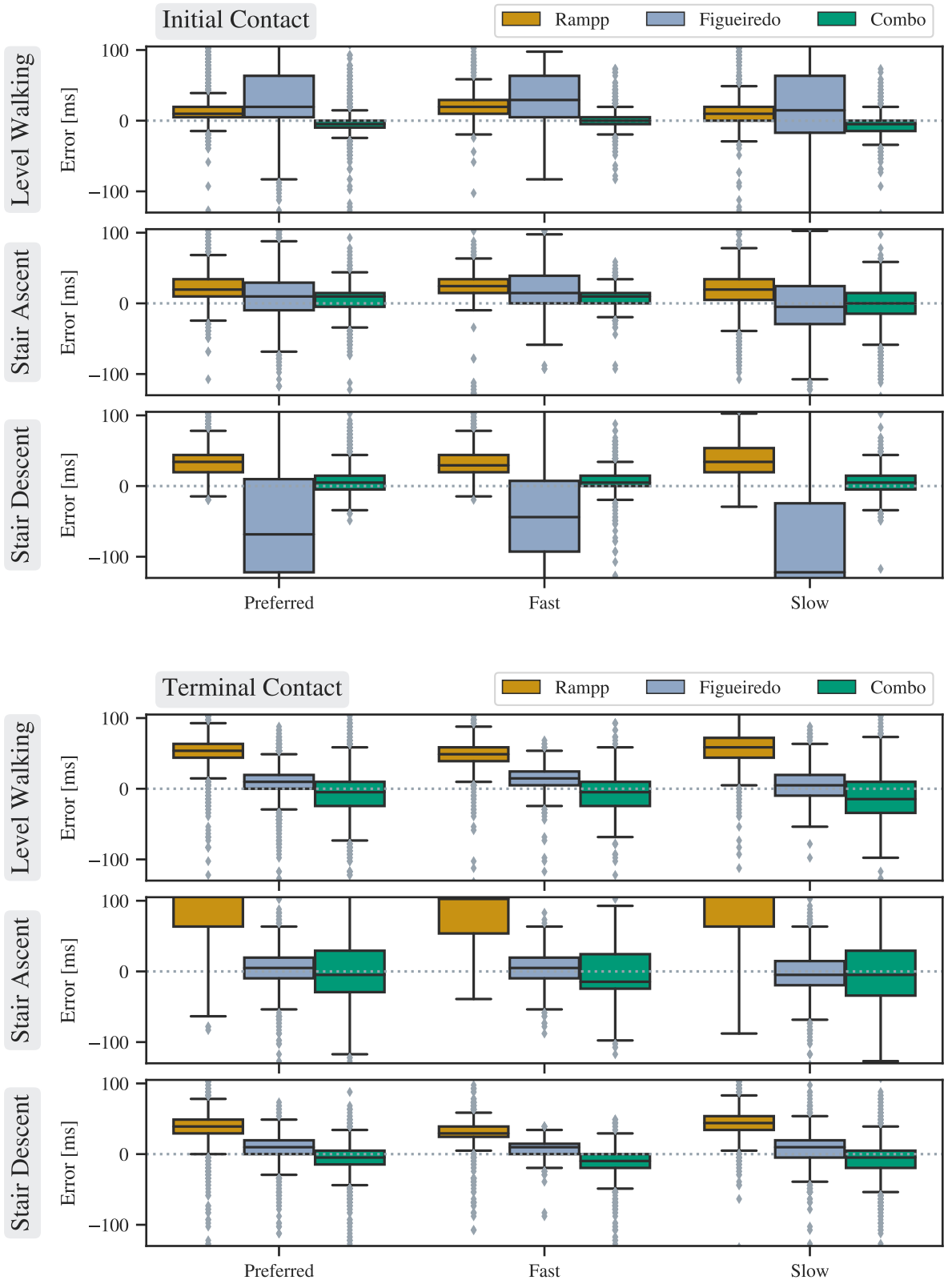

Figure 5.2: **Temporal errors of different algorithms.** The performance of the algorithms is analyzed depending on the *stride type* and the pace. Only values within −100 ms to 100 ms are displayed. The same plot with all values included can be found in Figure B.1 and B.2.

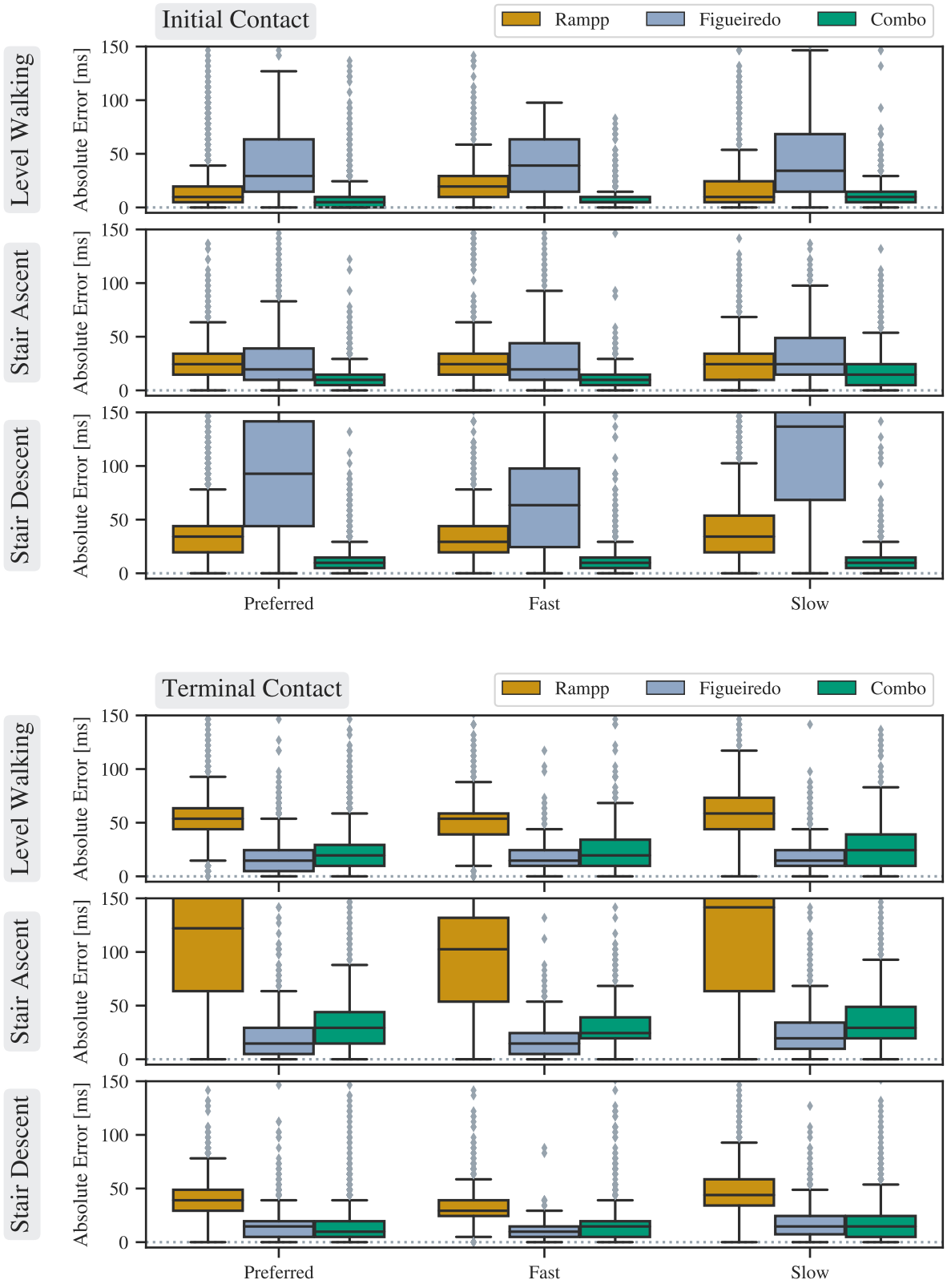

Figure 5.3: **Temporal absolute errors of different algorithms.** The performance of the algorithms is analyzed depending on the *stride type* and the pace. Only values up to 150 ms are displayed. The same plot with all values included can be found in Figure B.3 and B.4.

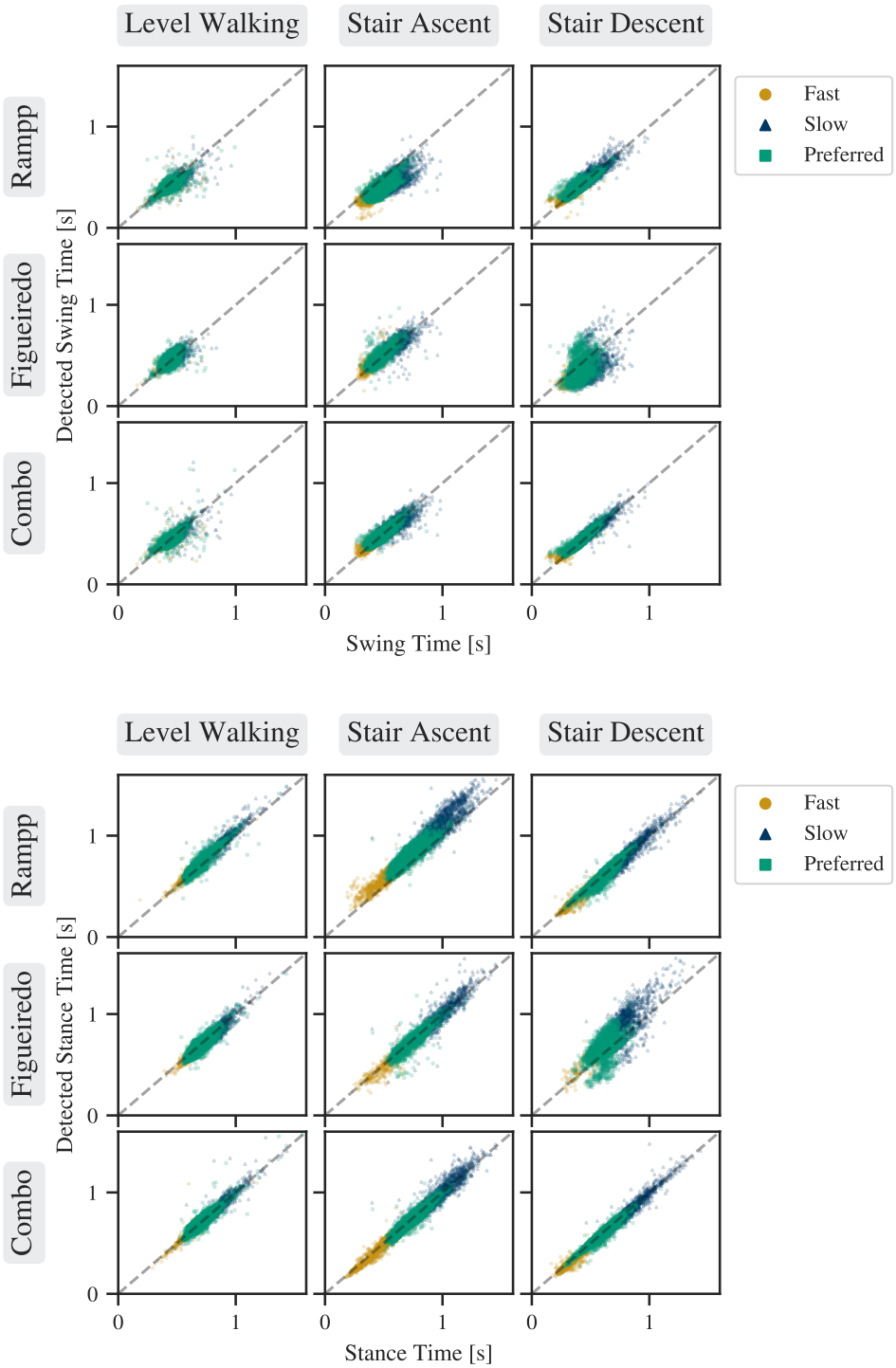

Figure 5.4: **Swing and stance time scatter plots.** The ground truth *swing* and *stance times* from the FSR data are displayed along the x-axis. Ideally all data points should be on the dashed line. The same plots but with more detail can be found in Appendix B.5 and B.6.

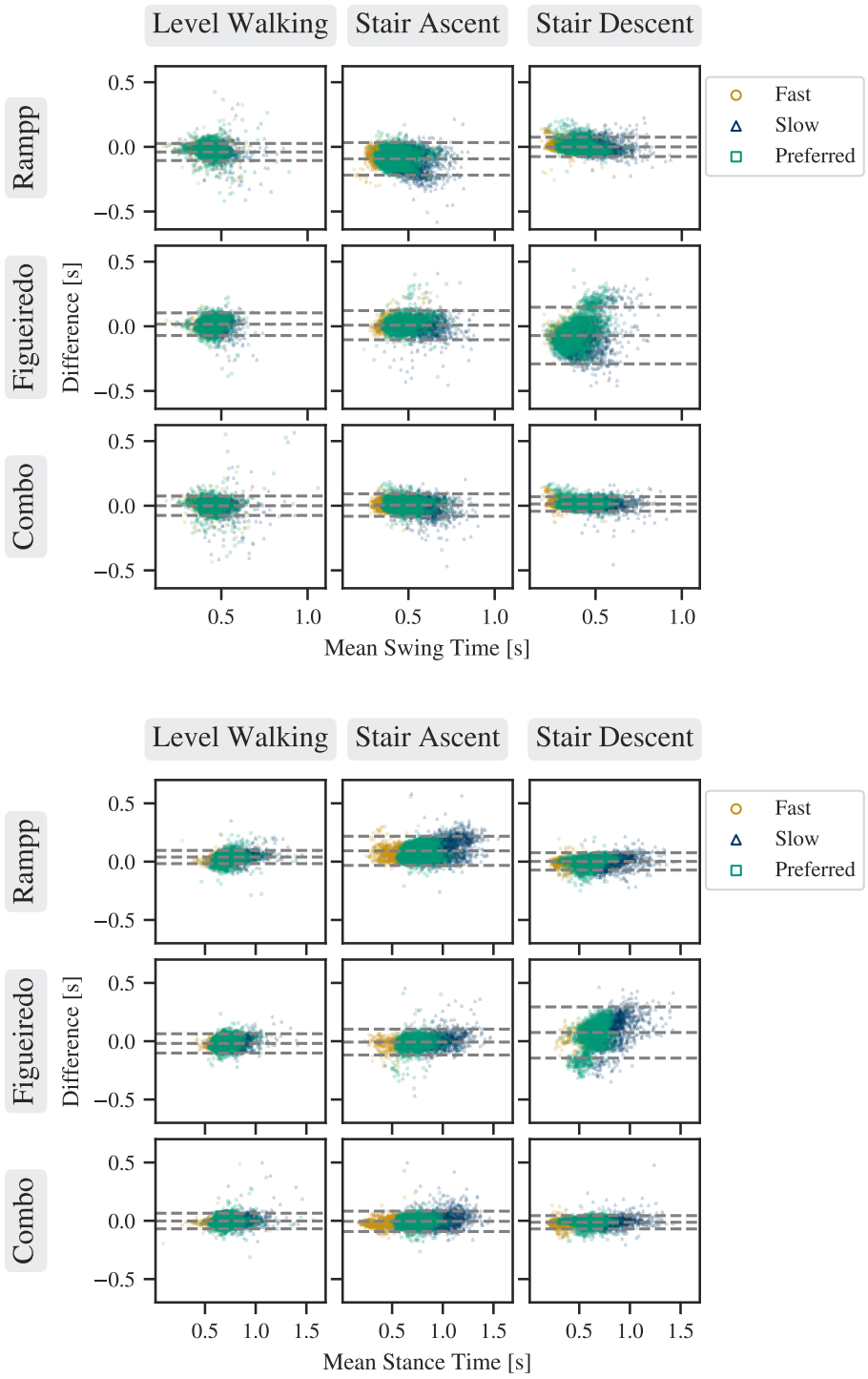

Figure 5.5: **Bland-Altmann plots for swing and stance time.** The arithmetic mean of the algorithm's parameter estimation and the ground truth is displayed on the x-axis. The y-axis shows the difference between these values. The three dashed lines correspond to the mean and 1.96σ of these differences, this means that 95% of the differences are between the dashed lines. A bigger version of these plots can be found in Appendix B.7 and Appendix B.8.

Table 5.6: Mean errors and standard deviation for different stride types and paces for the *stance time*.

Pace	Type	Rampp Mean Error [ms]	Figueiredo Mean Error [ms]	Combo Mean Error [ms]
Preferred	Asc.	89.0 ± 56.1	-10.0 ± 52.7	-5.6 ± 40.3
	Desc.	1.8 ± 36.0	61.1 ± 104.8	-11.0 ± 26.7
Slow	Asc.	114.5 ± 79.4	2.7 ± 64.7	2.5 ± 56.4
	Desc.	3.3 ± 45.5	106.3 ± 124.6	-10.7 ± 35.3
Fast	Asc.	73.8 ± 50.6	-18.0 ± 49.7	-10.5 ± 37.0
	Desc.	-0.4 ± 31.0	46.6 ± 73.4	-18.9 ± 25.7
Mixed	Level	39.2 ± 29.5	-19.0 ± 42.4	-2.2 ± 34.3

Table 5.7: Mean absolute errors with 95th percentile (P_{95th}) in milliseconds and *Spearman correlation coefficient* (SCC) for different stride types and paces for the *swing time*.

Pace	Type	Rampp MAE (P_{95th})	SCC	Figueiredo MAE (P_{95th})	SCC	Combo MAE (P_{95th})	SCC
Preferred	Asc.	91.9 (175.8)	0.58	38.6 (97.7)	0.73	33.1 (73.2)	0.76
	Desc.	26.4 (73.2)	0.82	100.8 (212.4)	0.41	21.1 (58.6)	0.92
Slow	Asc.	117.5 (239.3)	0.59	47.0 (117.2)	0.79	42.9 (102.5)	0.80
	Desc.	34.0 (92.8)	0.86	140.0 (278.3)	0.39	26.2 (68.4)	0.93
Fast	Asc.	77.0 (156.2)	0.71	38.4 (107.4)	0.81	31.4 (68.4)	0.84
	Desc.	22.4 (68.4)	0.87	69.2 (156.7)	0.63	23.9 (63.5)	0.91
Mixed	Level	44.8 (78.1)	0.76	38.4 (83.0)	0.50	26.0 (63.5)	0.67

Table 5.8: Mean absolute errors with 95th percentile (P_{95th}) in milliseconds and *Spearman correlation coefficient* (SCC) for different stride types and paces for the *stance time*.

Pace	Type	Rampp MAE (P_{95th})	SCC	Figueiredo MAE (P_{95th})	SCC	Combo MAE (P_{95th})	SCC
Preferred	Asc.	91.2 (170.9)	0.85	37.4 (92.8)	0.88	32.3 (73.2)	0.91
	Desc.	26.5 (73.2)	0.92	102.2 (210.0)	0.52	21.2 (58.6)	0.95
Slow	Asc.	117.6 (239.3)	0.89	45.5 (117.2)	0.93	42.2 (102.5)	0.94
	Desc.	34.5 (92.8)	0.94	141.8 (273.4)	0.67	26.1 (68.4)	0.97
Fast	Asc.	75.3 (151.4)	0.92	37.2 (107.4)	0.93	31.4 (68.4)	0.97
	Desc.	21.9 (58.6)	0.97	70.4 (156.2)	0.73	24.1 (58.6)	0.97
Mixed	Level	43.2 (78.1)	0.94	38.0 (83.0)	0.81	23.9 (58.6)	0.91

Chapter 6

Discussion

In this thesis, a gait event detection algorithm especially for stair ambulation was developed and evaluated. Established gait event detection algorithms designed for walking on level ground or inclined surfaces tend to reach their limits when applied to stair ambulation data due to the differing signal characteristics. To address this issue, various stair ambulation data was first recorded using the targeted sensor setup with IMUs attached to the instep of the foot. On this data, the behavior and results of two existing gait event detection algorithms [Ram15, Fig18] were then examined in more detail. Based on the findings, an improved algorithm for gait event detection for stair ascent and descent was finally developed and likewise evaluated.

In the following sections, the performance, limitations, and weaknesses of all algorithms used in this thesis are elaborated and compared to literature.

6.1 Processing Pressure Sensor Data

While most events were detected accurately from the FSR data, the algorithm did have difficulties to correctly detect the desired edges during slow locomotion (Figure 6.1 b)). The derivative threshold at 10% of the steepest slope did not fit the moderately steep slopes optimally, but a lower threshold at e.g., 5% of the steepest slope did not work for strides with a steep *midswing* signal such as in Figure 4.2. However, a derivative threshold that is slightly dependent on the *stride time* may be worth further investigation.

Additionally, the FSR data processing algorithm sometimes got stuck in local minima, if they did occur (Figure 6.1 a)).

Due to the varying and in some places very noisy FSR signal during *swing time* (Figure 4.2), an unmodified application of simple thresholds as described in some literature [Bob18, Han09]

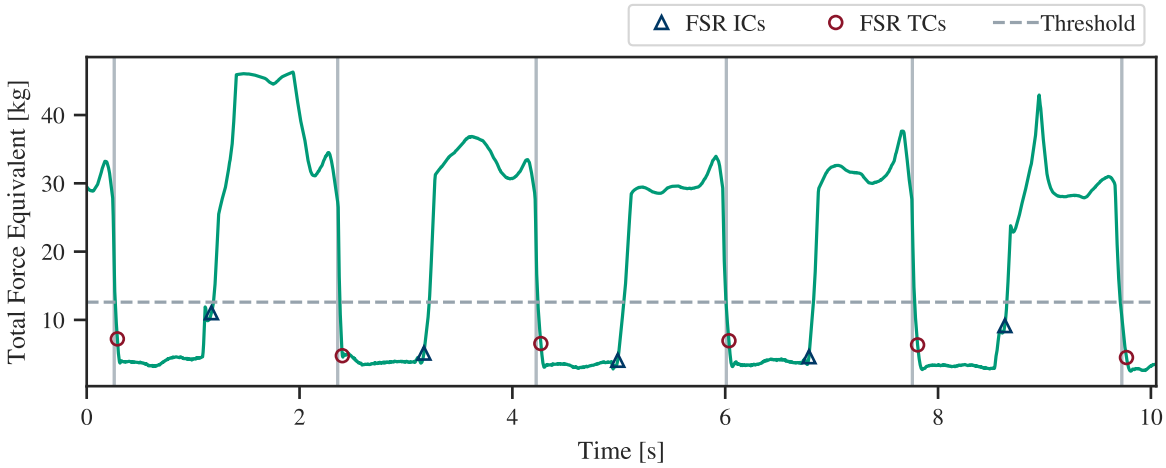

(a) In the first and last stride shown, the edge detection algorithm got stuck in local minima over 80 ms after the actual edge.

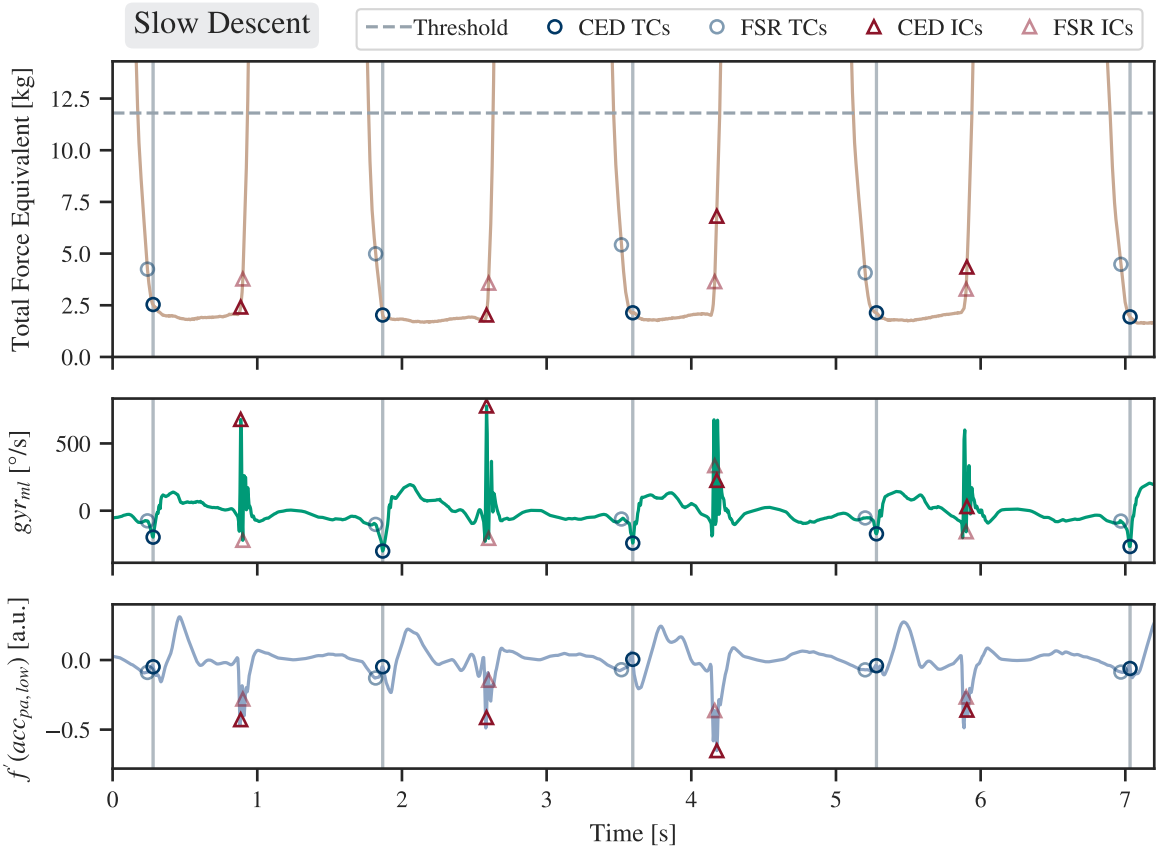

(b) Partially, the CED algorithm seemed to deliver better results than the processing of the FSR data. Due to the relatively moderate steepness of the edge, the FSR algorithm stopped its search early and errors of up to 80 ms can be observed.

Figure 6.1: **Systematic errors in the processing of the FSR data.**

was not possible. Instead the approach was loosely based on Hausdorff et al. [Hau95], which leads to different results (slightly earlier IC and later TC). As some authors [Fig18] who also used FSRs as a reference system did not specify their individual approach, a direct comparison of results may potentially be misleading.

Bobić et al. did not report concrete numbers on the mean absolute errors of their threshold-based approach for event detection with FSRs, but stated that it clearly outperformed the tested IMU gait event detection algorithms [Bob18]. The contact area approach by Catalfamo et al. achieved low absolute errors when compared to a threshold-based approach (22 ± 9 ms for IC and 10 ± 4 ms) [Cat08], however it was not applicable for this thesis due to the substantially lower number of pressure sensors used.

6.2 Rampp Event Detection

The RED tended to detect the IC late during stair descent, because of the characteristic additional broad peak in the gyr_{ml} signal. This peak is wrongly assumed as the *midswing* peak, thus the detection starts of with an initial search region that does not contain the actual IC (Figure 4.3).

Additionally, especially in gait patterns with harder treading, the gyr_{ml} signal exhibits disturbances between *midswing* and *stance phase*. These result in a very noisy derivative that does not reliably provide a sensible IC candidate (Figure 6.2). In the original paper, Rampp et al. [Ram15] might not have had problems with such high frequency noise due to their lower sampling rate at 102.4 Hz instead of 204.8 Hz. Furthermore, they did only record slow walking elderly people which of course do not exhibit the same impact forces and movement velocities as healthy younger people e.g., during fast stair ascent, and consequentially produce less noise due to overstimulation of the sensors and fast compensation movements. Most importantly, Rampp et al. did position the IMU laterally below the ankle instead of the instep and did only validate their algorithm for level walking gait, which can explain the differing results as well.

The TCs are also always detected late because the chosen feature (zero crossing) apparently does not fit the event perfectly. This is not so much of a problem during faster level walking or descent but becomes very apparent during stair ascent due to the especially shallow curve of the mediolateral gyroscope signal during ascent (Figure 6.2). Nevertheless, the effect can also be observed during slower level walking and stair descent.

Rampp et al. validated their algorithm with an instrumented walkway, that possibly detects the TC event later than the FSR algorithm used in this thesis. Nevertheless, the TCs detected at the angular velocity minimum seem to be at a valid location in comparison to the FSR signal and

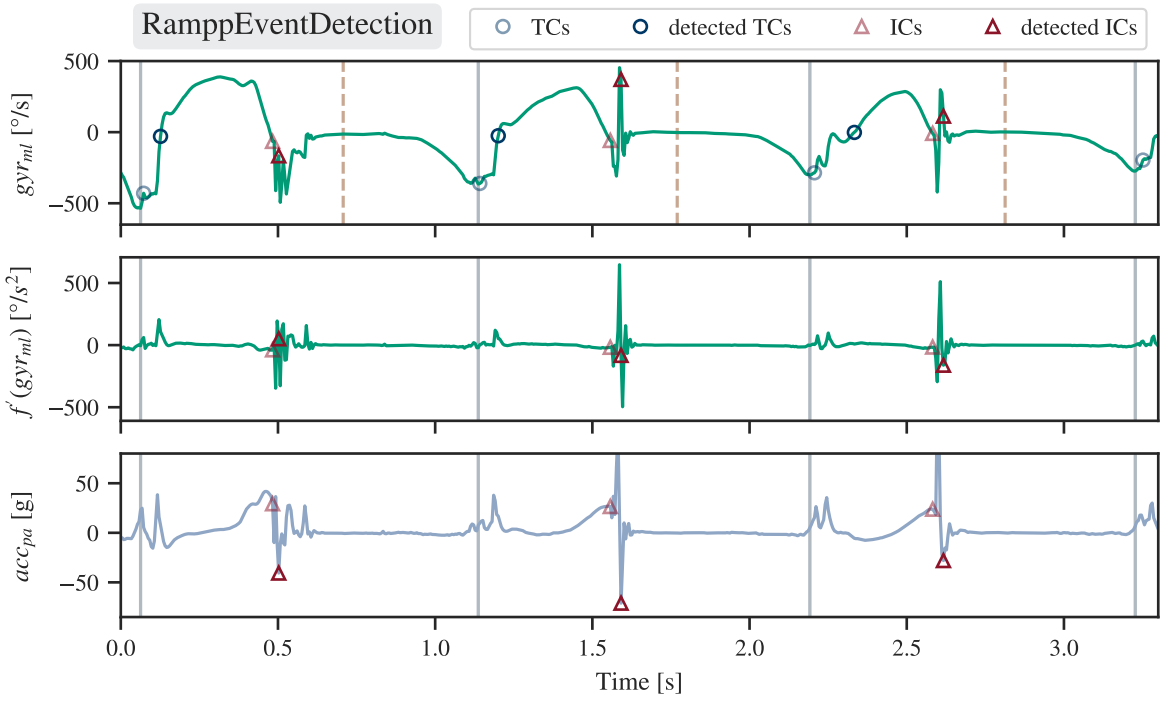

Figure 6.2: **Systematic errors in the RamppEventDetection algorithm.** The first step shown (level walking) exhibits a noisy gyr_{ml} signal and derivative. The other two steps (stair ascent) show a narrow peak after the *midswing* peak due to a gait pattern with hard tread. The ICs are still identified as intended. The flattened and otherwise altered gyroscope curve during the *swing phase* of the last step causes a late TC detection.

a later detection e.g., at the zero crossing would not be justifiable on the basis of this FSR signal (Figure 6.1). Consequentially, the error in the FSR algorithm may just have enhanced the TC detection error for the RED and it is likely, that the TCs are in fact located somewhere around the minimum in the gyr_{ml} signal rather than at the zero crossing.

Similarly to the results of this thesis, Rampp et al. [Ram15] also reported higher SCCs for *swing time* than for *stance time*. This effect is probably related to the smaller range of values for *swing time*, which is caused by mainly varying the length of *stance time* at different gait speeds [Man80] (also see Figure 5.4).

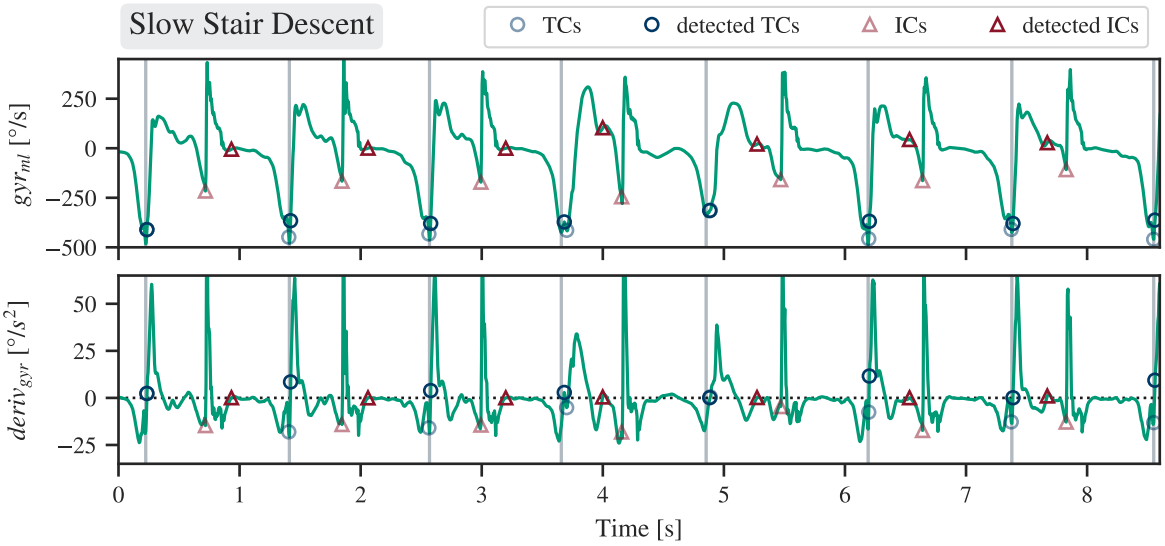

(a) During the first three strides, only the IC peak of the gyr_{ml} signal exceeds MAX_{thr}. Consequentially the IC can only be detected *after* the peak, which is over 150 ms too late. In the fourth stride, the *midswing* peak is high enough, but all following strides exhibit a minimum/plateau in the gyroscope signal over 100 ms before the actual IC which the algorithm then wrongly interpreted as the IC.

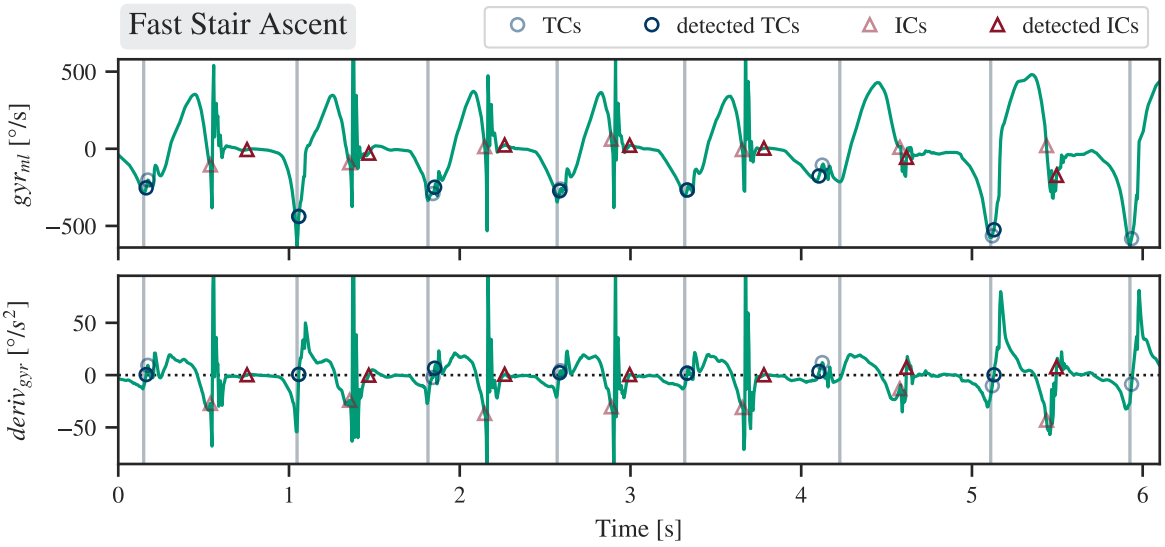

(b) During the first five strides, again only the IC peak does surpass the MAX_{thr} threshold. However, the error is mostly significantly smaller than during stair descent due to the narrower peak. The last shown stride (level walking) exhibits a very steep slope after its successfully detected *midswing* peak. Unfortunately, no sample value within this downward slope does fall exactly into the value range of $IC_{thr,mean} \pm IC_{thr,std}$ and the IC was then detected at the next minimum. The TC at 4.1 s is detected exceptionally well despite its odd location about 100 ms before the greater minimum and labeled stride border.

Figure 6.3: **Systematic errors in the FigueiredoEventDetection algorithm.**

6.3 Figueiredo Event Detection

The low detection rate was among other reasons caused by the very long reset time ($5 \cdot t_{stride}$) after one decision rule could not be satisfied properly. This means, that a variety of errors that occur in single strides can cause many strides afterwards to be skipped. One prominent reoccurring error is caused by the adaptive threshold strategy. Different *stride types* have different characteristic *midswing* peak heights, with the typical stair ascent maximum value falling below the typical MAX_{thr} of a level walking sequence. Consequentially, the algorithm has to reset almost every time when a transcending phase from level walking to stair ascent occurs and at minimum the first five strides of the stair ascent will be skipped. Additionally, the algorithm starts at the first maximum in the gyroscope signal, so only the IC is detected in the first stride and the stride is considered invalid by postprocessing.

This restart moment and the right MAX_{thr} value is especially crucial during stair descent and even stair ascent with a hard tread as the right maximum has to be picked. This issue and its effects are further illustrated in Figure 6.3. If the wrong maximum is selected, this does not result in any default state or even reset actions and thus leads to many false IC detections.

However, as also illustrated in Figure 6.3, fixed thresholds (and even more so ranges like IC_{thr}) are also a source of error as changes in *stride type* and individual gait patterns cannot be addressed.

In summary, the FED algorithm lacks the ability to view the stride as a whole due to its design for real-time gait event detection. With its remarkably reliable TC detection, it is well suited for *stride time* estimation during stair ambulation and level walking. The inadequate IC detection, however, precludes its use for *swing* and *stance time* calculation as well as any other IC-dependent gait parameters.

Figueiredo et al. reported incredibly low mean (absolute) errors e.g., 1.9 ± 9.1 ms delay for 0.8% of the ICs, 4.01 ± 1.9 ms advance for 1.2% of the ICs and the remaining 82% of the ICs were detected at exactly the right time during level walking [Fig18]. These remarkably good results could not even closely be reproduced in this thesis. The cause of this shortcoming needs to be further investigated. One possible source of error could be the higher sampling rate used in this thesis, which can be addressed through downsampling of the signal. Furthermore, Figueiredo et al. did not specify the value used as the smoothing factor k, so after visual inspection of various signal outcomes the value 0.2 was chosen. The effects of a slightly higher or lower smoothing factor can be further investigated, however $k = 0.05$ and $k = 0.4$ equally showed worse results. Finally, they also did not describe their FSR reference algorithm, so it is unclear what they were comparing their results with.

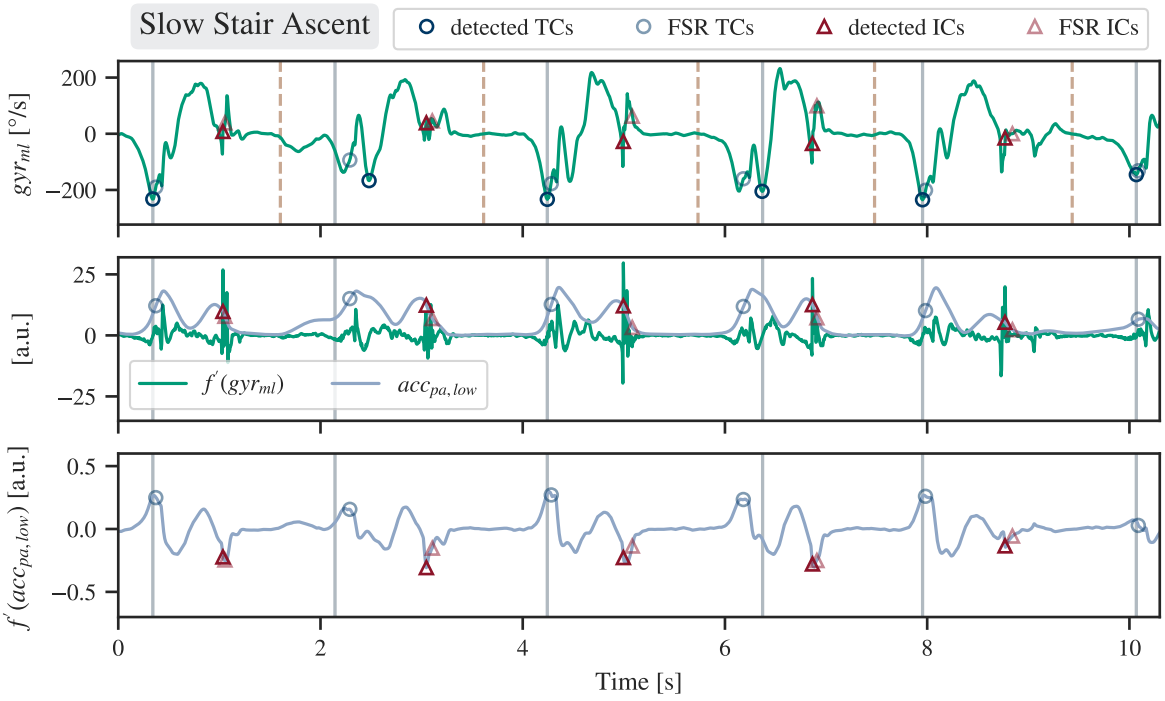

Figure 6.4: **Systematic errors in the ComboEventDetection algorithm.** The actual IC is over 50 ms after the $f'(acc_{pa,low})$ minimum for the second, third, and fourth stride shown. The detected TCs are mostly slightly early, except for the second and fourth stride, where an unusual extra minimum in the gyroscope signal is exhibited. The $acc_{pa,low}$ derivative however does look promising for a more reliable TC detection. Also note the wrongly labeled second stride border, that could have been a cause for further errors.

6.4 Combo Event Detection

The CED algorithm overall performed better for the IC detection than the other investigated algorithms. Nevertheless, the chosen feature is still not optimal, as shown in Figure 6.4.

The TC detection performance is worse than FED's. This is due to a sometimes occurring second minimum in the gyroscope signal. The actual TC most often seems to be located at the first minimum rather than the second one though the latter might be the global minimum within the search region (Figure 6.3 and Figure 6.4). Additionally, the gyroscope minimum is not the optimal feature even during strides were no extra second minimum appears. A further investigation into the $acc_{pa,low}$ derivative or maybe the low-pass filtered gyr_{ml} signal would be interesting.

In comparison with Formento et al. [For14], smaller mean (absolute) errors were observed for the CED IC (mean absolute error during stair ascent: 21 ± 17 ms and during stair descent:

38±36 ms) and TC detection (mean absolute error during stair ascent: 40±13 ms and during stair descent: 132±44 ms). These values are rather in the range of the RED results. Although the CED results are comparatively poor for stair ascent, they still indicate a better performance than the algorithm presented by Formento et al. [For14].

Bobić et al. [Bob18] did not specify any concrete numbers to the (absolute) errors of their evaluated event detection algorithms. Nonetheless, by comparing the plots it is safe to say, that CED outperformed their template-based algorithms at least for level walking and stair descent. However, they already mentioned in their discussion that the detected markers from the template-based approach did not precisely match the actual IC and TC events and nevertheless, the accelerometry template-based approach seemed very promising. Therefore, further research into template-based approaches would be valuable. In order to be applicable for stair ambulation, most likely *stride type* specific templates would be necessary due to the inherently different signal characteristics.

In comparison with the RED algorithm and the *stance time* results reported by Rampp et al. [Ram15], even the level walking event detection was improved by the CED algorithm or at least for *swing time* it was not substantially worsened (*swing time* absolute error: 25 ms, *stance time* absolute error: 33 ms). However, this could be due to the higher sampling rate used for RED than what the algorithm was designed for and due to the application to geriatric patients' gait by Rampp et al..

In general, the absolute differences and correlation coefficients showed that the performance of the algorithm is comparable to literature [Ram15, Bob18, For14]. Together with the relatively high number of differently aged subjects, it can be assumed that this algorithm is applicable for stair ambulation analysis with healthy subjects. However, although this study included multiple different stairs, gait paces, and gait strategies, it was still in a supervised environment, thus the algorithm's performance in unsupervised real-world scenarios still has to be evaluated. The applicability for subjects with altered gait e.g., due to very old age or PD has to be validated as well through application in real-world monitoring studies.

Furthermore, the detection of the *midstance* event should be added to enable trajectory reconstruction and thus make the calculation of spacial gait parameters such as *stride length* possible [Ram15].

A great advantage of the proposed gait analysis system is the ability to record data independently from gait analysis laboratories and therefore gain insights into realistic every-day gait patterns. This is useful for long-term home monitoring applications and even monitored stair ambulation analysis, as no instrumented staircases are needed.

Chapter 7

Conclusion and Outlook

The goal of this thesis was to develop a gait event detection algorithm to detect initial and terminal contact during stair ambulation. This algorithm should be applicable for free-living gait analysis and potentially long-term home monitoring to gain more realistic insights into daily-life gait characteristics. IMUs attached to the instep of the foot were chosen as a measurement system, as they provide an easy to use, unobtrusive, inexpensive, and light-weight solution to measure human gait with a high biomechanical resolution.

After inspection and evaluation of the gait event detection algorithms by Rampp et al. [Ram15] and Figueiredo et al. [Fig18], an improved algorithm for gait event detection for stair ambulation was developed.

The minimum in the medio-lateral gyroscope signal was chosen as the feature for TC detection and the IC was detected at the steepest downward slope of a low-pass filtered posterior-anterior acceleration signal. The developed algorithm is an improvement compared to the other two evaluated algorithms, however, both features chosen for IC and TC are reaching the limits of the reference system.

Nevertheless, the algorithm produced proper results comparable to literature. The temporal gait parameters *stance* and *swing time* could be detected with mean absolute errors between 21.1 ms (preferred descent *swing time*) and 32.3 ms (preferred ascent *stance time*) and 95% of absolute errors below 58.6 ms and 73.2 ms, respectively. Solely the errors for slow stair ascent were substantially higher with a mean absolute error of up to 42.9 ms and 95% of the absolute errors below 102.5 ms. Due to Rampp et al. choosing the zero crossing of the medio-lateral gyroscope signal as the TC feature, the absolute errors of their algorithm's results for all stair ascent scenarios were even higher. The algorithm of Figueiredo et al. on the other hand did struggle with low detection rates partially due to adaptive thresholds that were not applicable for

changing *stride types* and performed poorly with regard to IC detection especially during stair descent because the algorithm was not designed to expect a second – possibly greater – peak in the gyroscope signal after the usual *midswing* peak. The surprisingly accurate TC detection results of their algorithm however demonstrated that there is still room for improvement in the developed algorithm.

Relevant signal features especially for the TC detection should be reviewed in future work. Since the TC can not trivially be accurately detected from the gyroscope signal alone, other signals such as the (low-pass filtered) acceleration signal should be considered as well.

On the other hand, an investigation into template-based algorithms may be valuable. An algorithm of that form would probably benefit from *stride type* specific templates in order to adequately handle the inherently different signal characteristics. Another promising approach would be the development of a Hidden Markov Model to detect said gait events or the exploration of other machine learning methods for time-series analysis. Furthermore, an adaption for real-time gait event detection would make the algorithm suitable for further clinical applications such as functional electrical stimulation.

With the help of the events detected by the algorithm, it is possible to calculate other gait parameters taking into account the sensor side, e.g., asymmetries in the gait or *double* and *single support* times. In addition, it is also possible to add the data from the hip sensor, which opens up the possibility of determining further parameters relating to the center of gravity, such as trunk sway.

Future research, however, first needs to evaluate to what extend the developed algorithm is applicable to pathological gait, e.g., of patients with PD. Data collection for this purpose has already started and first experiments show mixed results.

Appendix A

Patents

A.1 Exoskeleton Ankle Robot

Publication Number	US20160331557A1
Date of Publication	June 21, 2015
Inventors	Kai-Yu Tong, Ling Fung Yeung, Corinna Ursula Ockenfeld, Sze Kit Ho, Hon-Wah Wai, Man-Kit Pang
Assignee	Hong Kong Polytechnic University HKPU
Abstract	A portable electrical motor-driven exoskeleton ankle joint robot with gear transmission and control system which is intended to provide walking assistance in different speed and walking conditions to persons with disability in walking or muscle weakness or joint problem.

A.2 Method for detecting a movement step and for determining the movement and / or movement speed of a legged body, in particular a pedestrian

Publication Number	DE102015209607A1
Date of Publication	November 26, 2015
Inventors	Estefania Munoz Diaz
Assignee	Deutsches Zentrum für Luft und Raumfahrt e.V.
Abstract	In the method of detecting a movement step performed by a body, in particular a pedestrian, comprising at least one pair of legs which are pivoted alternately and at a varying leg pivot angle α about a pivot axis for movement of the body during a one-step movement step, the change in the leg pivot angle α, about which one leg of a leg pair is pivoted in a movement step of the body relative to the vertical, is detected by means of a sensor for each movement step. Based on the amplitude of the course of the leg swing angle α during a movement step, the completion of the movement step, the step length and / or the speed are determined.

A.3 System and method for 3D gait assessment

Publication Number	US9307932B2
Date of Publication	May 16, 2013
Inventors	Benoît Mariani, Kamiar Aminian
Assignee	Ecole Polytechnique Federale de Lausanne (EPFL)

Abstract The invention relates to a system and a method for assessment of walking and miming gait in human. The method is preferably based on the fusion of a portable device featuring inertial sensors and several new dedicated signal processing algorithms: the detection of specific temporal events and parameters, 5 optimized fusion and de-drifted integration of inertial signals, automatic and online virtual alignment of sensors module, 3D foot kinematics estimation, a kinematic model for automatic online heel and toe position estimation, and finally the extraction of relevant and clinically meaning-full outcome parameters. Advantageously including at least one wireless inertial module attached to foot, the system provides common spatio-temporal parameters (gait cycle time, stride length, and stride velocity), with the 10 advantage of being able to work in unconstrained condition such as during turning or running. It furthermore may provide original parameters for each gait cycle, both temporal (load, foot-flat and push duration) and spatial (foot clearance and turning angle), and their inter-cycles variability. The system and method according to the invention allows the assessment of various aspects of gait which have shown recently to be of premium importance in research and clinical field, including foot clearance, 15 turns, gait initiation and termination, running, or gait variability. The system may be light weight, easy to wear and use, and suitable for any application requiring objective and quantitative evaluation of gait without heavy laboratory settings.

Appendix B

Additional Figures and Tables

Table B.1: Detection rates in percent for all pace/strategy and *stride type* combinations.

Pace	Type	Rampp	Figueiredo	Combo
Preferred	Asc.	100.00	58.93	99.74
	Desc.	99.72	62.57	99.95
Slow	Asc.	100.00	63.79	99.19
	Desc.	99.95	68.67	100.00
Fast	Asc.	93.24	42.26	99.72
	Desc.	82.81	19.99	99.79
Mixed	Level	99.89	72.25	99.61
	Asc.	98.42	56.29	99.60
	Desc.	95.86	54.20	99.93
Single Step	Asc.	100.00	73.60	99.30
	Desc.	99.91	66.96	99.48
Double Step	Asc.	96.97	63.94	98.18
	Desc.	93.20	57.10	99.70

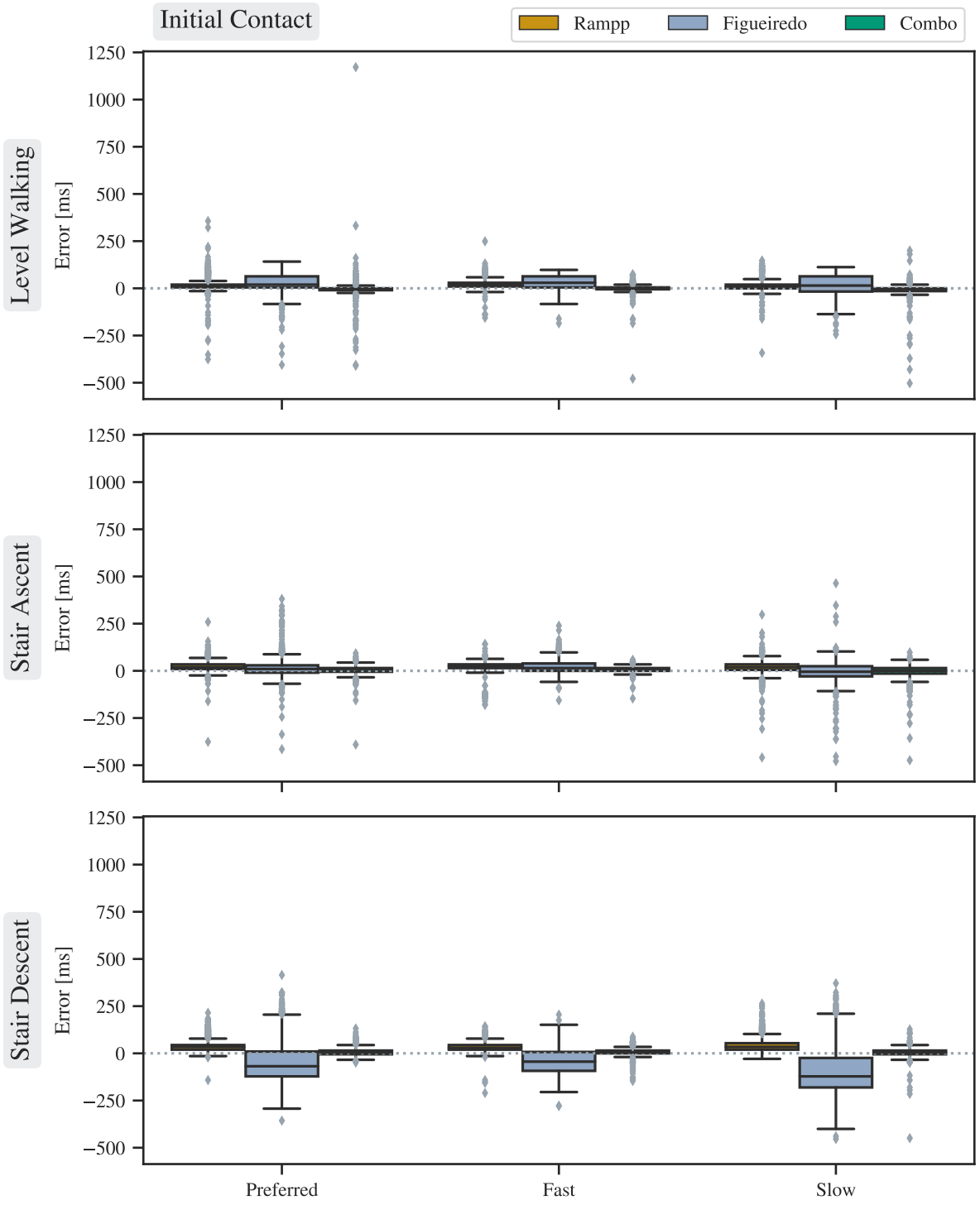

Figure B.1: Initial contact temporal errors with all outliers.

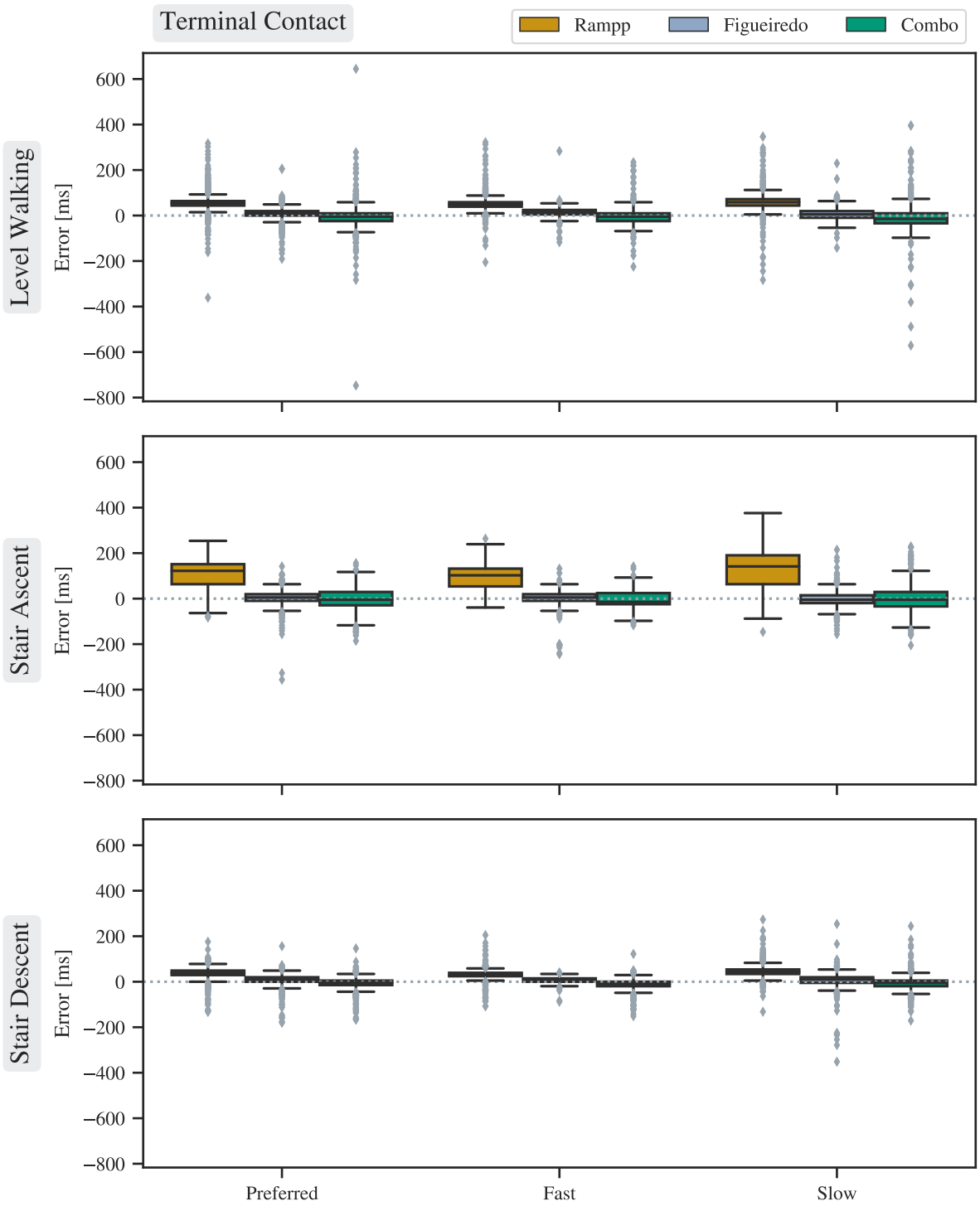

Figure B.2: Terminal contact temporal errors with all outliers.

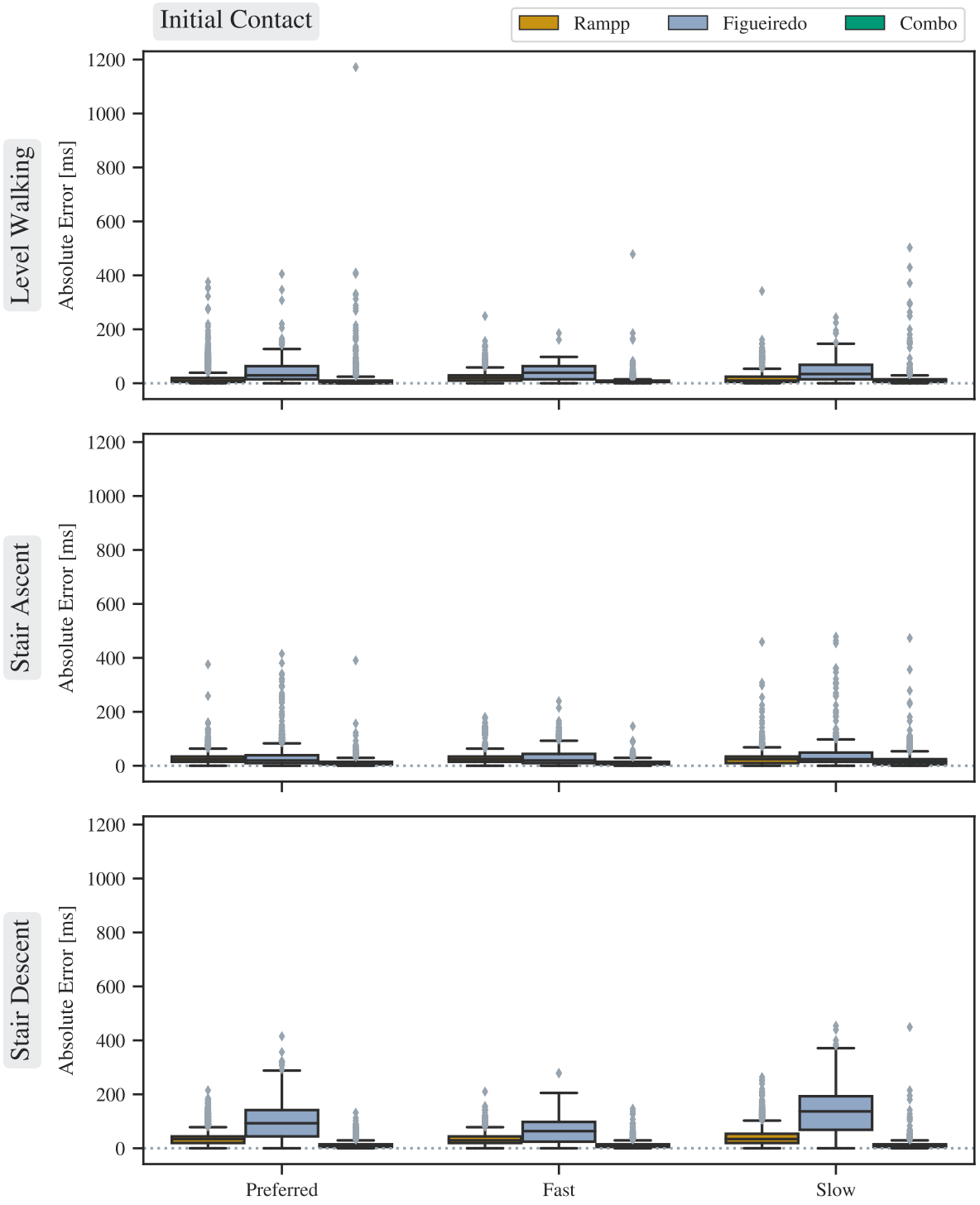

Figure B.3: Initial contact absolute temporal errors with all outliers.

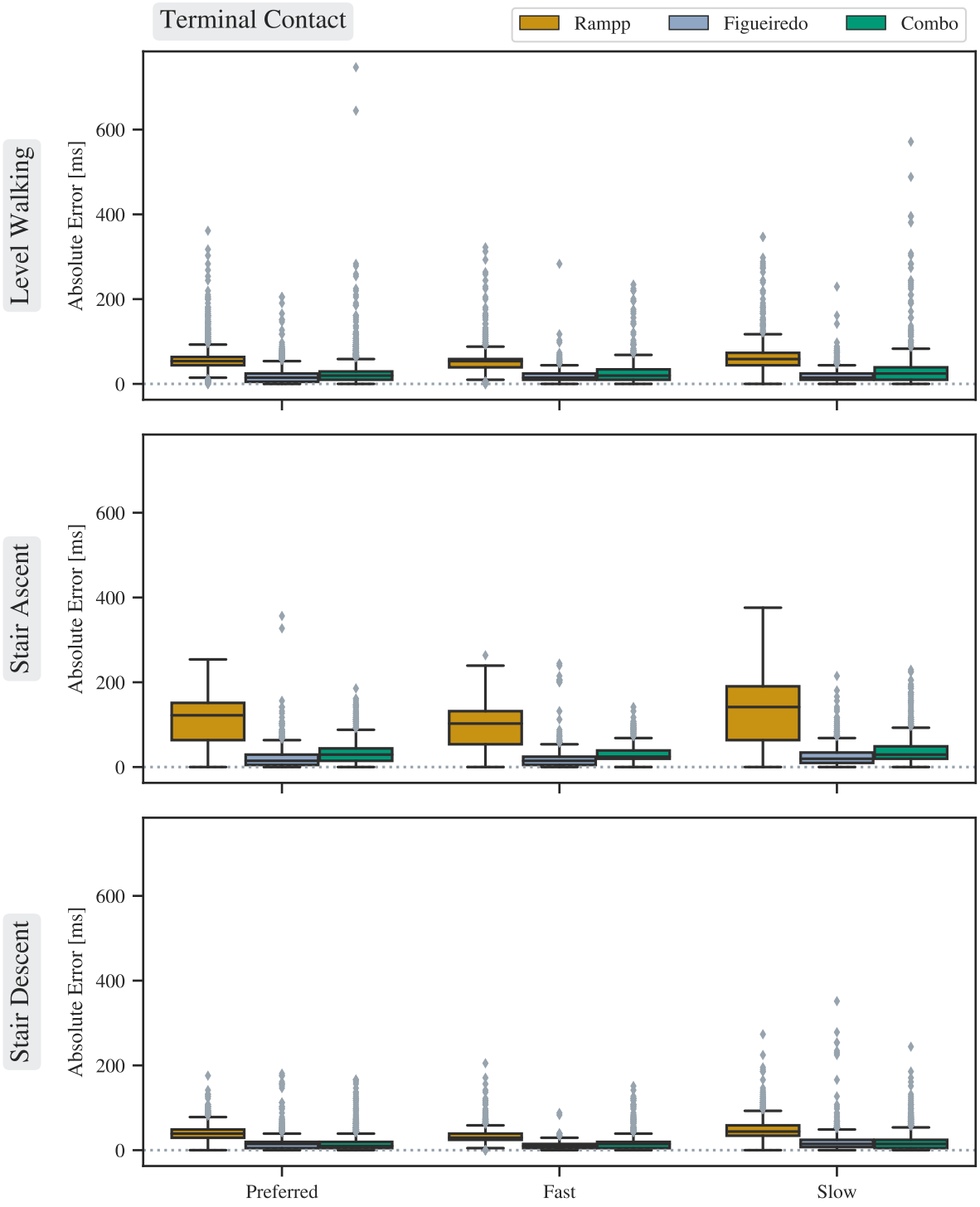

Figure B.4: Terminal contact absolute temporal errors with all outliers.

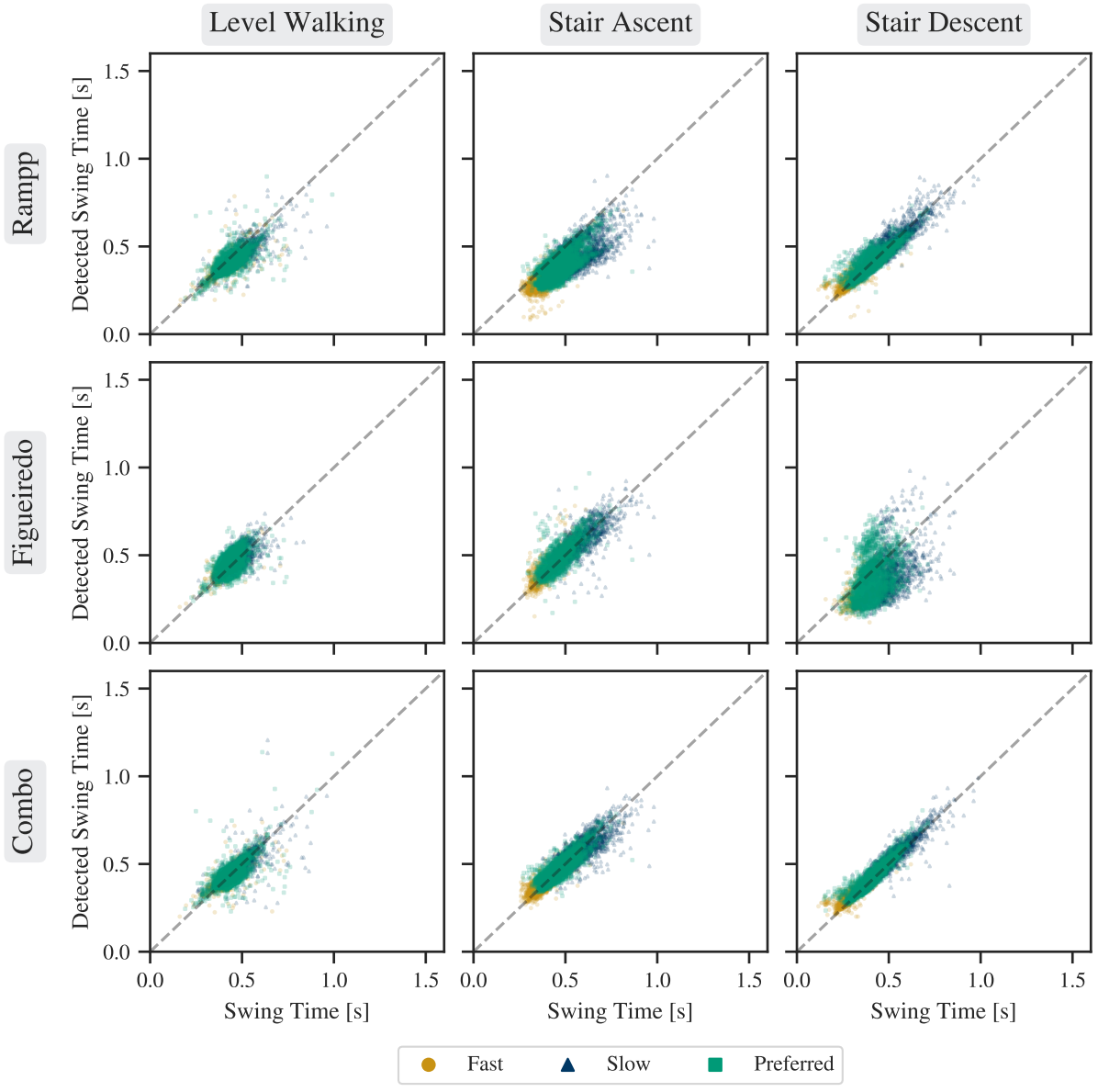

Figure B.5: More detailed *swing time* scatterplot.

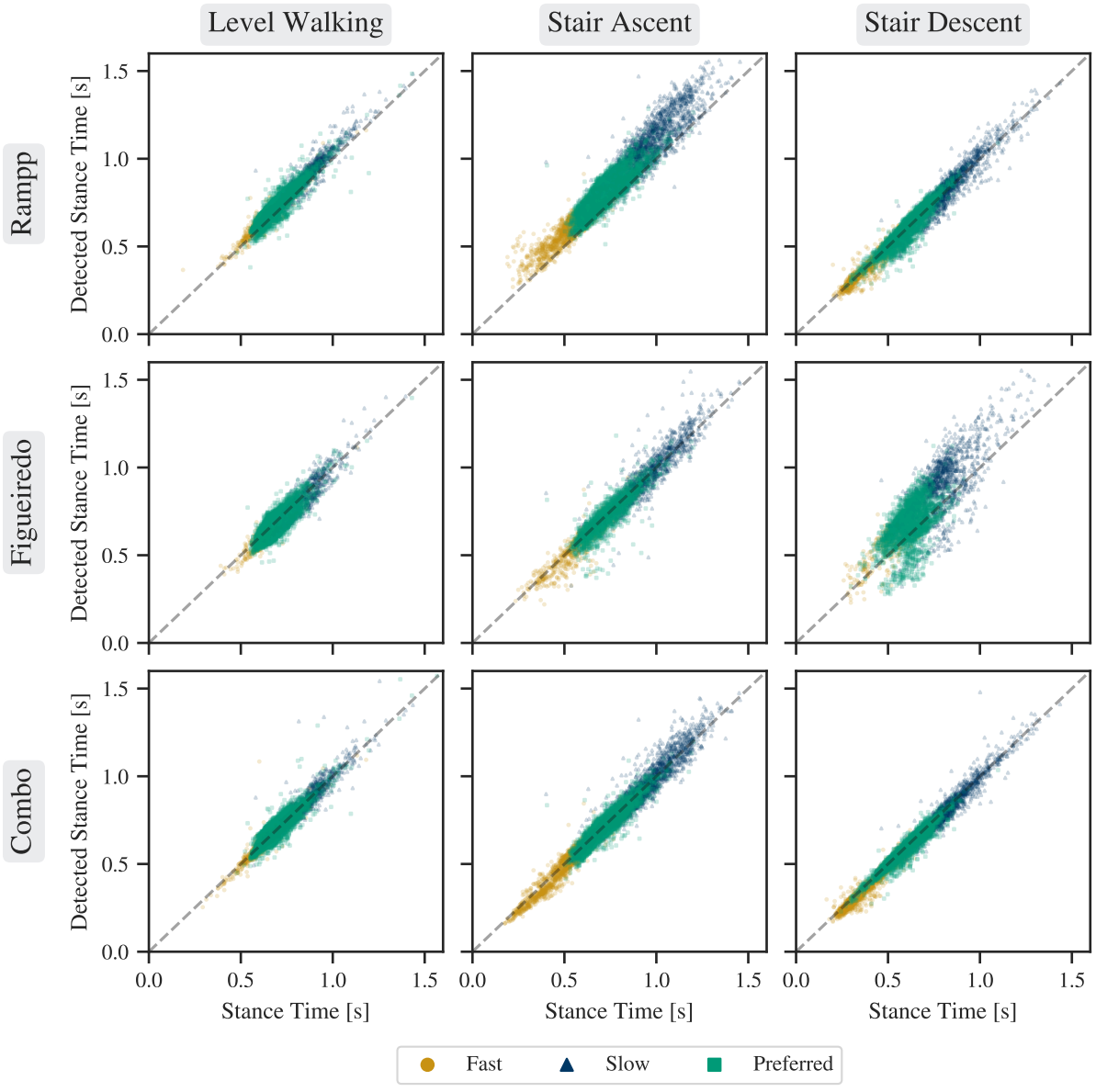

Figure B.6: More detailed *stance time* scatterplot.

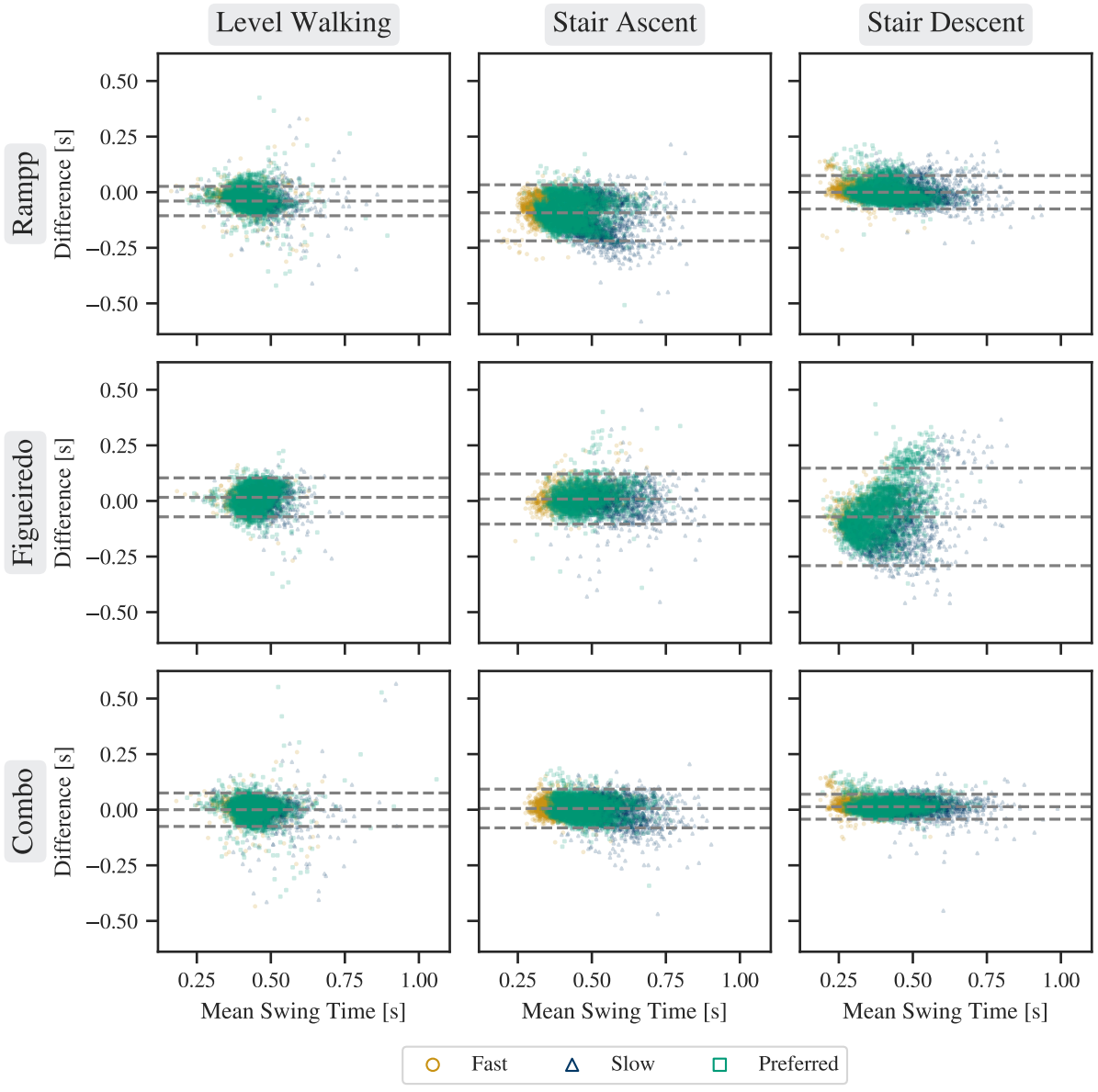

Figure B.7: More detailed *swing time* Bland-Altmann plot.

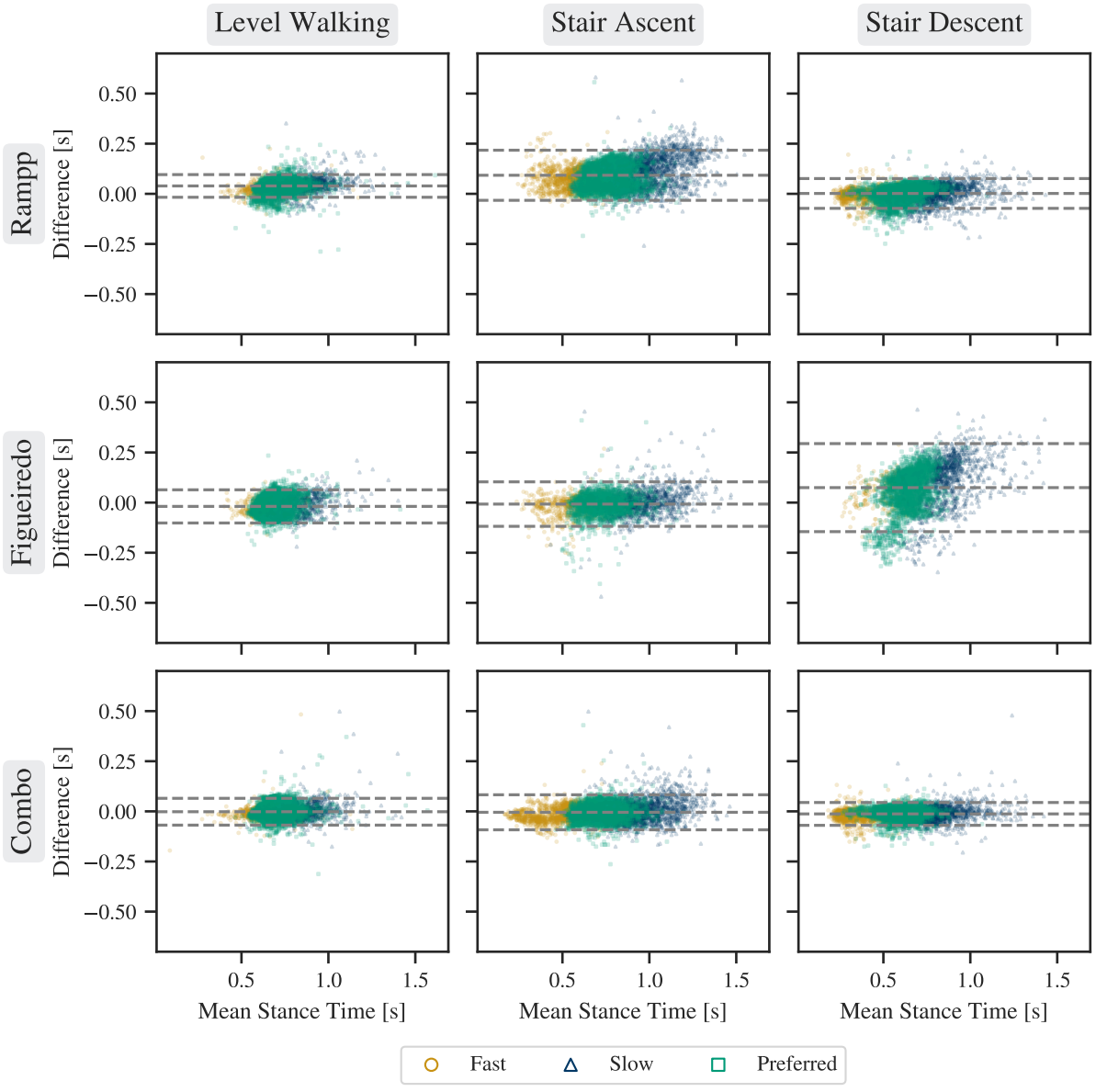

Figure B.8: More detailed *stance time* Bland-Altmann plot.

Table B.2: **Study protocol.** In *flying* mode, several meters of walking on level ground precede and succeed the stair ambulation phases and there is no standing phase between stair ascent and descent. In *standing* mode, walking starts and ends only a few steps before and after the stair and a standing phase separates stair ascent and descent.

No.	Stair	Speed/Strategy	Mode
1	staircase	preferred	flying
2		preferred	standing (up/down)
3		fast	standing (up/down)
4		slow	standing (up/down)
	Walk to next stair with 2-step stair on the way.		
5	flat stair / ramp	preferred	flying
6	flat stair	preferred	standing (down/up)
7		fast	standing (down/up)
8		slow	standing (down/up)
	Walk to next stair with flat stair (down) on the way.		
9	long stair	preferred	flying
10		preferred	standing (down/up)
11		fast	standing (down/up)
12		slow	standing (down/up)
13		single step	standing (down/up)
10		double step	standing (down/up)

Acronyms

CED ComboEventDetection. 41, 42, 44, 45, 57, 58

FBF Foot Body Frame. 12

FED FigueiredoEventDetection. 41, 42, 44, 45, 56, 57

FSF Foot Sensor Frame. 12, 25

FSM finite state machine. 28, 29

FSR force-sensing resistor. 13, 17, 21–23, 38, 51, 53, 54, 56

HD Huntington's disease. 2

IC initial contact. 3–5, 7, 8, 17, 21, 23, 24, 27–29, 33–35, 37, 38, 42, 43, 53, 54, 56–60, 79

IMU inertial measurement units. 2, 4–7, 10, 12, 16, 51, 53, 59

MEMS micro-electro-mechanical systems. 10

PD Parkinson's disease. 2, 6, 8, 38, 58, 60

RED RamppEventDetection. 41–43, 45, 53, 54, 58

SCC Spearman correlation coefficient. 44, 45, 54

TC terminal contact. 3–5, 8, 9, 17, 19, 21, 23–25, 27, 29, 33, 37, 38, 42–44, 53, 54, 56–60, 79

List of Figures

List of Tables

Bibliography

[Alb09] A. Albarbar, A. Badri, Jyoti K. Sinha, and A. Starr. Performance evaluation of MEMS accelerometers. *Measurement*, 42(5):790–795, jun 2009.

[Bao05] Minhang Bao. *Analysis and Design Principles of MEMS Devices*. Elsevier, Amsterdam Boston London, 2005.

[Bar13] Jens Barth, Cacilia Oberndorfer, Patrick Kugler, Dominik Schuldhaus, Jurgen Winkler, Jochen Klucken, and Bjorn Eskofier. Subsequence dynamic time warping as a method for robust step segmentation using gyroscope signals of daily life activities. In *2013 35th Annual International Conference of the IEEE Engineering in Medicine and Biology Society (EMBC)*. IEEE, jul 2013.

[Ben15] Earl T. Benser. Trends in inertial sensors and applications. In *2015 IEEE International Symposium on Inertial Sensors and Systems (ISISS) Proceedings*. IEEE, mar 2015.

[Ber09] Jeroen HM Bergmann, Ruth E Mayagoitia, and Ian CH Smith. A portable system for collecting anatomical joint angles during stair ascent: a comparison with an optical tracking device. *Dynamic Medicine*, 8(1), apr 2009.

[Ber18] M. Bertoli, A. Cereatti, D. Trojaniello, L. Avanzino, E. Pelosin, S. Del Din, L. Rochester, P. Ginis, E. Bekkers, A. Mirelman, J. Hausdorff, and U. Della Croce. Estimation of spatio-temporal parameters of gait from magneto-inertial measurement units: Multicenter validation among parkinson, mildly cognitively impaired and healthy older adults. *BioMedical Engineering OnLine*, 17, 2018.

[Bob18] Vladislava N. Bobic, Milica D. Djuric-Jovieic, Saa M. Radovanovic, Nataa T. Dragaevic, Vladimir S. Kostic, and Mirjana B. Popovic. Challenges of stride segmentation and their implementation for impaired gait. In *2018 40th Annual International Conference of the IEEE Engineering in Medicine and Biology Society (EMBC)*. IEEE, jul 2018.

[Bro15] Matthew A. Brodie, Kejia Wang, Kim Delbaere, Michela Persiani, Nigel H. Lovell, Stephen J. Redmond, Michael B. Del Rosario, and Stephen R. Lord. New methods to monitor stair ascents using a wearable pendant device reveal how behavior, fear, and frailty influence falls in octogenarians. *IEEE Transactions on Biomedical Engineering*, 62(11):2595–2601, nov 2015.

[Bro17] M. A. Brodie, M. J. Coppens, A. Ejupi, Y. J. Gschwind, J. Annegarn, D. Schoene, R. Wieching, S. R. Lord, and K. Delbaere. Comparison between clinical gait and daily-life gait assessments of fall risk in older people. *Geriatrics and Gerontology International*, 17(11):2274–2282, 2017.

[Bro19] Lorenzo Brognara, Pierpaolo Palumbo, Bernd Grimm, and Luca Palmerini. Assessing gait in parkinson's disease using wearable motion sensors: A systematic review. *Diseases*, 7(1):18, feb 2019.

[But30] S. Butterworth. On the theory of filter amplifiers. *Experimental Wireless and the Wireless Engineer*, 7:536–541, 1930.

[Cal17] Rafael Caldas, Marion Mundt, Wolfgang Potthast, Fernando Buarque de Lima Neto, and Bernd Markert. A systematic review of gait analysis methods based on inertial sensors and adaptive algorithms. *Gait & Posture*, 57:204–210, sep 2017.

[Car13] B. Carse, B. Meadows, R. Bowers, and P. Rowe. Affordable clinical gait analysis: An assessment of the marker tracking accuracy of a new low-cost optical 3d motion analysis system. *Physiotherapy*, 99(4):347 – 351, 2013.

[Car18] Ilaria Carpinella, Elisa Gervasoni, Denise Anastasi, Tiziana Lencioni, Davide Cattaneo, and Maurizio Ferrarin. Instrumental assessment of stair ascent in people with multiple sclerosis, stroke, and parkinson's disease: A wearable-sensor-based approach. *IEEE Transactions on Neural Systems and Rehabilitation Engineering*, 26(12):2324–2332, dec 2018.

[Cat08] Paola Catalfamo, David Moser, Salim Ghoussayni, and David Ewins. Detection of gait events using an f-scan in-shoe pressure measurement system. *Gait & Posture*, 28(3):420–426, oct 2008.

[Cat10] Paola Catalfamo, Salim Ghoussayni, and David Ewins. Gait event detection on level ground and incline walking using a rate gyroscope. *Sensors*, 10(6):5683–5702, jun 2010.

[Chu13] Jun-Uk Chu, Kang-Il Song, Sungmin Han, Soo Hyun Lee, Ji Yoon Kang, Dosik Hwang, Jun-Kyo Francis Suh, Kuiwon Choi, and Inchan Youn. Gait phase detection from sciatic nerve recordings in functional electrical stimulation systems for foot drop correction. *Physiological Measurement*, 34(5):541–565, apr 2013.

[Col05] Brian Coley, Bijan Najafi, Anisoara Paraschiv-Ionescu, and Kamiar Aminian. Stair climbing detection during daily physical activity using a miniature gyroscope. *Gait & Posture*, 22(4):287–294, dec 2005.

[Con17] Zachary J. Conway, Peter A. Silburn, Tim Blackmore, and Michael H. Cole. Evidence of compensatory joint kinetics during stair ascent and descent in parkinson's disease. *Gait & Posture*, 52:33–39, feb 2017.

[Cos02] Patrick A Costigan, Kevin J Deluzio, and Urs P Wyss. Knee and hip kinetics during normal stair climbing. *Gait & Posture*, 16(1):31–37, aug 2002.

[Din17] Silvia Del Din, Brook Galna, Alan Godfrey, Esther M J Bekkers, Elisa Pelosin, Freek Nieuwhof, Anat Mirelman, Jeffrey M Hausdorff, and Lynn Rochester. Analysis of free-living gait in older adults with and without parkinson's disease and with and without a history of falls: Identifying generic and disease-specific characteristics. *The Journals of Gerontology: Series A*, 74(4):500–506, dec 2017.

[Fer95] F. Ferraris, U. Grimaldi, and M. Parvis. Procedure for effortless in-field calibration of three-axis rate gyros and accelerometers. *Sensors and Materials*, 7:311–311, 1995.

[Fig18] Joana Figueiredo, Paulo Felix, Luis Costa, Juan C. Moreno, and Cristina P. Santos. Gait event detection in controlled and real-life situations: Repeated measures from healthy subjects. *IEEE Transactions on Neural Systems and Rehabilitation Engineering*, 26(10):1945–1956, oct 2018.

[For14] Paola Formento, Ruben Acevedo, Salim Ghoussayni, and David Ewins. Gait event detection during stair walking using a rate gyroscope. *Sensors*, 14(3):5470–5485, mar 2014.

[Gal19] I. Galperin, I. Hillel, S. Del Din, E. M. J. Bekkers, A. Nieuwboer, G. Abbruzzese, L. Avanzino, F. Nieuwhof, B. R. Bloem, L. Rochester, U. Della Croce, A. Cereatti, N. Giladi, A. Mirelman, and J. M. Hausdorff. Associations between daily-living physical activity and laboratory-based assessments of motor severity in patients with

falls and Parkinson's disease. *Parkinsonism and Related Disorders*, 62(January):85–90, 2019.

[Gar85] Everette S. Gardner. Exponential smoothing: The state of the art. *Journal of Forecasting*, 4(1):1–28, 1985.

[Gon15] Iván González, Jesús Fontecha, Ramón Hervás, and José Bravo. An ambulatory system for gait monitoring based on wireless sensorized insoles. *Sensors*, 15(7):16589–16613, jul 2015.

[Gus96] F. Gustafsson. Determining the initial states in forward-backward filtering. *IEEE Transactions on Signal Processing*, 44(4):988–992, 1996.

[Han09] Michael Hanlon and Ross Anderson. Real-time gait event detection using wearable sensors. *Gait & Posture*, 30(4):523–527, nov 2009.

[Hau95] Jeffrey M. Hausdorff, Zvi Ladin, and Jeanne Y. Wei. Footswitch system for measurement of the temporal parameters of gait. *Journal of Biomechanics*, 28(3):347–351, mar 1995.

[Hau98] Jeffrey M. Hausdorff, Merit E. Cudkowicz, Renée Firtion, Jeanne Y. Wei, and Ary L. Goldberger. Gait variability and basal ganglia disorders: Stride-to-stride variations of gait cycle timing in parkinson's disease and huntington's disease. *Movement Disorders*, 13(3):428–437, may 1998.

[Jar18] Delaram Jarchi, James Pope, Tracey K. M. Lee, Larisa Tamjidi, Amirhosein Mirzaei, and Saeid Sanei. A review on accelerometry-based gait analysis and emerging clinical applications. *IEEE Reviews in Biomedical Engineering*, 11:177–194, 2018.

[Jia18] Xianta Jiang, Kelvin Chu, Mahta Khoshnam, and Carlo Menon. A wearable gait phase detection system based on force myography techniques. *Sensors*, 18(4):1279, apr 2018.

[Kan15] Christoph M. Kanzler, Jens Barth, Alexander Rampp, Heiko Schlarb, Franz Rott, Jochen Klucken, and Bjoern M. Eskofier. Inertial sensor based and shoe size independent gait analysis including heel and toe clearance estimation. In *2015 37th Annual International Conference of the IEEE Engineering in Medicine and Biology Society (EMBC)*. IEEE, aug 2015.

[Kas05] Jean-Pierre Kassi, Markus O. Heller, Ulrich Stoeckle, Carsten Perka, and Georg N. Duda. Stair climbing is more critical than walking in pre-clinical assessment of primary stability in cementless THA in vitro. *Journal of Biomechanics*, 38(5):1143–1154, may 2005.

[Kel19] Keloth, Viswanathan, Jelfs, Arjunan, Raghav, and Kumar. Which gait parameters and walking patterns show the significant differences between parkinson's disease and healthy participants? *Biosensors*, 9(2):59, apr 2019.

[Kon08] Kyoungchul Kong and Masayoshi Tomizuka. Smooth and continuous human gait phase detection based on foot pressure patterns. In *2008 IEEE International Conference on Robotics and Automation*. IEEE, may 2008.

[Kon14] Win Kong, Mohamad Hanif Saad, M A Hannan, and Aini Hussain. Human gait state classification using artificial neural network. In *2014 IEEE Symposium on Computational Intelligence for Multimedia, Signal and Vision Processing (CIMSIVP)*. IEEE, dec 2014.

[Liz16] L Eduardo Cofré Lizama, Fary Khan, Peter VS Lee, and Mary P Galea. The use of laboratory gait analysis for understanding gait deterioration in people with multiple sclerosis. *Multiple Sclerosis Journal*, 22(14):1768–1776, jul 2016.

[MA16] M. Encarna Micó-Amigo, Idsart Kingma, Erik Ainsworth, Stefan Walgaard, Martijn Niessen, Rob C. van Lummel, and Jaap H. van Dieën. A novel accelerometry-based algorithm for the detection of step durations over short episodes of gait in healthy elderly. *Journal of NeuroEngineering and Rehabilitation*, 13(1), apr 2016.

[Man80] Roger A. Mann and John Hagy. Biomechanics of walking, running, and sprinting. *The American Journal of Sports Medicine*, 8(5):345–350, sep 1980.

[Man19] Miguel D. Sánchez Manchola, María J. Pinto Bernal, Marcela Munera, and Carlos A. Cifuentes. Gait phase detection for lower-limb exoskeletons using foot motion data from a single inertial measurement unit in hemiparetic individuals. *Sensors*, 19(13):2988, jul 2019.

[Mar17] Christine F. Martindale, Martin Strauss, Heiko Gassner, Julia List, Meinard Muller, Jochen Klucken, Zacharias Kohl, and Bjoern M. Eskofier. Segmentation of gait sequences using inertial sensor data in hereditary spastic paraplegia. In *2017 39th*

Annual International Conference of the IEEE Engineering in Medicine and Biology Society (EMBC). IEEE, jul 2017.

[McD01] Andrew L. McDonough, Mitchell Batavia, Fang C. Chen, Soonjung Kwon, and James Ziai. The validity and reliability of the GAITRite system's measurements: A preliminary evaluation. *Archives of Physical Medicine and Rehabilitation*, 82(3):419–425, mar 2001.

[McF88] Bradford J. McFadyen and David A. Winter. An integrated biomechanical analysis of normal stair ascent and descent. *Journal of Biomechanics*, 21(9):733–744, jan 1988.

[Mir19] Anat Mirelman, Paolo Bonato, Richard Camicioli, Terry D Ellis, Nir Giladi, Jamie L Hamilton, Chris J Hass, Jeffrey M Hausdorff, Elisa Pelosin, and Quincy J Almeida. Gait impairments in parkinson's disease. *The Lancet Neurology*, 18(7):697–708, jul 2019.

[Mui10] Susan W. Muir, Katherine Berg, Bert Chesworth, Neil Klar, and Mark Speechley. Quantifying the magnitude of risk for balance impairment on falls in community-dwelling older adults: a systematic review and meta-analysis. *Journal of Clinical Epidemiology*, 63(4):389–406, apr 2010.

[Nad03] S Nadeau, B.J McFadyen, and F Malouin. Frontal and sagittal plane analyses of the stair climbing task in healthy adults aged over 40 years: what are the challenges compared to level walking? *Clinical Biomechanics*, 18(10):950–959, dec 2003.

[Ngu19] An Nguyen, Nils Roth, Nooshin Haji Ghassemi, Julius Hannink, Thomas Seel, Jochen Klucken, Heiko Gassner, and Bjoern M. Eskofier. Development and clinical validation of inertial sensor-based gait-clustering methods in parkinson's disease. *Journal of NeuroEngineering and Rehabilitation*, 16(1), jun 2019.

[Nis21] Wesley Niswander and Kimberly Kontson. Evaluating the impact of IMU sensor location and walking task on accuracy of gait event detection algorithms. *Sensors*, 21(12):3989, jun 2021.

[OP11] Mooyeon Oh-Park, Cuiling Wang, and Joe Verghese. Stair negotiation time in community-dwelling older adults: Normative values and association with functional decline. *Archives of Physical Medicine and Rehabilitation*, 92(12):2006–2011, dec 2011.

[Par12] Poonam K. Pardasaney, Nancy K. Latham, Alan M. Jette, Robert C. Wagenaar, Pengsheng Ni, Mary D. Slavin, and Jonathan F. Bean. Sensitivity to change and responsiveness of four balance measures for community-dwelling older adults. *Physical Therapy*, 92(3):388–397, mar 2012.

[Pir16] Walter Pirker and Regina Katzenschlager. Gait disorders in adults and the elderly. *Wiener klinische Wochenschrift*, 129(3-4):81–95, oct 2016.

[Ram15] Alexander Rampp, Jens Barth, Samuel Schülein, Karl-Günter Gaßmann, Jochen Klucken, and Björn M. Eskofier. Inertial sensor-based stride parameter calculation from gait sequences in geriatric patients. *IEEE Transactions on Biomedical Engineering*, 62(4):1089–1097, 2015.

[Rie02] Robert Riener, Marco Rabuffetti, and Carlo Frigo. Stair ascent and descent at different inclinations. *Gait & Posture*, 15(1):32–44, feb 2002.

[Rud21] Julian Rudisch, Thomas JÃ¶llenbeck, Lutz Vogt, Thomas Cordes, Thomas JÃ¼rgen Klotzbier, Oliver Vogel, and Bettina Wollesen. Agreement and consistency of five different clinical gait analysis systems in the assessment of spatiotemporal gait parameters. *Gait & Posture*, 85:55–64, mar 2021.

[Rue10] Jan Rueterbories, Erika G. Spaich, Birgit Larsen, and Ole K. Andersen. Methods for gait event detection and analysis in ambulatory systems. *Medical Engineering & Physics*, 32(6):545–552, jul 2010.

[SC13] Anne Shumway-Cook, Catherine S. Taylor, Patricia Noritake Matsuda, Michael T. Studer, and Brady K. Whetten. Expanding the scoring system for the dynamic gait index. *Physical Therapy*, 93(11):1493–1506, nov 2013.

[Sch17] J. C. M. Schlachetzki, J. Barth, F. Marxreiter, J. Gossler, Z. Kohl, S. Reinfelder, H. Gassner, K. Aminian, B. M. Eskofier, J. Winkler, and J. Klucken. Wearable sensors objectively measure gait parameters in parkinson's disease. *PLOS ONE*, 12(10):1–18, 10 2017.

[Smi02] B.T. Smith, D.J. Coiro, R. Finson, R.R. Betz, and J. McCarthy. Evaluation of force-sensing resistors for gait event detection to trigger electrical stimulation to improve walking in the child with cerebral palsy. *IEEE Transactions on Neural Systems and Rehabilitation Engineering*, 10(1):22–29, mar 2002.

[Sta00] Jill K. Startzell, D. Alfred Owens, Lorraine M. Mulfinger, and Peter R. Cavanagh. Stair negotiation in older people: A review. *Journal of the American Geriatrics Society*, 48(5):567–580, may 2000.

[Sta11] J. Stamatakis, J. Cremers, D. Maquet, B. Macq, and G. Garraux. Gait feature extraction in parkinson's disease using low-cost accelerometers. In *2011 Annual International Conference of the IEEE Engineering in Medicine and Biology Society*. IEEE, aug 2011.

[Tun17] C. Tunca, N. Pehlivan, N. Ak, B. Arnrich, G. Salur, and C. Ersoy. Inertial sensor-based robust gait analysis in non-hospital settings for neurological disorders. *Sensors*, 17(4), 2017.

[Vir20] Pauli Virtanen, Ralf Gommers, Travis E. Oliphant, Matt Haberland, Tyler Reddy, David Cournapeau, Evgeni Burovski, Pearu Peterson, Warren Weckesser, Jonathan Bright, Stéfan J. van der Walt, Matthew Brett, Joshua Wilson, K. Jarrod Millman, Nikolay Mayorov, Andrew R. J. Nelson, Eric Jones, Robert Kern, Eric Larson, C J Carey, İlhan Polat, Yu Feng, Eric W. Moore, Jake VanderPlas, Denis Laxalde, Josef Perktold, Robert Cimrman, Ian Henriksen, E. A. Quintero, Charles R. Harris, Anne M. Archibald, Antônio H. Ribeiro, Fabian Pedregosa, Paul van Mulbregt, and SciPy 1.0 Contributors. SciPy 1.0: Fundamental Algorithms for Scientific Computing in Python. *Nature Methods*, 17:261–272, 2020.

[Vu20] Huong Thi Thu Vu, Dianbiao Dong, Hoang-Long Cao, Tom Verstraten, Dirk Lefeber, Bram Vanderborght, and Joost Geeroms. A review of gait phase detection algorithms for lower limb prostheses. *Sensors*, 20(14):3972, jul 2020.

[Wan14] Kejia Wang, Nigel H. Lovell, Michael B. Del Rosario, Ying Liu, Jingjing Wang, Michael R. Narayanan, Matthew A. D. Brodie, Kim Delbaere, Jasmine Menant, Stephen R. Lord, and Stephen J. Redmond. Inertial measurements of free-living activities: Assessing mobility to predict falls. In *2014 36th Annual International Conference of the IEEE Engineering in Medicine and Biology Society*. IEEE, 2014.

[Wan17] Kejia Wang, Kim Delbaere, Matthew A. D. Brodie, Nigel H. Lovell, Lauren Kark, Stephen R. Lord, and Stephen J. Redmond. Differences between gait on stairs and flat surfaces in relation to fall risk and future falls. *IEEE Journal of Biomedical and Health Informatics*, 21(6):1479–1486, nov 2017.

[Whi07] M. W. Whittle. Chapter 2 - normal gait. In *Gait Analysis (Fourth Edition)*, pages 47 – 100. Butterworth-Heinemann, Edinburgh, 2007.

[Won07] Wai Yin Wong, Man Sang Wong, and Kam Ho Lo. Clinical applications of sensors for human posture and movement analysis. *Prosthetics & Orthotics International*, 31(1):62–75, mar 2007.

[Woo07] Oliver J. Woodman. An introduction to inertial navigation. Technical Report UCAM-CL-TR-696, University of Cambridge, Computer Laboratory, August 2007.

[Wu02] Ge Wu, Sorin Siegler, Paul Allard, Chris Kirtley, Alberto Leardini, Dieter Rosenbaum, Mike Whittle, Darryl D D'Lima, Luca Cristofolini, Hartmut Witte, Oskar Schmid, and Ian Stokes. ISB recommendation on definitions of joint coordinate system of various joints for the reporting of human joint motion—part i: ankle, hip, and spine. *Journal of Biomechanics*, 35(4):543–548, apr 2002.